RICE UNIVERSITY

A Novel Phosphodiesterase of the GdpP Family Modulates Cyclic di-AMP Levels in Response to Cell Membrane Stress in Daptomycin-Resistant Enterococci

by

Xu Wang

A THESIS SUBMITTED
IN PARTIAL FULFILLMENT OF THE
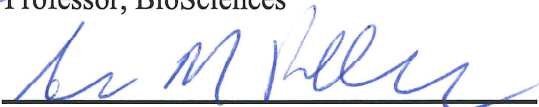REQUIREMENTS FOR THE DEGREE

Doctor of Philosophy

APPROVED, THESIS COMMITTEE

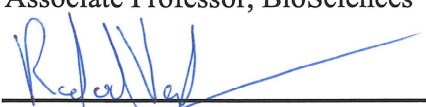Yousif Shamoo, Thesis Advisor
Professor, BioSciences

John S. Olson, Committee Chair
Professor, BioSciences

George N. Phillips, Jr.,
Professor, BioSciences

Yizhi Jane Tao,
Associate Professor, BioSciences

Rafael Verduzco,
Associate Professor, Chemical and
Biomolecular Engineering

HOUSTON, TEXAS
March 2017

ABSTRACT

A Novel Phosphodiesterase of the GdpP Family Modulates Cyclic di-AMP Levels in Response to Cell Membrane Stress in Daptomycin-Resistant Enterococci

by

Xu Wang

Antimicrobial resistance is a serious and growing threat to public health. The Centers for Disease Control estimates that at least 2 million people contract serious infections each year resulting in at least 23,000 deaths each year in the United States alone. To develop more effective treatments, it is important to understand the fundamental biology underlying the mechanisms of antibiotic resistance. Substitutions in the LiaFSR membrane stress response pathway are frequently associated with emergence of antimicrobial peptide resistance in both *Enterococcus faecalis* and *Enterococcus faecium*. Cyclic di-AMP (c-di-AMP) is an important signal molecule that affects many aspects of bacterial physiology including stress response. We have previously identified a mutation in a gene (designated *yybT*) of *E. faecalis* that was associated with development of daptomycin resistance. The adaptive mutation produced a change at position 440 in the predicted protein (*yybT*[I440S]). Here, we show that intracellular cyclic di-AMP signaling is present in enterococci and, based upon *in vitro* physicochemical characterization, we show that *E. faecalis yybT* encodes a cyclic dinucleotide phosphodiesterase of the GdpP family that exhibits specific activity toward c-di-AMP by hydrolyzing it to 5'pApA. The *E.*

faecalis GdpP^{I440S} substitution reduces cyclic di-AMP phosphodiesterase activity more than 11-fold leading to further increases in cyclic di-AMP levels. Additionally, deletions of *liaR* (encoding the response regulator of the LiaFSR system) that lead to daptomycin hypersusceptibility in both *E. faecalis* and *E. faecium* also resulted in increased cyclic-di-AMP levels suggesting that changes in the LiaFSR stress response pathway are linked to broader physiological changes. Taken together, our data show that modulation of cyclic di-AMP pools is strongly associated with antibiotic-induced cell membrane stress response via changes in GdpP activity and signaling through the LiaFSR system.

Acknowledgments

I would also like to thank the members of Arias lab at UT Medical School, who are nice collaborators to work with. Especially, I would like to thank Dr. Diana Panesso and Dr. Jinnethe Reyes.

I would like to thank Tao lab, Olson lab, Silberg lab, Matthew Bennett lab, Phillips lab, Carson lab and Nikonowicz lab for providing suggestions for my research and sharing equipment and reagents.

I would like to thank the Department of BioSciences. In particular, I would like to thank Dr. Janet Braam, Dr. Susan Cates, Ms. Angel Forward, Ms. Sandra Saunders, Mr. Juan Sanchez, and Mr. Gerald Mixon, who were always willing to provide help. I would like to thank National Institutes of Health for providing funding for my research, and the China Scholarship Council for the fellowship.

Last but not least, I want to express endless gratitude to my parents and my friends, who never hesitate to support my pursuit.

Contents

List of Figures

List of Tables

Nomenclature

BHI	Brain heart infusion
Bs	*Bacillus subtilis*
CdaA	Cyclic di-AMP synthase A
CdaS	Cyclic di-AMP synthase S, sporulation-specific
c-di-AMP	Cyclic di-adenosine monophosphate
c-di-GMP	Cyclic di-guanosine monophosphate
CLS	Cardiolipin synthase
DAC	Diadenylate cyclase
DAP	Daptomycin
DisA	DNA integrity scanning protein A
Efc	*Enterococci faecalis*
Efm	*Enterococci faecium*
GdpP	GGDEF domain protein containing phosphodiesterase
L. monocytogenes	*Listeria monocytogenes*
LTA	Lipoteichoic acid
MR	Molecular replacement
M. smegmatis	*Mycobacterium smegmatis*
MAD	Multi-wavelength anomalous dispersion
MIR	Multiple isomorphous replacement
MIC	Minimum Inhibitory Concentration

MR	Molecular replacement
MRSA	Methicillin-resistant *Staphylococcus aureus*
M. tuberculosis	*Mycobacterium tuberculosis*
PDE	phosphodiesterase
RpfA	Resuscitation promoting factor A
SAD	Single-wavelength anomalous dispersion
S. aureus	*Staphylococcus aureus*
S. coelicolor	*Streptomyces coelicolor*
S. pneumoniae	*Streptococcus pneumoniae*
SeMet	Selenomethionine
VRE	Vancomycin Resistant Enterococcus

Chapter 1

Introduction

1.1. *E. faecalis* GdpP is a putative cyclic di-AMP-specific phosphodiesterase.

GdpP (GGDEF domain protein containing phosphodiesterase) is a multi-domain protein containing two putative N-terminal transmembrane helices, a putative Per-Arnt-Sim (PAS) domain, a GGDEF domain and a DHH domain with a DHHA1 subdomain (Figure 1.1) (Rao et al., 2010). GdpP has been identified in several Gram-positive bacteria including *Bacillus subtilis* (Rao et al., 2010), *Lactococcus lactis* (Smith et al., 2012), *Streptococcus pyogenes* (Cho and Kang, 2013) and *Staphylococcus aureus* (Corrigan et al., 2011) with roles in bacterial growth and virulence.

In a previous study about *Enterococcus faecalis* (*E. faelicas*) evolutionary trajectories to antibiotic daptomycin (DAP) resistance, Miller *et al.* identified mutation I440S in a previously unidentified gene, designated *yybT* (Miller et al., 2013). Based on primary sequence alignment, I reasoned that YybT might be a member of the GdpP family (*E. faecalis yybT* will be referred to as *Efc gdpP* hereafter) (Corrigan et al., 2011). Since GdpP[I440S] was identified in the DAP-resistant *E. faecalis*, I postulated GdpP was also active in *E. faecalis*, and wanted to study the structure and functions of *Efc* GdpP and how the I440S adaptive mutation affects GdpP activity. From studies on the individual domains of GdpP homologs, several activities have been described.
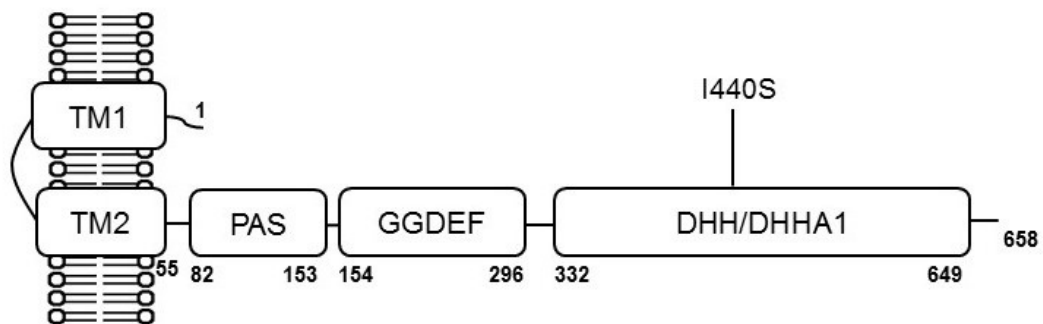
Figure 1.1 Domain organization of *E. faecalis* GdpP. *Efc GdpP is a multi-domain protein containing two putative N-terminal transmembrane helices, a Per-Arnt-Sim (PAS) domain, a GGDEF domain and a DHH domain with a DHHA1 subdomain. The DHH/DHHA1 domain has putative c-di-AMP phosphodiesterase active site while the*

GGDEF domain has putative ATPase activity. The daptomycin adaptive mutation I440S is in the DHH domain.

1.1.1. *Efc* GdpP PAS domain is a putative signal sensor domain.

PAS domains are important signaling input modules usually fused to a signal transduction or sensory protein (Henry and Crosson, 2011). They have been shown to detect a variety of environmental stimuli and transmit the information to other signaling output domains in the protein (Henry and Crosson, 2011). *B. subtilis* GdpP (*Bs*GdpP) and *G. thermodenitrificans* GdpP (*Gt*GdpP) have been demonstrated to have heme-binding PAS domains (Rao et al., 2010, 2011). The binding of heme to PAS domain can inhibit the activities of GGDEF domain and DHH/DHHA1 domain in *Bs*GdpP (Rao et al., 2010). No known ligand for the PAS domain of *Efc* GdpP has been established.

1.1.2. *Efc* GdpP GGDEF domain is a putative ATPase domain.

GGDEF was referred to the highly conserved Gly-Gly-Asp-Glu-Phe motif in this domain (Hecht and Newton, 1995). GGDEF domains typically have a diguanylate cyclase (DGC) activity to synthesize c-di-GMP from 2 GTP molecules (Rao et al., 2010). However, the GGDEF domain in *Bs*GdpP lacks the essential GGDEF motif, and has weak ATPase activity (Rao et al., 2010).

GGDEF domains were also recently reported to have a diadenylate cyclase activity that can synthesize cyclic di-AMP (c-di-AMP) from two ATP molecules (Hallberg et al., 2016). Three GGDEF domain proteins from Gram-negative bacteria, *Geobacter sulfurreducens* HyprA (also referred to as GSU1658), *Bdellovibrio bacteriovorus* DgcA (also referred to as Bd0367), and *Myxococcus xanthus* HyprB (also referred to as MXAN-2643), showed diadenylate cyclase activity *in* vitro and when they were over expressed in *E. coli* (Hallberg et al., 2016). However, since c-di-AMP has not been identified in Gram-negative bacteria, whether these observations are physiologically relevant will require further investigation. Nevertheless, it suggests *Efc* GdpP can synthesize c-di-AMP under certain conditions.

1.1.3. *Efc* GdpP DHH/DHHA1 domain is a putative phosphodiesterase domain.

The Asp-His-His (DHH/DHHA1) domain of *Bs*GdpP has a cyclic-dinucleotide (c-di-AMP and c-di-GMP) phosphodiesterase (PDE) activity *in vitro*, and can hydrolyze c-di-AMP and c-di-GMP to 5'pApA and 5'pGpG respectively (Rao et al., 2010). *S. aureus* GdpP (*Sa*GdpP) has c-di-AMP-specific PDE activity *in vivo* (Corrigan et al., 2011). The signaling molecule, ppGpp, can inhibit *Bs*GdpP PDE activity (Rao et al., 2010). Using a bioinformatic approach I was able to identify a potential DHH/DHHA1 domain in *Efc* GdpP suggesting a potential c-di-AMP phosphodiesterase activity.

1.2. Cyclic di-AMP is a new second messenger identified in some Gram-positive bacteria.

Interesting, cyclic di-AMP (c-di-AMP) is a putative substrate, as well as a putative product, of *Efc* GdpP. c-di-AMP is a recently discovered second messenger molecule (Figure 1.2). Since c-di-AMP could only be synthesized chemically in the twentieth century, the microbiological role of c-di-AMP was largely unknown until Witte *et al.* first discovered a c-di-AMP synthase in *B. subtilis* in 2008 (Bejerano-Sagie et al., 2006; Römling, 2008; Witte et al., 2008). Later on, c-di-AMP was identified in several other Gram-positive bacteria including *Listeria monocytogenes* (Witte et al., 2013), *Staphylococcus aureus* (Corrigan et al., 2011)*, Streptococcus pyogenes* (Cho and Kang, 2013), and *Streptococcus pneumoniae* (Bai et al., 2013)*.*
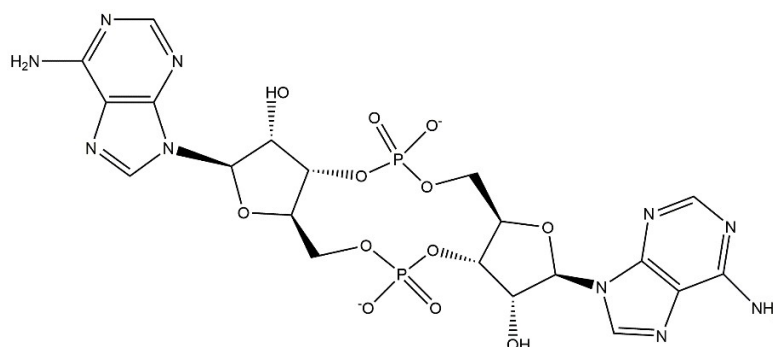
Figure 1.2 Structure of cyclic di-AMP. *Figure is produced by Chemdraw Professional.*

1.2.1. Synthesis and degradation of c-di-AMP

1.2.1.1. c-di-AMP is synthesized by diadenyl cyclase.

The ability to directly synthesize c-di-AMP from two ATP or ADP was first identified in a specific diadenylate cyclase (DAC) domain (Bai et al., 2012; Witte et al., 2008). To date, three DAC domain proteins have been discovered, including the most common DAC synthase referred to as c-di-AMP synthase A (CdaA, also referred to as YbbP), the sporulation-specific synthase CdaS (also referred to as YojJ), and the DNA integrity scanning protein A (Dis A) (Corrigan et al., 2013; Mehne et al., 2013, 2014; Oppenheimer-Shaanan et al., 2011a; Witte et al., 2008).

As mentioned above (Section 1.1.2), some GGDEF domains in Gram-negative bacteria also showed diadenylate cyclase activity (Hallberg et al., 2016)

1.2.1.2. c-di-AMP is hydrolyzed by phosphodiesterases.

In vivo levels of c-di-AMP are not only maintained by diadenyl cyclases but also by phosphodiesterases. The Asp-His-His (DHH/DHHA1) domain and His-Asp (HD) domain hydrolyze c-di-AMP to 5'pApA or AMP (Huynh et al., 2015; Rao et al., 2010). A study of *L. monocytogenes* c-di-AMP phosphodiesterases showed that DHH/DHHA1 family phosphodiesterases are more important than HD family phosphodiesterases for bacterial virulence and intracellular growth (Huynh et al., 2015).

1.2.2. Molecular mechanism of c-di-AMP signaling

Genes encoding c-di-AMP synthases and phosphodiesterases are widespread in Gram-positive bacteria and some archaea (Rao et al., 2010; Römling, 2008) and are usually found together suggesting a dynamic interplay of activities that maintains the steady-state level of c-di-AMP *in vivo*. c-di-AMP has been shown to bind both of RNAs and proteins (Corrigan et al., 2013; Nelson et al., 2013) and therefore there are many potential downstream targets for c-di-AMP signaling. As a second massager, c-di-AMP not only participates in regulating metabolism, but also quorum sensing consistent with a broad role in bacterial physiology.

1.2.2.1. c-di-AMP can regulate gene expression by binding to an RNA riboswitch.

c-di-AMP can regulate cell signaling at the level of protein translation through riboswitches, which are structure-dependent regulators located in the 5' or 3' untranslated region of mRNA (Nelson et al., 2013). Studies have shown that two c-di-AMP molecules can bind to the *ydaO* riboswitch motif, leading to global conformational changes in the mRNA structure to form terminators (Nelson et al., 2013). *ydaO* riboswitches control a broad range of gene expression, including genes encoding c-di-AMP synthases CdaA and DisA, and genes for cell wall metabolism, amino acid and ion transport, amino acid transport, and other signal transduction pathways (Barrick et al., 2004; Block et al., 2010). These reports provide further evidence that c-di-AMP is an important molecule in cell signaling.

1.2.2.2. c-di-AMP regulates enzyme activity by directly binding to the protein.

In addition to regulating gene expression via binding to specific mRNAs, c-di-AMP can also bind directly to some proteins, and control their activities via allosteric regulation (Corrigan and Gründling, 2013; Corrigan et al., 2013). Several c-di-AMP receptors have been identified by protein pull-down assays (Corrigan et al., 2013). Interestingly, most of them regulate transmembrane cation transport. The most conserved c-di-AMP synthases and phosphodiesterases are membrane proteins or membrane associated suggesting that like many signaling pathways c-di-AMP transduces or responds to environmental changes leading to improved cellular fitness.

1.2.3. Pathways regulated by c-di-AMP

1.2.3.1. c-di-AMP is essential for bacterial growth.

Both c-di-AMP depletion and accumulation are toxic for bacteria. Deletion of the genes encoding c-di-AMP synthase in the genome is fatal for bacilli (Luo and Helmann, 2012; Mehne et al., 2013). Intracellular c-di-AMP accumulation also inhibits growth, and causes aberrant small and curled morphologies (Bai et al., 2013; Luo and Helmann, 2012; Mehne et al., 2013; Smith et al., 2012). These observations suggest maintaining c-di-AMP in a certain level is important for bacteria growth and fitness.

1.2.3.2. c-di-AMP signals DNA damage.

c-di-AMP, together with c-di-AMP synthase DisA, have been shown to report on DNA damage in *B. subtilis* (Oppenheimer-Shaanan et al., 2011a). *B. subtilis* DisA scans the chromosomal DNA for double-stranded breaks and synthesize c-di-AMP (Oppenheimer-Shaanan et al., 2011a). The DNA lesions can stop DisA scanning and downregulate DiaA activity, which leads to decreased c-di-AMP levels in *B. subtilis* (Oppenheimer-Shaanan et al., 2011a).

1.2.3.3. c-di-AMP regulates potassium homeostasis.

In *S. aureus* and *B. subtilis*, c-di-AMP directly interacts with proteins involved in K^+ transport, including cation proton antiporter CpaA, K^+ transporter gating component KtrA, and KdpD in a K^+ response module (Corrigan et al., 2013; Kim et al., 2015). c-di-AMP controls the translation of K^+ transporter KtrAB by *ydaO* riboswitch (Kim et al., 2015; Nelson et al., 2013; Ren and Patel, 2014). Moreover, binding of c-di-AMP to KtrA inhibits K^+ uptake (Kim et al., 2015). These data suggests c-di-AMP plays an important role in osmotic stress response (Corrigan et al., 2013).

1.2.3.4. c-di-AMP regulates cell wall biosynthesis.

In several Gram-positive organisms, increased intracellular c-di-AMP levels can make bacteria resistant to cell wall stress (Luo and Helmann, 2012; Smith et al., 2012; Witte et al., 2013). In *S. coelicolor*, c-di-AMP can down regulate the expression

of cell wall hydrolase RpfA (Resuscitation Promoting Factor A) (Commichau et al., 2015). In an *S. aureus* lipoteichoic acid (LTA)-deficient strain, increased cellular c-di-AMP levels upregulated the amount of highly cross-linked peptidoglycan in the cell wall, which suggested that increased c-di-AMP levels may help strengthen the cell wall to protect bacteria against cell wall stress (Corrigan et al., 2011).

1.2.3.5. c-di-AMP regulates biofilm formation.

Several groups have reported that c-di-AMP can regulate biofilm formation (Gundlach et al., 2016; Peng et al., 2016). However, by knocking out different genes in different organisms led to varying biofilm phenotypes. A comparison of these studies is complicated by the observation that the different groups used different methods to test biofilm formation. In the experience of our research group the type of biofilm assay employed can often lead to substantially different conclusions about the ability to form biofilms.

For instance, Peng *et al.* knocked out a DHH/DHHA1 c-di-AMP phosphodiesterase protein PdeA in *Streptococcus mutans*, and measured biofilm formation by a crystal violet assay (Peng et al., 2016). Peng *et al.* found that increased c-di-AMP promotes biofilm formation by upregulating the expression of glucan synthase GtfB (Peng et al., 2016). However, when Gundlach *et al.* knocked out c-di-AMP phosphodiesterases GdpP and PgpH in *Bacillus subtilis*, and tested biofilm formation by complex colony formation assays their results showed that upregulating c-di-AMP levels could activate transcription factor SinR to inhibit *B.*

subtilis biofilm formation (Gundlach et al., 2016). These observations suggest that c-di-AMP may play different or more complex roles in different organisms in response to different stimuli.

1.2.4. c-di-AMP is involved in antibiotic resistance.

Increased intracellular c-di-AMP levels in bacteria have also been associated with increased tolerance to some antibiotics, including lysostaphin, oxacillin and penicillin G (Corrigan et al., 2011; Luo and Helmann, 2012; Smith et al., 2012). As mentioned above, c-di-AMP accumulation can upregulate highly cross-linked peptidoglycan to strengthen the cell wall (Corrigan et al., 2011). One of the reasons that increased c-di-AMP levels can protect bacteria from antibiotics targeting cell wall and cell membrane is that c-di-AMP regulates some aspects of cell wall biosynthesis and structure.

1.3. c-di-AMP is a putative second messenger in enterococci.

Although c-di-AMP has been identified in several Gram-positive bacteria, the cyclic dinucleotide signaling pathway and its potential role in signal transduction had not been characterized in the important clinical pathogen enterococci.

1.3.1. Multidrug-resistant enterococci are rising.

Enterococci are facultative anaerobic Gram-positive bacteria and are the cause of multiple human infections including endocarditis, bacteremia, nervous

system infections and urinary tract infections (Arias et al., 2011; Byappanahalli et al., 2012; Wang et al., 2014). Since enterococci can acquire antibiotic resistant cassette from other Gram-positive pathogens by conjugation and can accumulate mutations for novel antibiotics resistance, multidrug-resistant (MDR) enterococci emerged rapidly in decades (HICPAC, 1995; Rice et al., 1995).

Among MDR enterococcus, vancomycin-resistant enterococci (VRE) is a serious public health threat that is resistant to almost all antibiotics clinically available (Arias and Murray, 2012). VRE infections usually affect critically ill and immunocompromised patients with increased prevalence in healthcare-associated infections (9,820 in 2000 to 20,000 in 2013 in the United States) and cause 1,300 deaths in the United States each year (CDC, 2013). The cyclic lipopeptide daptomycin (DAP) is frequently used as a drug of last resort against recalcitrant VRE infections (Arias and Murray, 2012).

1.3.2. Daptomycin is an efficacious antibiotic to treat vancomycin-resistant enterococci.

Daptomycin (DAP) is a cyclic lipopeptide antibiotic produced by *Streptomyces roseosporus* during fermentation (Figure 1.3) (Arias et al., 2011). DAP is an efficacious antibiotic not only for VRE but also for other MDR pathogens such as methicillin-resistant *S. aureus* (MRSA) (Purrello et al., 2016).
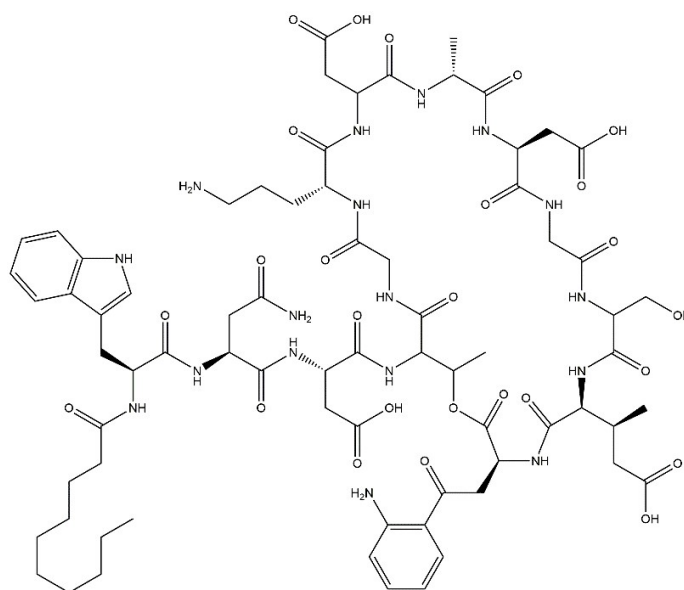
Figure 1.3 Structure of daptomycin. *Figure is produced by Chemdraw Professional.*

Several studies have been performed for the mechanism of DAP action (Jung et al., 2004; Müller et al., 2016; Robbel and Marahiel, 2010). The antibacterial activity of DAP depends highly on the concentration of Ca^{2+} (Hodinka et al., 1987; Jung et al., 2004). Ca^{2+} can induce DAP monomers to form micelles to approach cell membranes (Jung et al., 2004). DAP micelles than disassociate, and DAP inserts into the cell membrane in a phosphatidylglycerol-dependent manner (Jung et al., 2004). The insertion can interrupt cell wall synthesis and cause cation leakage, which results in cell death (Jung et al., 2004; Müller et al., 2016; Pogliano et al., 2012).

1.3.3. Mutations identified in DAP-resistant VRE showed a potential relationship between the LiaFSR cell membrane stress signaling pathway and c-di-AMP levels.

Although DAP is effective against VRE, widespread clinical applications of DAP select for DAP resistance (Arias et al., 2011). In a previous study, Miller *et al.* used quantitative experimental evolution of a polymorphic population of *Enterococcus faecalis* S613 (hereafter referred to as: *Efc* S613) to identify common evolutionary trajectories leading to DAP resistance (Miller et al., 2013). All the initial mutations associated with resistance appeared directly within the *liaFSR* pathway including *liaF* and *liaR* (Miller et al., 2013; Palmer et al., 2011). LiaFSR is a three-component membrane stress response regulon (Figure 1.4) (Wolf et al., 2010) that includes a transmembrane histidine kinase (LiaS) that is predicted to activate its cognate response regulator (LiaR) by phosphorylation in response to cell envelope stress (Schrecke et al., 2013). Upon activation, LiaR regulates downstream genes by binding DNA in a sequence specific manner including the *liaFSR* and *liaXYZ* operons (Davlieva et al., 2015a; Miller et al., 2013; Schrecke et al., 2013). Studies in *B. subtilis* have suggested that LiaF is an inhibitor of LiaS that attenuates signal response (Schrecke et al., 2013; Wolf et al., 2010).
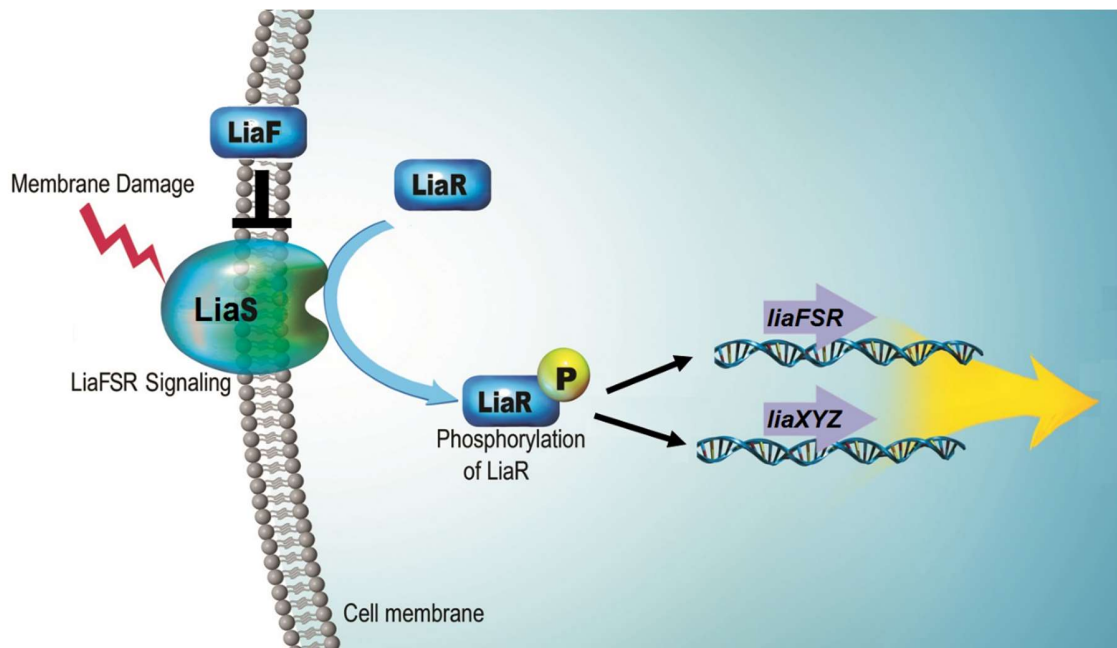
Figure 1.4 LiaFSR pathway in enterococci. *Cell envelope stress can active LiaS. LiaS then activates LiaR by phosphorylation, which leads to LiaR dimerization. LiaR dimers can regulate downstream gene expressions. LiaF can inhibit LiaS activity.* (Davlieva et al., 2015b; Miller et al., 2013; Schrecke et al., 2013; Wolf et al., 2010)

After an initial set of mutations within the LiaFSR pathway, a second group of genes showed clear indications of being important to adaptation to DAP and included *cls* (encoding a cardiolipin synthase) and *gdpP*.

In addition to *gdpP*, I was able to identify potential homologs to a c-di-AMP synthase A (CdaA) and another cyclic-dinucleotide phosphodiesterase PgpH in the *E. faecalis* genome (ADDP01000030.1) (Huynh et al., 2015; Mehne et al., 2013). Thus, I postulated that if *yybT* was indeed a *gdpP* homolog, the c-di-AMP signaling pathway

may be important in enterococci and may influence different processes including the adaptive response to antimicrobial peptides like DAP. Interestingly, DAP-resistant strains containing $gdpP^{I440S}$ were found in association with mutations in the LiaFSR system such as $liaR^{D191N}$, suggesting a potential epistatic link to the LiaFSR regulon (Miller et al., 2013). Although $gdpP^{I440S}$ has not been observed in clinical isolates, the possibility that it was a phosphodiesterase provided the first indication that there might be a relationship between the LiaFSR pathway, cyclic dinucleotide signaling and DAP resistance.

1.4. Goals of this project

It is challenging to develop effective clinical therapies against enterococci since they rapidly accumulate mutations to acquire resistance against most antibiotics (Arias et al., 2011). Our ability to develop new antibiotics or new therapeutic approaches to infections by enterococci would greatly benefit from a better understanding of how they respond to antibiotic stress. Based upon the earlier work of Miller et al., that c-di-AMP signaling was not only present in enterococci but was important to their stress response including those related to the membrane damage response pathway LiaFSR (Miller et al., 2013).

In this study, I show for the first time that c-di-AMP is a second messenger in enterococci. Using *in vitro* enzymatic activity assays, I show that *E. faecalis* GdpP (*Efc* GdpP) is a *bone fide* c-di-AMP specific phosphodiesterase. The GdpP^{I440S} substitution identified during selection to DAP has reduced activity both *in vitro* and *in vivo* and

leads to accumulation of c-di-AMP. I also show my structural studies of *Efc* GdpP and *E. faecium* GdpP (*Efm* GdpP). As there is no structure of full-length GdpP protein, GdpP protein structure solved by crystallography will reveal the putative substrate and inhibitor binding sites and how the five domains in GdpP regulate each other. Additionally, I provide data that link the LiaFSR and LiaXYZ pathways and changes in c-di-AMP levels. I show that a putative c-di-AMP phosphodiesterase XpaC is under direct LiaR regulation. Taken together, my data suggest that the membrane stress response of enterococci via GdpP or LiaFSR signaling, affects c-di-AMP levels. The changes in c-di-AMP may have important physiological implications for the adaptive response to antibiotics in enterococci. Results obtained from this project improve our understanding of ways the mutations in the genome help enterococci resist DAP. It also provides new possible targets for antibacterial therapies of DAP-resistant Gram-positive pathogens.

Chapter 2

Materials and Methods

2.1. Enterococci strains and growth media

Enterococci strains used in this study are listed in Table 2.1. *E. faecalis* (*Efc*) OG1RF harboring pMSP3535 and recombinant plasmids were grown in brain heart infusion (BHI) supplied with 10 µg/ml erythromycin and nisin as described in (Bryan et al., 2000). Other *Efc* strains were grown in LBHI broth (80% lysogeny broth (LB) and 20% brain heart infusion (BHI)) as described in (Miller et al., 2013). *E. faecium* (*Efm*) HOU503 was grown in LBHI. Other *E. faecium* strains were grown in BHI. When DAP was added, 50 mg/L $CaCl_2$ was supplied to the medium (Miller et al., 2013).

Table 2.1 Summary of enterococci strains used in this study.

Strains	Genotype or description	Reference or source
E. faecalis strains		
S613	Wild type clinical VRE[a] strain	(Arias et al., 2011; Reyes et al., 2015)
OG1RF	Wild type laboratory vancomycin-susceptible strain	(Arias et al., 2011; Reyes et al., 2015)
R712	Clinical daptomycin-resistant strain derived from S613. *lia*F$^{\Delta I177}$ *cls*$^{\Delta K61}$ *gdpD*$^{\Delta I170}$	(Arias et al., 2011; Reyes et al., 2015)
TDR7	Experimental daptomycin-resistant strain derived from S813. *liaX*^{V289fs} *cls*^{R217Q}	(Miller et al., 2013)
S613_D17C9[b]	*lia*F$^{\Delta I177}$, *prg*U^{G105G}, EFE19809.1/19808.1 intergenic 34bp deletion	This study
S613_D18A10[b]	*liaF*$^{\Delta I177}$, *xpaC*$^{1-163fs}$, *dacA*^{E554K}, *prgU*^{N103N}, EFE19809.1/19808.1 34bp intergenic deletion, G$\rightarrow$T in EFE19513.1/ EFE19514.1 intergenic region	This study
OG1RF_Δ*liaR*	Δ*liaR*	(Reyes et al., 2015)
OG1RF_Δ*liaR*::*liaR*	OG1RF_Δ*liaR* with *liaR* complementation *in cis*	(Reyes et al., 2015)
OG1RF_*liaX*$^{1-289}$	OG1RF with a stop codon inserted after LiaX residue 289	Arias Lab
OG1RF_Δ*liaX*	Δ*liaX*	Arias Lab
OG1RF_Δ*liaY*	Δ*liaY*	Arias Lab
OG1RF_Δ*liaZ*	Δ*liaZ*	Arias Lab
OG1RF_Δ*liaYZ*	Δ*liaYZ*	Arias Lab
OG1RF:: pMSP3535::*gdpP*	pMSP3535::*gdpP-Efc*	This study
OG1RF:: pMSP3535::*gdpP*^{I440S}	pMSP3535::*gdpP*^{I440S}-*Efc*	This study
OG1RF:: pMSP3535	pMSP3535	This study
E. faecium strains		
HOU503	Clinical daptomycin-tolerant VRE strain with *liaR*^{W37C} and *liaS*^{T120A}.	(Panesso et al., 2015)
HOU503F	HOU503 fusidic acid-resistant derivative	(Panesso et al., 2015)

HOU503F_ΔliaR	ΔliaR	(Panesso et al., 2015)
HOU503F_ΔliaR::liaR	HOU503F_ΔliaR with liaR complementation in cis	(Panesso et al., 2015)
R497F	Fusidic acid-resistant derivative of the clinical daptomycin-resistant vancomycin-susceptible E. faecium strain R497 with liaR^{W37C}, liaS^{T120A}, and cls^{ins110}	(Panesso et al., 2015)
R497F_ΔliaR	ΔliaR	(Panesso et al., 2015)
R497F_ΔliaR::liaR	F497F_ΔliaR with liaR complementation in cis	(Panesso et al., 2015)

[a]VRE: vancomycin-resistant enterococci.

[b]Please see Table 4.1 for details of *Efc* S613_D17C9 and *Efc* S613_D18A10.

2.2. Measurement of intracellular c-di-AMP by competitive ELISA

A c-di-AMP competitive enzyme-linked immunosorbent assay (ELISA) protocols were optimized from *Underwood et al., 2014* (Underwood et al., 2014) to measure the intracellular c-di-AMP concentrations in *Efc* and *Efm*.

To prepare samples for c-di-AMP measurement, enterococcus cells were grown to late exponential phase ($OD_{600} \sim 1.0$ for *E. faecalis*, and $OD_{600} \sim 1.2$ for *E. faecium*). Cell pellets from 45 mL or 90 mL cultures were washed by 5 mL PBS 3 times, and re-suspended in 0.5 mL 50 mM Tris-HCl pH 8.0. Cells were opened by sonication on ice for 1 min total time (10 s on and 3 min off at output 6/50% duty cycle in every cycle). Samples were boiled at 95°C for 5 min. Supernatants were

collected after centrifugation at 12,000g for 15 min. Samples were used immediately for the following steps.

Streptococcus pneumoniae CabP (*Spn* CabP) was purified as described *Bai et al., 2014* (Bai et al., 2014). Nunc MaxiSorp Immuno 96-well microplate (Fisher Scientific) was coated with 100 μL/well coating buffer containing 200 μg/mL *Spn* CabP at 4°C for 17-18 hr. Plates were washed by PBST (PBS with 0.05% (v/v) Tween 20) three times, and then blocked by the addition 100 μL/well 1% (w/v) bovine serum albumin (BSA) in PBS for 1 h at room temperature. Plates were washed again with PBST three times. 2'-[Biotin]-AHC-c-diAMP (Biolog B106) was added to samples to 25 nM final concentration. 100 μL of each sample was added to the plate, and incubated at room temperature for 3 h. The plate was washed by PBST three times. HRP-Conjugated Streptavidin (ThermoFisher) was diluted 1:10,000 in PBS, and 100 μL was added to each well. The plate was incubated in the dark at room temperature for 1.5 h, and was washed with PBST three times. 100 μL/well substrate buffer (as described in (Underwood et al., 2014)) was then added to the plate. The plate was incubated in the dark for 1h, and 2 M H_2SO_4 was added to stop the reaction. The absorbance at 492 nm was measured by plate reader (BioRad). The absorbance at 630 nm was used as baseline absorbance. Coating buffer and substrate buffer was prepared as described by Underwood et al. (Underwood et al., 2014). A H_2O_2 final concentration of 0.2% was used in the substrate buffer.

2.3. Plasmid construction for protein overexpression

The *Efc gdpP* and subdomains were amplified by PCR from *Efc* S613 using specific primers (Table 2.2) with PfuUltraII DNA Polymerase. Mutations Y212A, D419A, I440S, D499A in E*fc* GdpP were generated by site directed mutagenesis (Table 2.2). The *Efm gdpP* and subdomains were amplified from *Efm* R494 by PCR using specific primer listed in Table 2.3. The *xpaC* genes were amplified from *Efc* S613, *Efm* HOU503 and MRSA 131 by PCR using specific primers listed in Table 2.4.

PCR products were digested by appropriate restriction endonucleases and cloned into pET-28a (Novagen) for expression in *E. coli* BL21, or into pMSP3535 (Bryan et al., 2000) for expression in *Efc* OG1RF.

Table 2.2 Primers used in this study for molecular cloning of *Efc gdpP*.

Primer	Sequence
Efc GdpP with N-His tag forward primer for pET-28a	TTCTCCCATGGATGCATCATCATCACCATCACGAAAACTTGTATTTCCAGGGGATGCAAAAGAAGAGAATTCAA
Efc GdpP with N-His tag reverse primer for pET-28a	TTCTCAAGCTTTCACTCCTGTTCATACATTTC
Efc GdpP with C-His tag forward primer for pET-28a	TTCTCCCATGGATGCAAAAGAAGAGAATTCAA
Efc GdpP with C-His tag reverse primer for pET-28a	TTCTCAAGCTTTCAATGGTGATGATGATGATGTTCGTTCAAATAGAACTGCCCCTCCTGTTCATACATTTC
Efc GdpP$_{167-300}$ with N-His tag forward primer	TTCTCCCATGGATGCATCATCATCACCATCACGAAAACTTGTATTTCCAGGGGAAAGTCGAAATGCAAACGGCTATT
Efc GdpP$_{167-300}$ with N-His tag reverse primer	TTCTCAAGCTTTCAATCTTTGGCTTCTTTTAC
Efc GdpP$_{82-159}$ with N-His tag forward primer	TTCTCCCATGGATGCATCATCATCACCATCACGAAAACTTGTATTTCCAGGGGGGTACCTGTGGGAATTATTACG
Efc GdpP$_{82-159}$ with N-His tag reverse primer	TTCTCAAGCTTTCATTTAGTGATATCTTCAAAAGT
Efc GdpP$_{332-658}$ with N-His tag forward primer	TTCTCCCATGGATGCATCATCATCACCATCACGAAAACTTGTATTTCCAGGGGATTATTGCGGAATCTGCTGAC
Efc GdpP$_{56-658}$ with N-His tag forward primer	TTCTCCCATGGATGCATCATCATCACCATCACGAAAACTTGTATTTCCAGGGGGTAGAAATTACAAACGTAGAA
Efc GdpP$_{309-658}$ forward primer for pET-28a	TTCTCCCATGGATGCATCATCATCACCATCACGAAAACTTGTATTTCCAGGGGATGCAAAAGAAGAGAATTCAA
Efc GdpP forward primer for pMSP3535	TTCTCACTAGTATTGGAGGCAAAAAAATGCATCATCATCACCATCACGAAAACTTGTATTTCCAGGGACAAAAGAAGAGAATTCAAAAAAACG

Efc GdpP reverse primer for pMSP3535	TTCTCCTCGAGTCACTCCTGTTCATACATTTCATT
GST-GdpP forward primer	TTCTTGGATCCATGCAAAAGAAGAGAATC
GST-GdpP reverse primer	TTCTTCTCGAGTCACTCCTGTTCATACATT
Efc GdpP Y212A mutagenesis forward primer	GGATGGACCAAGCCAAAGTTTTTTA
Efc GdpP Y212A mutagenesis reverse primer	TAAAAAACTTTGGCTTGGTCCATCC
Efc GdpP D419A mutagenesis forward primer	GTAGCTTACCATAAACCGTCTCTAT
Efc GdpP D419A mutagenesis reverse primer	ATAGAGACGGTTTATGGTAAGCTAC
Efc GdpP I440S mutagenesis forward primer	AAGTGGTAAGCATTGATCACCATCG
Efc GdpP I440S mutagenesis reverse primer	CGATGGTGATCAATGCTTACCACTT
Efc GdpP D499A mutagenesis forward primer	GAATTGTGGTTGCTACGAAAAGTTT
Efc GdpP D499A mutagenesis reverse primer	AAACTTTTCGTAGCAACCACAATTC

Table 2.3 Primers used in this study for molecular cloning of *Efm gdpP*.

Primer	Sequence
Efm GdpP with N-His tag forward primer for pET-28a	TTCTCCCATGGATGCATCATCATCACCATCACGAAA ACTTGTATTTCCAGGGGGGAAAATAAAAACAATCAT TTATCC
Efm GdpP with N-His tag reverse primer for pET-28a	TTCTCGAATTCTTACTCCTTATC ATATATTTG
Efm GdpP$_{338-657}$ with N-His tag forward primer for pET-28a	TTCTCCCATGGATGCATCATCATCACCATCACGAAA ACTTGTATTTCCAGGGGGGTGTTTATCAT GGGGCACAAG
Efm GdpP$_{137-298}$ with N-His tag forward primer for pET-28a	TTCTCCCATGGATGCATCATCATCACCATCACGAAA ACTTGTATTTCCAGGGGGGATAAAACATTTCAGTTT GATATG
Efm GdpP$_{137-298}$ with N-His tag reverse primer for pET-28a	TTCTCGAATTCTTATTTTACCTCTTTCACGACAAC
Efm GdpP$_{83-657}$ with N-His tag reverse primer for pET-28a	TTCTCCCATGGATGCATCATCATCACCATCACGAAA ACTTGTATTTCCAGGGGGCCTGTAGGAGTGATTGC
Efm GdpP$_{338-500}$ with N-His tag reverse primer for pET-28a	TTCTCGAATTCTTAATTTGTATCTACAACCATCCCTG C
Efm GdpP$_{83-167}$ with N-His tag reverse primer for pET-28a	TTCTCGAATTCTTAGTTAAAACTCCATCAGACG

Table 2.4 Primers used in this study for molecular cloning of *xpaC*.

Primer	Sequence
Efc S613 & TX1467 XpaC with N-terminal His-tag forward primer for pET-28a	TTCTCGAATTCATGCATCATCATCACCATCACAACA AATTAAATACAAAA
Efc S613 & TX1467 XpaC no-tag reverse primer for pET-28a	TTCTCAAGCTTTTATTGCTGGTCTTCGTTTAC
Efc S613 & TX1467 XpaC forward primer for pET-28a N-terminal His-tag	TTCTCGAATTCAACAAATTAAATACAAAATTAC
Efc S613 & TX1467 XpaC with C-terminal His-tag forward primer for pET-28a	TTCTCCCATGGATGAACAAATTAAATACAAAATTAC TG
Efc S613 & TX1467 XpaC with C-terminal His-tag reverse primer for pET-28a	TTCTCAAGCTTTTAGTGATGGTGATGATGATGTTG CTGGTCTTCGTTTACTTGAGG
Efc S613 XpaC^{K163fs} with C-terminal His-tag reverse primer for pET-28a	TTCTCAAGCTTCTAGTGATGGTGATGATGATGATTT TTCATACGTTTGTTTTTTAC
Efc S613 XpaC no-tag forward primer for pMSP3535	TTCTCACTAGTATAGGAGGAACTATATAAATGAAC AAATTAAATACAAAATTACTG
Efc S613 XpaC unremovable N-terminal His-tag forward primer for pMSP3535	TTCTCACTAGTATAGGAGGAACTATATAAATGCAT CATCATCACCATCACAACAAATTAAATACAAAATTA CTG
Efc S613 XpaC removable N-terminal His-tag forward primer for pMSP3535	TCTCACTAGTATAGGAGGAACTATATAAATGCATC ATCATCACCATCACGAAAACTTGTATTTCCAGGGA AACAAATTAAATACAAAATTACTG
Efc S613 XpaC no-tag reverse primer for pMSP3535	TTCTCCTCGAGTTATTGCTGGTCTTCGTTTACTTG
Efc S613 XpaC unremovable C-terminal His-tag reverse primer for pMSP3535	TTCTCCTCGAGTTAGTGATGGTGATGATGATGTTG CTGGTCTTCGTTTACTTG
Efc S613 XpaC removable C-terminal His-tag reverse primer for	TTCTCCTCGAGTTAGTGATGGTGATGATGATGTCC CTGGAAATACAAGTTTTCTTGCTGGTCTTCGTTTAC

pMSP3535	TTG
Efc S613 XpaC[1-163] no-tag reverse primer for pMSP3535	TTCTCCTCGAGCTAATTTTTCATACGTTTGTTTTTTAC
Efc S613 XpaC[1-163] unremovable C-terminal His-tag reverse primer for pMSP3535	TTCTCCTCGAGTTAGTGATGGTGATGATGATGATTTTTCATACGTTTGTTTTTTAC
Efc S613 XpaC[1-163] removable C-terminal His-tag reverse primer for pMSP3535	TTCTCCTCGAGTTAGTGATGGTGATGATGATGTCCCTGGAAATACAAGTTTTCATTTTTCATACGTTTGTTTTTTAC
Efm HOU503 XpaC with removable N-terminal His-tag forward primer for pET-28a	TTCTCCCATGGATGCATCATCATCACCATCACGAAAACTTGTATTTCCAGGGGATAAAACGAAATTGGCCGTGGC
Efm HOU503 XpaC no-tag reverse primer for pET-28a	TTCTCGAATTCTTAATCCTTTTGTTCTGGTTC
Efm HOU503 XpaC no-tag forward primer for pET-28a	TTCTCCCATGGATGATAAAACGAAATTGGCCGTGGC
Efm HOU503 XpaC with C-terminal His-tag reverse primer for pET-28a	TTCTCGAATTCTTAGTGATGGTGATGATGATGATCCTTTTGTTCTGGTTCATA
MRSA 131 XpaC with removable N-terminal His-tag forward primer for pET-28a	TTCTCCCATGGATGCATCATCATCACCATCACGAAAACTTGTATTTCCAGGGGACAGTGAGATATAATATTTCTCA
MRSA 131 XpaC no-tag reverse primer for pET-28a	TTCTCAAGCTTTCAATCTTGATGATGTTTTTGATGTAAC
MRSA 131 XpaC no-tag forward primer for pET-28a	TTCTCCCATGGATGACAGTGAGATATAATATTTCTC
MRSA 131 XpaC with unremovable C-terminal His-tag reverse primer for pET-28a	TTCTCAAGCTTTCAGTGATGGTGATGATGATGATCTTGATGATGTTTTTGATGTAAC
MRSA 131 XpaC with unremovable N-terminal His-tag forward primer for pET-28a	TTCTCCCATGGATGCATCATCATCACCATCACACAGTGAGATATAATATTTCTCA

2.4. Expression and purification of *E. faecalis* GdpP

Overnight cultures of *E. coli* BL21 carrying the *Efc* GdpP expression vector pET28a-*Efc*_GdpP was diluted 1:100 in 8L 2xYT medium supplemented with 50 mg/L kanamycin. To express protein for crystallization, additional 5 μM heme (Sigma) was added to the cultures. Cultures were shaken at 37°C until the OD_{600} reached 0.6~0.7. 0.5 mM IPTG was then added to induce protein expression. Cultures were shaken at 16°C for 20 h before being harvested by centrifugation. Cells were resuspended by a Ni-NTA buffer A (50 mM Tris pH 7.4, 20 mM Imidazole, 500 mM NaCl, 10 mM   -mercaptoethanol, 0.2 mM PMSF, 5% Glycerol (v/v)), and opened by sonication on ice with 3 cycles of 2 min on and 3 min off at output 6/50% duty cycle. Supernatants were collected by centrifugation at 24,000 rpm for 1 h at 4°C. The protein was purified initially with a gravity Ni-NTA column, and was step eluted by Ni-NTA buffer B (50 mM Tris pH 7.4, 200 mM Imidazole, 440 mM NaCl, 9 mM β-mercaptoethanol, 0.2 mM PMSF, 5% Glycerol (v/v)). The fractions containing target protein were collected and dialyzed overnight at 4°C against gel filtration buffer (25 mM CHES pH 8.6, 200 mM NaCl). Protein was subsequently concentrated and further purified on a HiLoad 16/60 Superdex 200 gel filtration column. Fractions containing target protein were collected. Fresh protein should be used for the following experiments as storage at -80°C reduces activity.

2.5. Product analysis of GdpP reactions by HPLC

For ATPase activity, 10 μM protein and 100 μM ATP was incubated at 28°C for 2 h in a reaction buffer containing 40 mM Tris pH 7.5 and 10 mM $MgCl_2$. For phosphodiesterase activity, 10 μM protein was incubated with 100 μM c-di-AMP or c-di-GMP at 28°C for 2 h in a reaction buffer containing 100 mM Tris pH 8.3, 20 mM KCl, and 0.5 mM $MnCl_2$. 1mM ppGpp was added to the reaction buffer in experiments to estimate ppGpp inhibition of GdpP phosphodiesterase activity. Reactions were stopped and protein precipitated by addition of trifluoroacetic acid (TFA) to 1% (v/v) final concentration and incubated on ice for 15 min. Precipitants were removed by centrifugation. A total of 10 μL nucleotide standards or samples were injected into RP C-18 column (Hamilton #79674), and eluted with a gradient of 0 to 100% (Buffer A: 0.1M KH2PO4, 4 mM tetrabutylammonium bromide, pH 6.0. Buffer B: 60% Buffer A, 40% methanol, pH 5.5.).

2.6. Kinetics Measurement of the phosphodiesterase activity

The protocols were optimized from the coralyne fluorescence turn-on assay described in (Zhou et al., 2014) to measure the phosphodiesterase kinetics of *Efc* GdpP$_{309-658}$. 2.5 μM *Efc* GdpP$_{309-658}$ was incubated with 0-1750 μM c-di-AMP (Biolog) at 37 °C in thermal cycler. The reaction buffer contains 50mM CHES pH9.2, 20mM KCl, 0.5 mM $MnCl_2$, and 1 mM fluorinated octyl maltoside (Anatrace). The reactions were stopped after incubated for 0, 2 min, 4 min, and 6 min by heated up to 95 °C for

3 min. Precipitated proteins were removed by 96-well filter plate (EconoSpin). c-di-AMP concentrations were measured by mixed with coralyne buffer to a final condition contained 100 mM coralyne (Sigma), 50 mM CHES pH9.2, and 3 mM KI. Fluorescence intensities (ex. 420 nm, em. 475 nm) were measured by plate reader (BioRad).

2.7. Expression *Efc* GdpP and *Efc* GdpP[I440S] in *E. faecalis* OG1RF

The *Efc* OG1RF strains with recombinant plasmids were grown in BHI with 10 μg/ml erythromycin. The overnight cultures of *Efc* OG1RF with recombinant plasmids were diluted 1:100 to BHI with 10 μg/ml erythromycin on the second day, and 20 ng/ml nisin was added when the OD_{600} was ~0.5. Cultures were incubated at 37°C shaken at 225 rpm overnight. On the third day, the overnight cultures were then re-diluted into BHI with 10 μg/ml erythromycin, 20 ng/ml nisin. Cells were harvested after their OD_{600} reaching 1.5 (late exponential phase of *Efc* OG1RF strains with pMSP3535 plasmids) for c-di-AMP measurements.

2.8. Kinetics measurement of the ATPase activity

The steady-state kinetic parameters were determined using EnzChek® Phosphate Assay Kit (Life Technologies) by measuring the release of inorganic phosphate (Pi) hydrolyzed from ATP. The reactions were set up in 96-well plate, and were monitored by Bio-Rad plate reader.

2.9. Structural modeling

The structural model of *Efc* GdpP DHH-DHHA1 domain was built using Phyre2 server. The Mn^{+2} ions positions were predicted by alignment to *Mycobacterium tuberculosis* phosphodiesterase Rv2837c (Protein Data Bank entry 5CET) (He et al., 2015).

2.10. Expression and Purification of *Efc* GST-GdpP

Overnight cultures of *E. coli* BL21 with recombinant plasmid pET28a-*Efc*_GST-GdpP was diluted 1:100 in 8L 2xYT with 100 mg/L ampicillin. 0.5 mM IPTG was added when the culture reached an OD600 of ~0.7-0.8. Culture was shaken at 16°C for 20 h before harvesting by centrifugation.

Cells were resuspended in Lysis Buffer A (50mM Tris pH8.0, 150 mM NaCl, 5% Glycerol (v/v)). Cells were opened by sonication. Supernatant was collected after centrifugation at 24,000 rpm for 1 h at 4°C. The protein was purified with 5ml glutathione agarose (Thermo scientific #16100), and eluted by an Elution Buffer (50mM Tris pH 8.0, 150 mM NaCl, 10 mM reduced glutathione, 5% Glycerol (v/v)). The fractions containing GST-GdpP were collected and dialyzed at 4°C overnight against the Dialysis Buffer (50mM Tris pH8.0, 200mM NaCl). Unfrozen protein was used for the heme reconstitution assay.

2.11. Quantitative PCR

RNA isolation and cDNA synthesis were performed as described in *Miller et al., 2013* (Miller et al., 2013). Quantitative PCR was performed using B-R SYBR® Green SuperMix Kit (Quanta) and real-time thermal cycler (Bio Rad). Primers for qPCR are listed in Table 2.5.

Table 2.5 Primers used in this study for quantitative PCR.

Target gene		Sequence
Primers for *Efc* S613 and *Efc* OG1RF genes		
liaF	Forward primer	ATTGGCGTTTTACTTGTGGC
	Reverse primer	ATCAACATAAACCAAACAGCCG
liaR	Forward primer	AGTGTATCCGGCGATTGAAG
	Reverse primer	TCTTATGCGTCACTTCAGGTTC
liaY	Forward primer	TGATTGGCTAGGAATTGACCC
	Reverse primer	AGAGAATGCCTGGAAATCCTG
liaZ	Forward primer	GGGAAATGAACTTTGGCTTCTC
	Reverse primer	TTTCGATAAATTGTGATCCGTAACG
cdaA	Forward primer	TCAACCAGAAGTGCGAAGAG
	Reverse primer	CCGTTTTGACATGTACTGAATGG
cdaR	Forward primer	AGATGCCAAAGGTCAAGTCC
	Reverse primer	GTGGCGTACCTGTCATACTAAC
gdpP	Forward primer	GAGGCGATTAAAGAGTACCCAG
	Reverse primer	CTTGTGAGATCGATAGAGACGG
xpaC	Forward primer	GCTGTCGCTAGAGAATATGGC
	Reverse primer	CAACTCACGATAATGGGCTTC

relA	Forward primer	GACTTGCTTCGTCAGTTCATC
	Reverse primer	CCAAAAGGGAATCCAGTAGAGG
relQ	Forward primer	CAGGACGTGTGAAACCAGTAG
	Reverse primer	AGTGCGACTACCTGGTAAATG
relA	Forward primer	GACTTGCTTCGTCAGTTCATC
	Reverse primer	CCAAAAGGGAATCCAGTAGAGG
relQ	Forward primer	CAGGACGTGTGAAACCAGTAG
	Reverse primer	AGTGCGACTACCTGGTAAATG
Primers for *Efc* S613 genes		
liaS	Forward primer	CAAGCACAACGAACAGAAACC
	Reverse primer	CTTCTAGACTGATAGGACGCAAG
liaX	Forward primer	TGGTGATGTGTCTATTTCCGC
	Reverse primer	GATATTCCCATTTGCAGAGCTTG
ghd2	Forward primer	AGCCAAGCAAGAACAGAAGC
	Reverse primer	ATTGCGACATTCCCACTACC
pgpH	Forward primer	TGCTGATACTTGTGAGGCTG
	Reverse primer	TCTCTTTCATCGTTAACCCGC
cspA	Forward primer	TGGAAACAGGTACAGTAAAATGG
	Reverse primer	CGTCACCTTGGATAGCTGAG
EFE19808.1	Forward primer	TTTCATTCCCTCGTGGCG
	Reverse primer	AGAACATAAAGACGGTCCAGC
perM	Forward primer	TCACATCGTTCAAGCCACC
	Reverse primer	TTGAGCTTAGTCCCAGTTGC
Primers for *Efc* OG1RF genes		
liaX	Forward primer	CTTCTAGACTGATAGGACGCAAG
	Reverse primer	ACAAGCACAACGAACAGAAAC
liaX	Forward primer	GACCTACTGTTGATTCGTTTGAAG

	Reverse primer	CAATTTCTGCGTTGACTTCGTC
pgpH	Forward primer	GGCCATCTGAAATTCTGTCTTG
	Reverse primer	TCCACAAACACGAGAAGCAG
gdhA	Forward primer	GGTCCAAGTACAGATGTTCCAG
	Reverse primer	GGCTTCCCCAGTATCCTAAAG

Chapter 3

GdpP Modulates c-di-AMP Levels in Enterococci

3.1. Introduction

While c-di-AMP was detected in many Gram-positive bacteria, it had not been studied in enterococci. Since the *Efc* S613 genome (ADDP01000030.1) has potential homologs to c-di-AMP synthase CdaA and phosphodiesterases GdpP and PgpH, a role for c-di-AMP in enterococci seemed reasonable (Huynh et al., 2015; Mehne et al., 2013). Additionally, as the adaptive mutant *Efc gdpP*[I440S] was identified in DAP-resistant *Efc* strains via experimental evolution, *Efc* GdpP was a good candidate to be a critical component of any cellular c-di-AMP signaling pathways (Miller et al., 2013).

In this chapter, I show that c-di-AMP is present in enterococci. Using *in vitro* and *in vivo* assays, I demonstrate that *Efc* GdpP is an c-di-AMP specific

phosphodiesterase and regulates intracellular c-di-AMP levels. I also show that the DAP adaptive mutation I440S strongly diminishes *Efc* GdpP phosphodiesterase activity and upregulates c-di-AMP levels, which suggests c-di-AMP accumulation may protect bacteria from cell wall stress.

3.2. The nucleotide signaling molecule c-di-AMP is present at physiologically relevant levels in enterococci.

As c-di-AMP signaling has not been previously identified in enterococci, it was essential to test whether c-di-AMP was present at levels consistent with being a second messenger *in vivo*.

In order to measure c-di-AMP levels I optimized a c-di-AMP specific competitive enzyme-linked immunosorbent assay (ELISA) for detecting c-di-AMP (Underwood et al., 2014). The assay was initially developed and applied to *E coli* expressing *M. tuberculosis* c-di-AMP synthase DisA and had to be refined for the measurement of c-di-AMP in enterococci (Underwood et al., 2014). I measured c-di-AMP levels in *Efc* S613 and its DAP-resistant derivative *Efc* R712, a vancomycin-resistant strain-pair isolated from the bloodstream of a patient before and after DAP treatment respectively. Additionally, I included a laboratory strain of *E. faecalis* (*Efc* OG1RF) (Table 3.1) (Arias et al., 2011; Bourgogne et al., 2008). Samples were collected at late exponential phase ($OD_{600} \sim 1.0$). As shown in Figure 3.1, *Efc* S613 and *Efc* OG1RF strains produced c-di-AMP. The c-di-AMP level was 113±81

pM/OD$_{600}$, and 112±47 pM/OD$_{600}$ for *Efc* S613 and *Efc* OG1RF, respectively, at late exponential phase. 5In *Efc* R712 (DAP-resistant derivative of *Efc* S613), the c-di-AMP level was 349±104 pM/OD$_{600}$, more than 3-fold higher than *Efc* S613 (Table 3.1 and Figure 3.1).

Table 3.1 Summary of enterococci strains in this study and their measured c-di-AMP concentrations and MICs to daptomycin.

Strains	Genotype or description	Intracellular [c-di-AMP][a] (pM/OD$_{600}$)	DAP MICs[b] (µg/ml)	Reference or source
E. faecalis strains				
S613	Wild type clinical VRE[c] strain	113±81	0.5	(Arias et al., 2011; Reyes et al., 2015)
OG1RF	Wild type laboratory vancomycin-susceptible strain	112±47	2	(Arias et al., 2011; Reyes et al., 2015)
R712	Clinical daptomycin-resistant strain derived from S613. *liaF*$^{\Delta I177}$ *cls*$^{\Delta K61}$ *gdpD*$^{\Delta I170}$	349±104	12	(Arias et al., 2011; Reyes et al., 2015)
TDR7	Experimental daptomycin-resistant strain derived from S813. *liaX*^{V289fs} *cls*^{R217Q}	268±97	12	(Miller et al., 2013)
S613_D17C9[d]	*lia*F$^{\Delta I177}$, *prg*U^{G105G}, EFE19809.1/19808.1 intergenic 34bp deletion	735±118	3	This study
S613_D18A10[d]	*liaF*$^{\Delta I177}$, *xpaC*$^{1-163fs}$, *dacA*^{E554K}, *prgU*^{N103N}, EFE19809.1/19808.1 34bp intergenic deletion, G→T in EFE19513.1/ EFE19514.1 intergenic region	1493±61	3	This study
OG1RF_*liaX*$^{1-289}$	OG1RF with a stop codon inserted after LiaX residue 289	111±7	12	Arias Lab
OG1RF_Δ*liaX*	Δ*liaX*	101±7	12	Arias Lab
OG1RF_Δ*liaY*	Δ*liaY*	26±33	2	Arias Lab

Table continued.

Strains	Genotype or description	Intracellular [c-di-AMP][a] (pM/OD$_{600}$)	DAP MICs[b] (µg/ml)	Reference or source
OG1RF_Δ*liaZ*	Δ*liaZ*	14±7	2	Arias Lab
OG1RF_Δ*liaYZ*	Δ*liaYZ*	64±12	2-3	Arias Lab
OG1RF:: pMSP3535::*gdpP*	pMSP3535::*gdpP-Efc*	115±9	0.5	This study
OG1RF:: pMSP3535::*gdpP*[I440S]	pMSP3535::*gdpP*[I440S]-*Efc*	152±3	0.5	This study
OG1RF:: pMSP3535	pMSP3535	158±3	0.5	This study
E. faecium strains				
HOU503	Clinical daptomycin-tolerant VRE strain with *liaR*[W37C] and *liaS*[T120A].	766±318	3	(Panesso et al., 2015)
HOU503F	HOU503 fusidic acid-resistant derivative	542±133	3	(Panesso et al., 2015)
R497F	Fusidic acid-resistant derivative of the clinical daptomycin-resistant vancomycin-susceptible *E. faecium* strain R497 with *liaR*[W37C], *liaS*[T120A], and *cls*[ins110]	549±150	24	(Panesso et al., 2015)

[a]Errors correspond to standard deviations among three individual measurements.

[b]MIC: Minimum Inhibitory Concentration. The MICs were measured by Etest (bioMérieux) on MH (Mueller Hinton) agar.

[c]VRE: vancomycin-resistant enterococci.
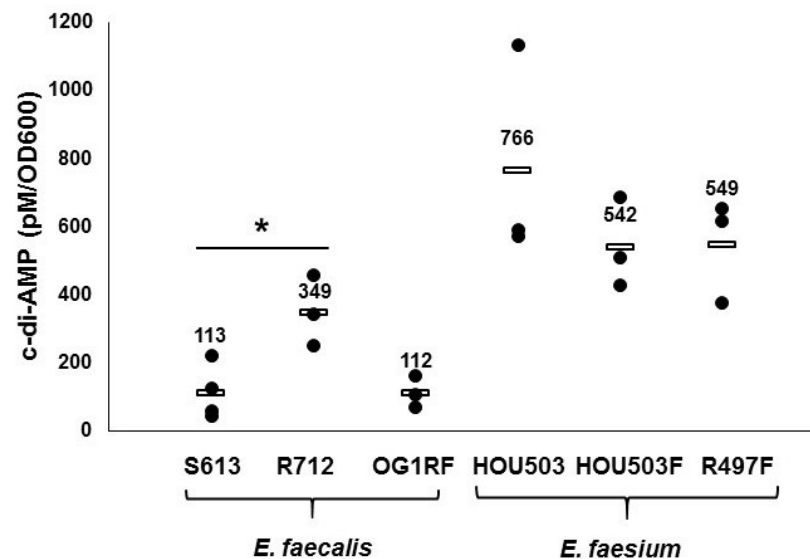
Figure 3.1 c-di-AMP is present in enterococci. *Intracellular c-di-AMP concentrations were measured by an enzyme-linked immunosorbent assay (ELISA)* (Underwood et al., 2014)*. c-di-AMP was detected in both of E. faecalis and E. faecium. Each c-di-AMP measurement was made from at least three independent biological measurements. (See Table 3.1 for strain descriptions.)*

To determine whether c-di-AMP signaling is present in other enterococci strains, a DAP-tolerant and vancomycin-resistant *Efm* clinical isolate HOU503 (referred to as *Efm* HOU503 hereafter) and its fusidic acid-resistant derivative *Efm* HOU503F were tested (Table 3.1) (Panesso et al., 2015). The c-di-AMP level was 766 ± 318 pM/OD_{600} and 542 ± 133 pM/OD_{600} for *Efm* HOU503 and *Efm* HOU503F at late exponential phase ($OD_{600} \sim 1.2$) (Table 3.1 and Figure 3.1) both significantly higher than those of *E. faecalis*. Interestingly, it has been reported that the c-di-AMP level in *S. pneumoniae* is ~ 25 pM/OD_{620} (Bai et al., 2013) and that c-di-AMP is present in cytoplasmic extracts from other Gram-positive bacteria. Using alternative methods to measure c-di-AMP, *B. subtilis* has ~ 1.7 μM/1 L culture (Oppenheimer-Shaanan et al., 2011a) and 3.33 ± 0.44 ng/mg bacterial dry weight in *S. aureus* (Corrigan et al., 2011). While c-di-AMP signaling molecules have been identified in a number of bacteria, the presence of c-di-AMP in *E. faecalis* and *E. faecium* had not been reported before and our results demonstrate that c-di-AMP is present in enterococci at levels to be a *bone fide in vivo* signal.

3.3. *E. faecalis* GdpP has phosphodiesterase activity.

Based on primary sequence homology, I hypothesized that the gene product of unknown function, previously annotated as *Efc* YybT, was a potential cyclic dinucleotide phosphodiesterase of the GdpP family (*Efc* GdpP) (Corrigan et al., 2011; Rao et al., 2010; Witte et al., 2013). *Efc* GdpP is a multi-domain protein containing two putative N-terminal transmembrane helices, a Per-Arnt-Sim (PAS) domain, a

GGDEF domain and a DHH domain with a DHHA1 subdomain (Figure 1.1) (Rao et al., 2010). The PAS domain is a putative signal input module and is frequently involved in signal transduction in orthologous systems (discussed below) (Rao et al., 2011). The GGDEF domain often has diguanylate cyclase activity (discussed below) (Ryjenkov et al., 2005). Thus, based on homology (Figure 3.2), I postulated that the putative DHH/DHHA1 domain of *Efc* GdpP would have cyclic dinucleotide phosphodiesterase activity (Corrigan et al., 2011; Rao et al., 2010; Witte et al., 2013).

```
Enterococcus_EFE19635.1        338 DIYIMGHRYPDMDALGSAFGVARLASFNNRKAWIVLDENEIIPDVKRVLEAIKEYPELEE
Bacillus_WP_003242517.1        339 NVIIMGHKFPDMDSIGAAIGILKVAQANNKDGFIVIDPNQIGSSVQRLIGEIKKYEELWS
Staphylococcus_WP_001081634.1  337 KVIIMGHKRPDIDAIGAAIGVSRFAMMNNLEAYIVLNETDIDPTLRRVMNEIDKKPELRE
Lactococcus_WP_011835587.1     338 DVFIVGHRFTDMDALGAAVAMKAFANMSGKEAFVVYDPEQLDVERAINKYNESSDGFT
Streptococcus_AGQ28355.1       360 NVFIVGHRKLDMDALGSAVGMQFFAGNIIENSFAVYNPDEYSPDIERAIERLQ--ADGKT
Geobacillus_WP_011888454.1     340 KVLIMGHKIPDMDALGAAIGILKVVQSNQKEGFLVVDAMKTDAGAQRLLEEIKKQADIWA
Mycobacterium_pdb_5CET          26 RVGVVCHVHPDADTIGAGLALALVLDGCGKRVEVSFAAPATLPESLRSLPGC-------H
                                        *    * *

Enterococcus_EFE19635.1        398 RIISFKEAMKRKKESSLLVMVDYHKPS-LSISQELYERFDKVVIIDHHRRGDEFPAKPLL
Bacillus_WP_003242517.1        399 RFITPEEAMEISNDDTLLVIVDTHKPS-IVMEERLVNKIEHIVVIDHHRRGEEFIRDPLL
Staphylococcus_WP_001081634.1  397 RFITSDDAWDVMTSKTTVVIVDTHKPE-IVLDENVLNKANRKVVIDHHRRGESFISNPLL
Lactococcus_WP_011835587.1     398 HIVRLETAQKLKKKDSLLIMVDHSKTS-QTLNLDFYKSFEKLVVIDHHRRDDDFPEHALL
Streptococcus_AGQ28355.1       418 RLISVSQAMGIVTPRSLLIMVDHSKIS-ITLSKEFYEQFQNVIVVDHHRRDDDFPDNAIL
Geobacillus_WP_011888454.1     400 RCIKPEQALELITEDTLLIVVDTHRPS-IVIEERLYRADHIVVIDHHRRGEEFIEAPIL
Mycobacterium_pdb_5CET          79 LLVRPE-VM--RRDVDLVVTVDIPSVDRLGALGDLTDSGRELLVIDHHASNDLFGT---A
                                                 ▲                              ▲

Enterococcus_EFE19635.1        457 SYIESSASSASELVTELIEYQSNSANKLQAFEATMMLAGIVVDTKSFNTRTTARTFDVAS
Bacillus_WP_003242517.1        458 VYMEPYASSTAELVTELLEYQPK-RLKINMIEATALLAGIIVDTKSFSLRTGSRTFDAAS
Staphylococcus_WP_001081634.1  456 IYMEPYASSTAELVTELLEYQPT-EQRLTRLESTVMYAGIIVDTRNFTLRTGSRTFDAAS
Lactococcus_WP_011835587.1     457 SYIESSASSASELTVEILQFHDNNQRKMSTIEASIVLAGIELDTKNFIKATTERTFEAAA
Streptococcus_AGQ28355.1       475 TFIESGASSAAELVTELIQFQNA-KKRLNKIQASVLMAGIMLDTKNFSTRVTSRTFDVAS
Geobacillus_WP_011888454.1     459 VYMEPYASSTSELVTELLEYQPK-RVKLSMLEATALLAGIVVDTKSFTLRTGSRTFDAAS
Mycobacterium_pdb_5CET         133 NFIDPSADSTTTMVAEILDAWGK---PIDPRVAHCIYAGLATDTGSFRWA-SVRGYRLAA
                                                                          ▲

Enterococcus_EFE19635.1        517 YLRTCGADSSLVQYLLSSD-LTSYLEMN-NLISKSEYVTKDTVVVAGS--EDKEYDS---
Bacillus_WP_003242517.1        517 YLRAKGADTVLVQKFLKET-VDSYIKRA-KLIQHTVLYKDNIAIASLPENEEEYFDQ---
Staphylococcus_WP_001081634.1  515 YLRAHGADTILTQHFLKDD-VDTYINRS-ELIRTVKVEDNGIAIAHGS--DDKIYHP---
Lactococcus_WP_011835587.1     517 YLRSRGSDNDLIKMIMATD-FEKYKKTN-EIVLNSQIILPGIALGIGL--KEEKYDN---
Streptococcus_AGQ28355.1       534 YLRSKGSDSVEIQNISATD-FEEYKQIN-EIILQGERLGDSIIVAAGE--KNHLYSN---
Geobacillus_WP_011888454.1     518 YLRAQGADTVLVQKLLRES-VANYVKRA-KLIERAAIDEHGIAIAKGD--ENEVHDQ---
Mycobacterium_pdb_5CET         189 RLVEIGVDNATVSRTLMDSHPFTWLPLLSRVLGSAQLVSEAV-GGRGL--VYVVVDNREW

Enterococcus_EFE19635.1        570 -----VTAAKTADTLLSMAGINAAFVITKRTDQQIGISARSNGSINVQIIMENLGGGGHF
Bacillus_WP_003242517.1        572 -----VLIAQCAADSLLSMSEVEASFAVARRDEQTVCISARSLGEVNVQIIMEALEGGGHL
Staphylococcus_WP_001081634.1  568 -----VTVAQCAADSLLSLEGIEASYVARREDNLIGISARSLGSVNVQLTMEALGGGGHL
Lactococcus_WP_011835587.1     570 -----IATAKAADTLLDMAGITAAFTITQHTNGYISISARSRNGFNVQTIMEQMGGGGHF
Streptococcus_AGQ28355.1       587 -----VIASKAADTILSMAHVEASFVIVETASHKIAISARSRSKINVQRVMEKLGGGGHF
Geobacillus_WP_011888454.1     573 -----VLIAQTADTLLTLSGVVASFVISKRGDGTVGISARSLGDVNVQVIMERLGGGGHL
Mycobacterium_pdb_5CET         247 VAARSEEVESIVDIVRTTQQAEVAAVFKEVEPHRWSVSMRAK-TVNLAAVASGFGGGGHR

Enterococcus_EFE19635.1        625 TNAAVQLSNVTVAEVKEQLLDVIRQNINEMYEQ----E
Bacillus_WP_003242517.1        627 TNAATQLSGIVSVSEALERLKHAIDEYFEGGVQ-----R
Staphylococcus_WP_001081634.1  623 TNAATQLKGVTVEEAIAQLQQAITEQLSRSED-----A
Lactococcus_WP_011835587.1     625 NNAATQIYEKNIQEVQDDLIEILKERENE--------K
Streptococcus_AGQ28355.1       642 NLAACQLTDTSLPQAKHLLLKTINMTMKETGEV-E--S
Geobacillus_WP_011888454.1     628 TNAAAQLSDVTVGEAEQQLREAIHDYFEGGKP-----V
Mycobacterium_pdb_5CET         306 LAAGY-TTTGSIDDAVASLRAAIGLTRAPPPPPLRSGC
```

Figure 3.2 Alignment of DHH-DHHA1 domains. *Figure shows the alignment of the DHH-DHHA1 domains of E. faecalis GdpP, Bacillus subtilis GdpP (referred as YybT in* (Rao et al., 2010)*), Staphylococcus aureus GdpP* (Corrigan et al., 2011)*, Lactococcus lactis GdpP (Smith et al., 2012), Streptococcus pyogenes GdpP (Cho and Kang, 2013), Geobacillus thermodenitrificans GdpP (referred as YybT in* (Rao et al., 2011)*), and Mycobacterium tuberculosis phosphodiesterase Rv2837c (He et al., 2015). The*

asterisks highlight the conserved residues for metal ion coordination with the alignment to M. tuberculosis Rv2837c (He et al., 2015). The triangles highlight the mutated residues Ile400, Asp419, and Asp499 in E. faecalis GdpP. Note that I440, the position mutated during adaptation to daptomycin is conserved (Miller et al., 2013).

3.3.1. *Efc* GdpP has c-di-AMP specific phosphodiesterase *in vitro*.

3.3.1.1. HPLC chromatography shows *Efc* GdpP hydrolyzes c-di-AMP to 5'pApA.

To test whether *Efc* GdpP has phosphodiesterase, *Efc* GdpP and the DHH/DHHA1 domain (residues 309-658 referred to as GdpP$_{309\text{-}658}$, Figure 1.1) were characterized *in vitro*. Purified wild type protein was incubated with c-di-AMP or c-di-GMP, and the products were analyzed by reverse phase HPLC. As shown in Figure 3.3A and Figure 3.3B, the incubation of GdpP with c-di-AMP resulted in the decrease of the cyclic dinucleotide peak and the formation of new product corresponding to linear dinucleotide 5'pApA without generating AMP or 3'pApA. This result indicates that *Efc* GdpP hydrolyzes c-di-AMP solely into 5'pApA and is consistent with the activity of *B. subtilis* GdpP measured previously (Rao et al., 2010). I also determined the phosphodiesterase activity of GdpP on c-di-GMP. Based on HPLC analysis, c-di-GMP is not likely to be a physiological substrate of *Efc* GdpP, although it has a weak ability to hydrolyze c-di-GMP to 5'pGpG (Figure 3.3 C, D).
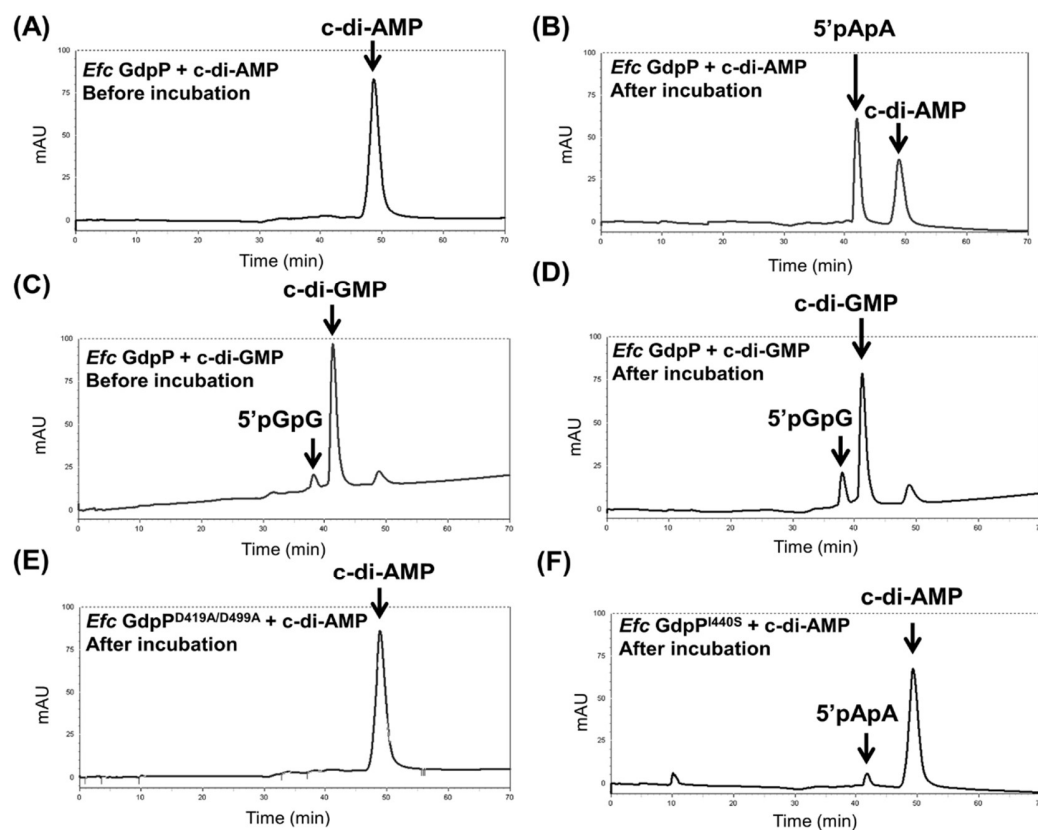
Figure 3.3 *Efc* GdpP has phosphodiesterase activity with specificity for c-di-AMP. *Reverse phase HPLC analysis of products from incubation of wild-type Efc GdpP and variants with cyclic dinucleotides at 28˚C for 2 h with 100 mM Tris pH 8.3, 20mM KCl, and 0.5mM MnCl₂. Wild type Efc GdpP and c-di-AMP: (A) before and (B) after incubation. Wild-type Efc GdpP with c-di-GMP: (C) before and (D) after incubation. (E) Efc GdpP^D419A/D499A after incubation with c-di-AMP. (F) Efc GdpP^I440S after incubation with c-di-AMP.*

3.3.1.2. *Efc* GdpP phosphodiesterase is more active in high pH range.

The pH dependence of *Efc* GdpP activity was measured using reverse phase HPLC. *Efc* GdpP exhibited the highest enzymatic activity at pHs of 9.8 to 10.3 (Figure 3.4). The optimal pH of *Efc* GdpP (9.8-10.1) is much higher than the optimal pH of its homolog *B. subtilis* GdpP, which is between 8.5 and 9.0 (Rao et al, 2010).
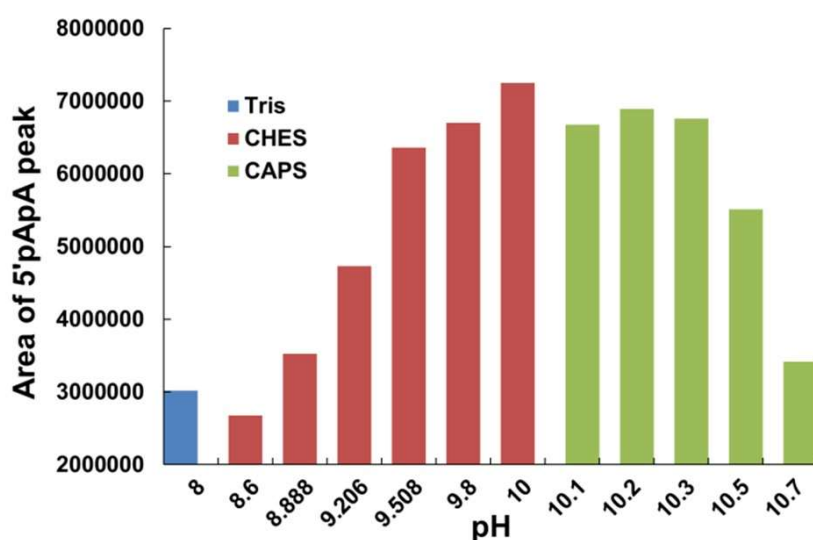
Figure 3.4 pH dependence of *Efc* GdpP. *100mM Tris, 50mM CHES or 50mM CAPS were used to adjust pH. The reaction contained 20 mM KCl, 0.5 mM MnCl₂. 10μM Efc GdpP and 100μM c-di-AMP. Assays were performed at 25℃ for 2 h before products were analyzed by reverse phase HPLC (see Materials and Methods). The area of 5'pApA peaks in the HPLC chromatography is plotted.*

3.3.1.3. Mn^{+2} dependence of *Efc* GdpP phosphodiesterase activity.

Once the specificity for c-di-AMP was established, I quantitated the phosphodiesterase activity using the coralyne fluorescence turn-on assay (Zhou et al., 2014). c-di-AMP, but not 5'pApA, can bind to the fluorescence dye coralyne and enhance its fluorescence emission (Zhou et al., 2014). Halide ions can quench the fluorescence of free coralyne to decrease the noise (Zhou et al., 2014). Since coralyne affected the binding of c-di-AMP to *Efc* GdpP, I could only perform end-point assays to study phosphodiesterase activity. The original coralyne assay protocols published by Zhou *et al.* can only measure accurate c-di-AMP concentrations between 1 μM and 50 μM. By using filter plate (EconoSpin) to remove protein precipitates and trying different c-di-AMP/coralyne incubation conditions, I successfully optimized the protocols (please see Section 2.7 for details). The optimized coralyne assay can be used to accurately measure c-di-AMP concentrations between 1 μM and 2mM.

Since divalent cations, such as Mn^{+2} and Mg^{+2}, can activate *B. subtilis* GdpP phosphodiesterase activity *in vitro* (Rao et al., 2011), the Coralyne assay was first used to study the Mn^{+2} dependence of *Efc* GdpP phosphodiesterase activity. Figure 3.5 shows the optimal concentration of Mn^{+2} is very broad with good activity from 0.01mM to 1mM.
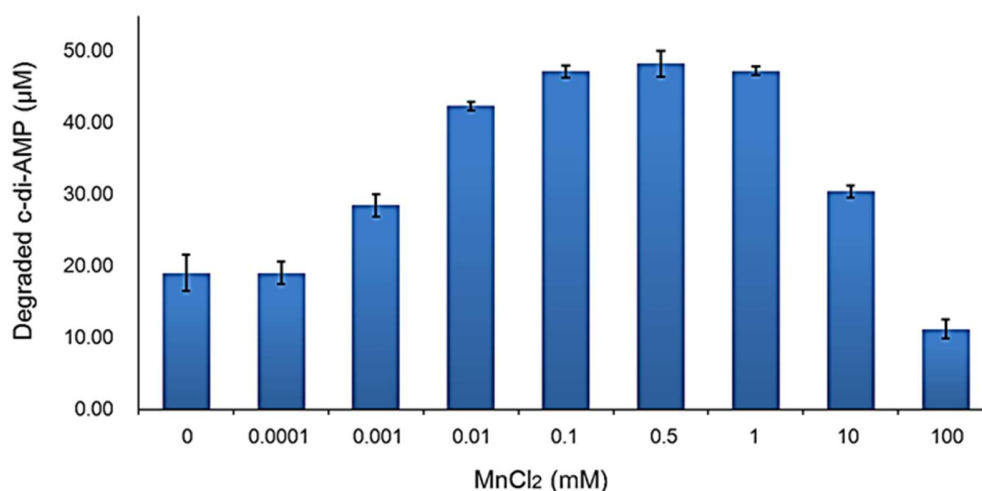
Figure 3.5 Mn^{+2} dependence of *Efc* GdpP phosphodiesterase activity. *5μM Efc GdpP was incubated with 80 μM c-di-AMP at 25℃ for 3 h before analyzed by the coralyne assay (Zhou et al., 2014). The reaction contained 50 mM CHES pH 9.2 and 20mM KCl.*

3.3.1.4. *Efc* GdpP phosphodiesterase kinetics measured by coralyne fluorescence turn-on assay.

I quantitated the phosphodiesterase activity of DHH/DHHA1 domain alone (*Efc* GdpP$_{309-658}$) and the full-length protein using the coralyne activity assay fluorescence turn-on assay (Zhou et al., 2014). Activity for the full-length protein was weak (Figure 3.6A) and saturating conditions of c-di-AMP were not practical to establish, while the activity of *Efc* GdpP$_{309-658}$ was ~13 times higher allowing me to

reach saturating conditions and establish kinetic parameters. The kinetic data for GdpP$_{309-658}$ were clearly multiphasic and could be fit to two phases to produce two K_{m}s extending over the conditions from 0-300 and 300-1750 µM c-di-AMP (Figure 3.6B). The Michaelis-Menten reaction rate constants calculated separately for the two phases produce very similar values of k_{cat} but a 3.3-fold change of K_{m} (K_{m1}= 51.81 ± 8.42 µM, k_{cat1}= 0.048 ± 0.003 s^{-1}, K_{m2}= 224.2 ± 30.26 µM, k_{cat2}= 0.21 ± 0.01 s^{-1}) (Figure 3.6B).

Since *Efc* GdpP$_{309-658}$ was difficult to purify with a strong tendency to aggregate and adsorb non-specifically, protein aggregation might be one reason for the apparent multiphasic kinetics. I screened 99 detergent reagents in different concentrations to help removing protein aggregation. I found that the detergent fluorinated octyl maltoside at 1 mM could reduce aggregation and produced protein that was 2 times more active (K_{m1}= 443.6 ± 97.53 µM, k_{cat1}= 0.42 ± 0.16 s^{-1}, K_{m2}= 132.6 ± 20.05 µM, k_{cat2}= 0.49 ± 0.01 s^{-1}, please see Figure 3.6 D and E for data analysis) (Figure 3.6 D-F). Taken together, the poor behavior of the protein during purification and the importance of fluorinated octyl maltoside to increase activity suggests that the multiphasic kinetics I observed may reflect the tendency of the protein to adsorb/aggregate as a less active population and that increasing the substrate concentration to >300 mM mitigated that effect to increase activity. Alternatively, a conformational change within the DHH/DHHA1 domain could occur at higher c-di-AMP concentrations and be a physiological feature of GdpP. Thus,

when toxic levels of c-di-AMP are reached, GdpP phosphodiesterase activity may increase.

(A)

(B)

(C)

(D)

(E)

(F)

Michaelis-Menten Reaction rate constants		K_m (μM)	k_{cat} (s^{-1})
Detergent	[c-di-AMP] range (μM)		
With Detergent	0 - 300	443.6±97.53	0.42±0.16
	300 - 1750	132.6±20.05	0.49±0.01
	0 - 1750	537.9±64.67	0.65±0.03
Without Detergent	0 - 250	51.81±8.42	0.048±0.003
	250 - 1750	224.2±30.26	0.21±0.01
	0 - 1750	820.5±119.5	0.35±0.03
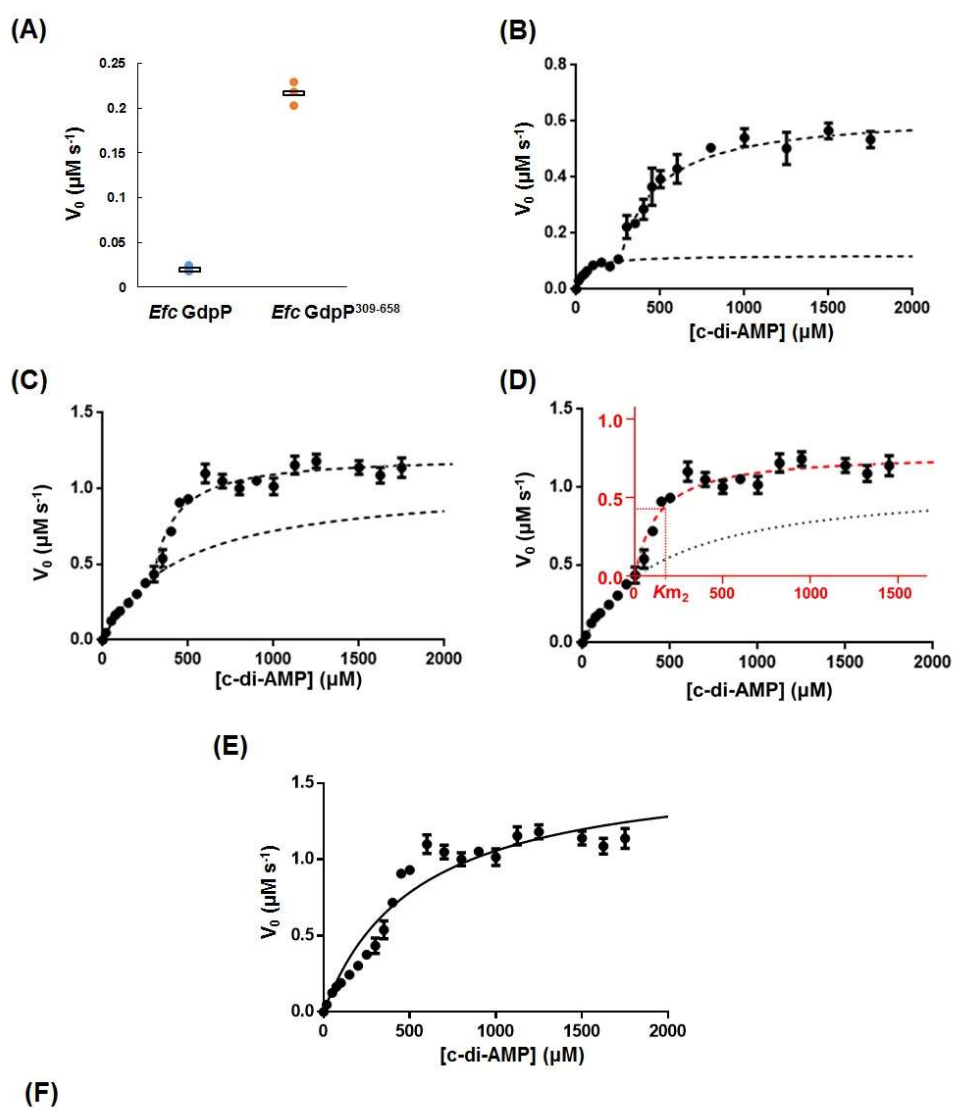
Figure 3.6 Steady-state kinetic analysis of *E. faecalis* GdpP DHH/DHHA1 domain (*Efc* GdpP$_{309-658}$) phosphodiesterase activity at 37°C. *(A) Comparison of the phosphodiesterase activity of full-length Efc GdpP and Efc GdpP$_{309-658}$. 10 μM Efc GdpP or 2.5 μM Efc GdpP$_{309-658}$ were incubated with 1mM c-di-AMP at 37 °C. The reaction rates were normalized to 1μM protein. The reactions contained 50 mM CHES pH9.2, 20 mM KCl, and 0.5 mM MnCl$_2$. (B) The enzymatic kinetics curve of Efc GdpP$_{309-658}$ without detergent. The reactions contained 2.5 μM Efc GdpP$_{309-658}$, 50 mM CHES pH9.2, 20 mM KCl, and 0.5 mM MnCl$_2$. (C-E) Steady-state kinetic analysis of Efc GdpP DHH/DHHA1 domain (Efc GdpP$_{309-658}$) phosphodiesterase activity at 37 °C with detergent. The reaction contained 2.5 μM Efc GdpP$_{309-658}$, 50 mM CHES pH 9.2, 20 mM KCl, 0.5mM MnCl$_2$, and 1mM fluorinated octyl maltoside. To determine the reaction rate constants of the second stage (300-1750 μM c-di-AMP), the axis was shift from (0, 0) to (300, 0.4348) (red) (D). V$_0$=0.4348 was the mean of the reaction rates of 2.5 μM Efc GdpP$_{309-658}$ with 300 μM c-di-AMP. In Figure (E) the kinetics curve was fit into one Michaelis-Menten model. (F) Kinetics comparison of Efc GdpP and Efc GdpP$_{309-658}$ without and with 1mM fluorinated octyl maltoside.*

Table 3.2 Summary of Steady-state kinetics of c-di-AMP-specific phosphodiesterases in Gram-positive bacteria.

Strain	Protein	Domain Organization	c-di-AMP-specific Phosphodiesterase Activity		Reference
			k_{cat}	K_m	
B. subtilis 168	GdpP[84-659]	PAS – GGDEF – DHH – DHHA1	0.55 ± 0.02 s^{-1}	1.3 ± 0.24 μM	(Rao et al., 2011)
E. faecalis S613[a]	GdpP[309-658]	DHH – DHHA1	$k_{cat1} = 0.42 \pm 0.16$ s^{-1} $k_{cat2} = 0.49 \pm 0.01$ s^{-1}	$K_{m1} = 443.6 \pm 97.5$ μM $K_{m2} = 132.6 \pm 20.1$ μM	This study
M. smegmatis MC155	MsPDE	DHH – DHHA1	0.52 ± 0.03 s^{-1}	6.80 ± 0.84 μM	(Tang et al., 2015)
M. tuberculosis H37Rv	Rv2837c	DHH – DHHA1	0.23 ± 0.02 s^{-1}	30.89 ± 6.71 μM	(He et al., 2016)
S. pneumoniae ST581	Pde1[51-657]	PAS – DHH – DHHA1	0.121 ± 0.037 s^{-1}	36.40 ± 17.43 μM	(Bai et al., 2013)
S. pneumoniae ST581	Pde2	DHH – DHHA1	0.027 ± 0.007 s^{-1}	16.75 ± 8.70 μM	(Bai et al., 2013)

[a]The enzyme kinetics of *E. faecalis* S613 GdpP[309-658] were measured in the presence of detergent (1mM fluorinated octyl maltoside). Please see Section 3.3.1.4 for details.

Table 3.2 shows the enzyme kinetics of Gram-positive bacterial c-di-AMP phosphodiesterases from previously published results. *Efc* GdpP$_{309-658}$ shows similar k_{cat} to other phosphodiesterases, but a much higher K_m (Table 3.2). Since the intracellular c-di-AMP levels in *B. subtilis* were measured by a different method (~1.7 µM/1 L culture) (Oppenheimer-Shaanan et al., 2011b) and there is no report for c-di-AMP levels in *M. smegmatis* and *M. tuberculosis.*, it is hard to explain the high K_m of *Efc* GdpP$_{309-658}$. Since the cellular c-di-AMP level in *S. pneumoniae* ST581 (~25pM/OD$_{620}$) is lower than that in *Efc* S613 (113$\pm$81 pM/OD$_{600}$) (Bai et al., 2013), the high K_m of *Efc* GdpP$_{309-658}$ may relate to the high c-di-AMP basal level in *E. faecalis*.

Additionally, there are no enzyme kinetics studies for the c-di-AMP phosphodiesterase PgpH in enterococcus or other Gram-positive bacteria and therefore it is hard to predict which enzyme is the predominant phosphodiesterase in enterococci for c-di-AMP regulation *in vivo*. Previously published work has suggested that *L. monocytogenes*, PgpH is essential for regular cell growth, and thus GdpP plays an important role during bacterial virulence (Huynh et al., 2015).

3.3.1.5. Aspartate 419 and 499 are essential to *Efc* GdpP phosphodiesterase activity.

As the activity of *Efc* GdpP was low, I wished to eliminate any possibility that the modest phosphodiesterase activity observed by the HPLC and coralyne assays

were not the result of some contaminant. To do this I designed an inactive version of variant of the protein to link phosphodiesterase activity to *Efc* GdpP. Based on a comparison of the *Efc* GdpP sequence with that of others phosphodiesterases, Asp residues 419 and 499 are predicted to be ligands for the metal ion binding site required for phosphodiesterase activity (Figure 3.2 and Figure 3.7) (Rao et al., 2010). To test whether Asp 419 and 499 are required for phosphodiesterase activity, I generated the double mutant *Efc* GdpP[D419A/D499A]. As expected, no activity was detected after incubation of *Efc* GdpP[D419A/D499A] with c-di-AMP (Figure 3.3E). These results indicate that alignment of the primary sequences for *Efc* GdpP to other members of the DHH protein family phosphodiesterases has correctly identified residues essential to activity and support my conclusion that *Efc* GdpP is a *bone fide* cyclic dinucleotide phosphodiesterase.
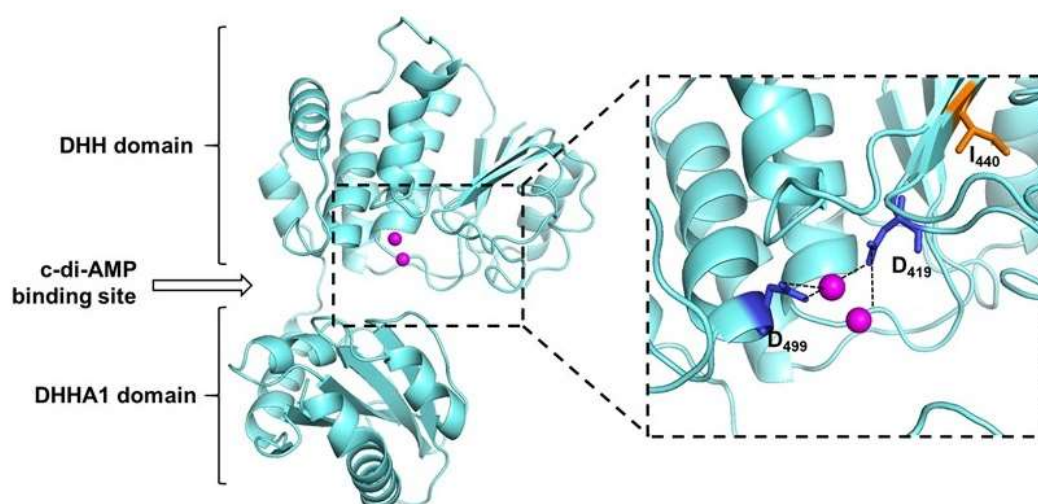
Figure 3.7 Predicted structure of *Efc* GdpP. *Predicted structure model of Efc GdpP DHH/DHHA1 domain indicating the presumptive phosphodiesterase active site and proximal position of I440S. Two Mn^{+2} ions are shown as spheres in magenta. Asp residues 419 and 499 are in blue, and Ile 440 is in orange. The structural model was built using the Phyre2 server. The Mn^{+2} positions are predicted by alignment with Mycobacterium tuberculosis phosphodiesterase Rv2837c (PDB 5CET) (He et al., 2015).*

3.3.2. Adaptive GdpP mutation I440S that correlates with daptomycin resistance in *E. faecalis* S613 strongly decreases GdpP phosphodiesterase activity *in vitro*.

In *Efc* GdpP, the adaptive mutation I440S is located in the putative DHH domain (Figure 1.1), and is proximal to the predicted substrate binding site (Figure 3.7) (He et al., 2015). To elucidate how the adaptive mutation may facilitate DAP resistance, I determined the phosphodiesterase activity of *Efc* GdpP^{I440S} toward its potential physiological substrate c-di-AMP. As shown in (Figure 3.3F), incubation of c-di-AMP with GdpP^{I440S} showed an 11-fold reduction in the ability to hydrolyze c-di-AMP to 5'pApA. Thus, the *gdpP*^{I440S} was identified in the DAP adaptive isolates (Miller et al., 2013), and may lead to c-di-AMP accumulation in these strains, suggesting that high intracellular c-di-AMP levels are important for *E. faecalis* physiology during DAP induced membrane stress.

3.3.3. *Efc* GdpP regulates *E. faecalis* intracellular c-di-AMP level.

To further test whether *Efc* GdpP has phosphodiesterase activity *in vivo*, the gene coding wild-type *Efc* GdpP was subcloned into the nisin-inducible vector pMSP3535 (Bryan et al., 2000) and transformed into *Efc* OG1RF. As shown in Figure 3.8 and Table 3.1, overexpression of *Efc* GdpP decreased cellular c-di-AMP levels by about 27% when compared to the empty plasmid. The decreased c-di-AMP levels in cells expressing *Efc* GdpP from the plasmid pMSP3535 were statistically significant compared with the control strain (p=0.008).

Since *Efc* GdpP[I440S] showed decreased phosphodiesterase *in vitro*, I expected that expression of the mutant *Efc* GdpP[I440S] from the plasmid pMSP335 would lead to restored levels of c-di-AMP. While there was a very modest decrease in c-di-AMP levels, it was not statistically significant (p=0.078). There could be a number of reasons for the inability of *Efc* GdpP[I440S] to fully restore c-di-AMP levels compared with negative control (OG1RF::pMSP3535). First, the mutation I440S decreases the phosphodiesterase activity by around 11-fold, but does not completely abolish it. Second, since *Efc* GdpP[I440S] is being expressed along with the genomic copies of the wild type GdpP in addition to the c-di-AMP synthesis and regulatory genes, the net effect of the *Efc* GdpP[I440S] might be compensated for by the homeostatic machinery of the cell. I observed a slight c-di-AMP level increase in *Efc* OG1RF:: pMSP3535 compared with *Efc* OG1RF (158 ± 3 pM/OD$_{600}$ versus 112 ± 47 pM/OD$_{600}$, p=0.225, see Table 3.1, Figure 3.1, and Figure 3.8 for details), which may be caused by addition of nisin, since higher c-di-AMP levels were also detected when *Efc* OG1RF::pMSP3535

when cultured with nisin versus its absence (data not shown). Together, my data highly suggest that *Efc* GdpP has phosphodiesterase activity *in vivo*, and can regulate intracellular c-di-AMP levels.
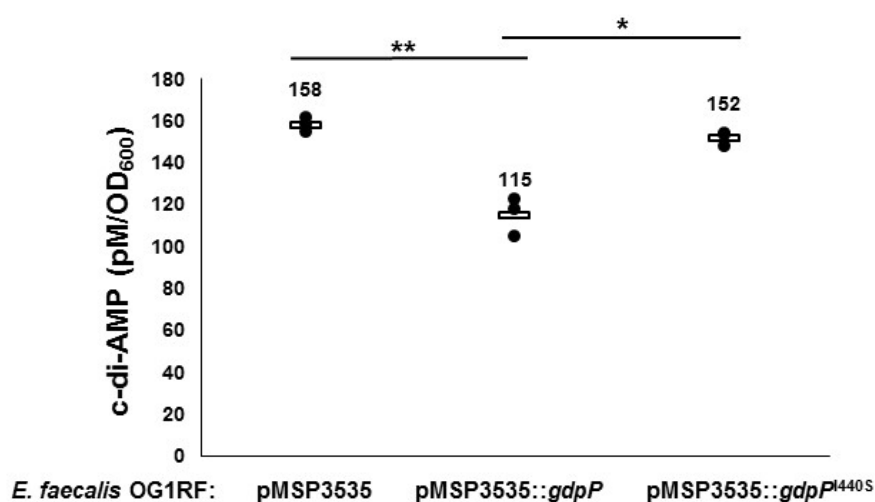
Figure 3.8 Expression of the c-di-AMP phosphodiesterase *Efc* GdpP in trans leads to reduced c-di-AMP levels *in vivo*. *Intracellular concentrations of c-di-AMP in Efc OG1RF during expression of Efc GdpP or Efc GdpP[I440S]. Expression of Efc GdpP leads to a statistically decreases in c-di-AMP levels (~27%). Expression of Efc GdpP[I440S] does not lead to significant changes in c-di-AMP. Each strain has three biological independent measurements.*

3.3.4. *E. faecalis* GdpP[I440S] is more sensitive to inhibition by ppGpp *in vitro*.

Several studies on GdpP family proteins, such as *B. subtilis* GdpP and *S. aureus* GdpP, have reported that ppGpp can inhibit GdpP phosphodiesterase activity (Corrigan et al., 2015; Rao et al., 2010). ppGpp is a stringent response signaling molecule, and accumulates in some bacteria during nutrient starvation (Kalia et al., 2013). In *B. subtilis*, ppGpp binds to *B. subtilis* GdpP, and inhibits phosphodiesterase activity (referred to as YybT in (Rao et al., 2010)).

To determine whether ppGpp is a direct inhibitor of *Efc* GdpP, 1mM ppGpp was incubated with 10 μM *Efc* GdpP and 100 μM c-di-AMP. Figure 3.9A shows that ppGpp inhibits *Efc* GdpP phosphodiesterase activity very modestly, but does not completely abolish it, even though the molar ratio of c-di-AMP to ppGpp was 10:1. My data suggests that ppGpp is a very weak inhibitor of *Efc* GdpP phosphodiesterase activity *in vitro*.

When 1mM ppGpp was added to the reaction system of 10μM *Efc* GdpP[I440S] and 100μM c-di-AMP, no c-di-AMP was hydrolyzed to 5'pApA after incubation for 2 h (Figure 3.9B) and indicates that the residual phosphodiesterase activity of *Efc* GdpP[I440S] can be inhibited by ppGpp *in vitro*. This data suggests that *Efc* GdpP[I440S] could be more sensitive to ppGpp inhibition than wild type *Efc* GdpP *in vivo*.
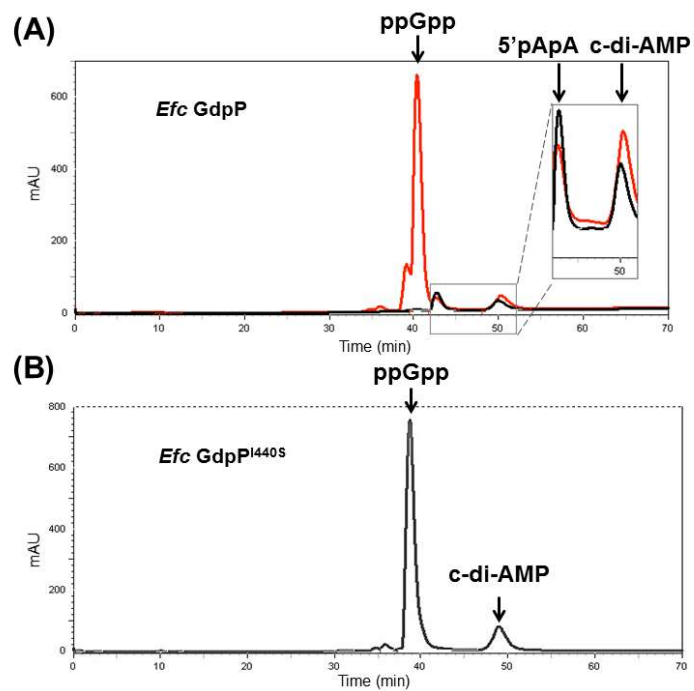
Figure 3.9 ppGpp is able to modestly inhibit *Efc* GdpP phosphodiesterase activity. *(A) Reverse phase HPLC analysis of products from incubation of wild type Efc GdpP and c-di-AMP with (red) and without (black) 1mM ppGpp after incubation for 2 h at 28°C. (B) Efc GdpP^{I440S} with c-di-AMP and ppGpp after 2hr incubation at 28°C showing no significant 5'pApA production.*

3.4. *Efc* GdpP has ATPase activity, but not diadenylate cyclase activity *in vitro*.

3.4.1. *Efc* GdpP has ATPase activity *in vitro*.

Efc GdpP has a putative GGDEF domain which is unusual as the previously described GdpP family proteins typically lack the conserved GGDEF motif (Cho and Kang, 2013; Corrigan et al., 2011; Rao et al., 2010, 2011). Proteins containing GGDEF domains in Gram-negative bacteria often have diguanylate cyclase activity, which can synthesize c-di-GMP from 2 GTPs (Ryjenkov et al., 2005). But the GGDEF domain in *B. subtilis* GdpP has only a very weak ATPase activity (referred to as YybT in (Rao et al., 2010)).

Primary sequence alignment indicated that *Efc* GdpP (similar to *B. subtilis* GdpP) contains a modified GGDEF domain with a highly divergent amino acid sequence (Figure 3.10). The GGDEF domain in *B. subtilis* GdpP, can bind ATP and slowly convert it to ADP (Rao et al., 2010). To test whether *Efc* GdpP exhibited ATPase activity, I incubated 100 μM ATP with 10 μM *Efc* GdpP, and analyzed the products by reverse phase HPLC. The chromatographic analysis revealed that *Efc* GdpP could hydrolyze ATP leading to the formation of ADP after incubation (Figure 3.11A, B).

```
Enterococcus_EFE19635.1        154 EN----------TYRFSVNKEQHTITFEDITKESNLYQEKVEMQTAIG-IVSVDNYDDVT
Bacillus_WP_003242517.1        141 LR----------KFRVVIKRDERLLYFFDVTEQIQIEKLYENERTVLA-YIFLDNYDDVT
Staphylococcus_WP_001081634.1  138 NQY---------HFQVRYSENDHCLYFFDITEQVQTNELYENSKPIIA-TLFLDNYDEIT
Streptococcus_AGQ28355.1       150 EDISQTFEVSGNKYTSYIDVSSGIFYFFDSFVGNRQLADASMLRPVVG-IISVDNYDDIT
Geobacillus_WP_011888454.1     142 GK----------QLKVIVHRHERLLYFFDVTEHMELRRRYEIERLVLA-IIFLDNYDEIT
Caulobacter_AAA87378.1         291 TD----------QLTGLHNRRYMTGQLDSLVKRATLGGD-----PVSALLIDIDFFKKIN
```

```
Enterococcus_EFE19635.1        203 DTMDEK-EISYLNSFITTMVSDWMDQYKV-FYKRINAERYFFIAQWEDIQKMMDEKFSIL
Bacillus_WP_003242517.1        190 QGLDDQ-TRSTMNSQVTSLLNAWAQEYGI-FLKRTSSERFIAVLNEHILTELENSKFSIL
Staphylococcus_WP_001081634.1  188 QNMNDT-QRSEINSMVTRVISRWATEYNI-FTKRYSSDQFVAYLNQKILADLEESKFDIL
Streptococcus_AGQ28355.1       210 DDLSDA-DTSKINSFVANFIDEFMESKRI-FYRRVNMDRYYFFTDFKTLNDLMDNKFSVL
Geobacillus_WP_011888454.1     191 QGMDDQ-AKSQMNSLVTSVLNRWANDYGI-FLKRTSSDRFIAVLNEHIITQLEKSKFSIL
Caulobacter_AAA87378.1         336 DTFGHDIGDEVLREFALRLASN---VRAIDLPCRYGGEEFVVIMPDTALAD----ALRIA
                                                                               *****
```

```
Enterococcus_EFE19635.1        261 DTIRKESANH---------EVAITLSMGIAYGGP--TLD-QTGTTAQLNLDTALVRGGDQ
Bacillus_WP_003242517.1        249 DEVREKTSFD---------GVALTLSVGVGASVS--SLK-ELGDLAQSSLDLALGRGGDQ
Staphylococcus_WP_001081634.1  247 SQLREKSVGY---------RAQLTLSIGVGEGTE--NLI-DLGELSQSGLDLALGRGGDQ
Streptococcus_AGQ28355.1       269 EEFRKEAQDA---------QRPLTLSIGISFGEE--NHS-QIGQ----------------
Geobacillus_WP_011888454.1     249 DEVREQTAKH---------QAQITLSIGIGAGVS--SLP-ELGDLAQSSLDLALGRGGDQ
Caulobacter_AAA87378.1         389 ERIRMHVSGSPFTVAHGREMLNVTISIGVSATAGEGDTPEALLKRADEGVYQAKASGRNA
```

```
Enterococcus_EFE19635.1        309 VVVK
Bacillus_WP_003242517.1        297 VAIK
Staphylococcus_WP_001081634.1  295 VAIK
Streptococcus_AGQ28355.1           ----
Geobacillus_WP_011888454.1     297 VAIK
Caulobacter_AAA87378.1         449 V--V
```

Figure 3.10 Proposed Alignment of the GGDEF domains. *Proposed alignment of the GGDEF domains of E. faecalis GdpP, Bacillus subtilis GdpP (referred as YybT in (Rao et al., 2010)), Staphylococcus aureus GdpP* (Corrigan et al., 2011)*, Streptococcus pyogenes GdpP (Cho and Kang, 2013), Geobacillus thermodenitrificans GdpP (referred as YybT in (Rao et al., 2011)), and the GGDEF domain in Caulobacter crescentus PleD with diguanylate cyclase activity (Paul et al., 2004). The conserved GGD(E)EF motif is highlighted.*
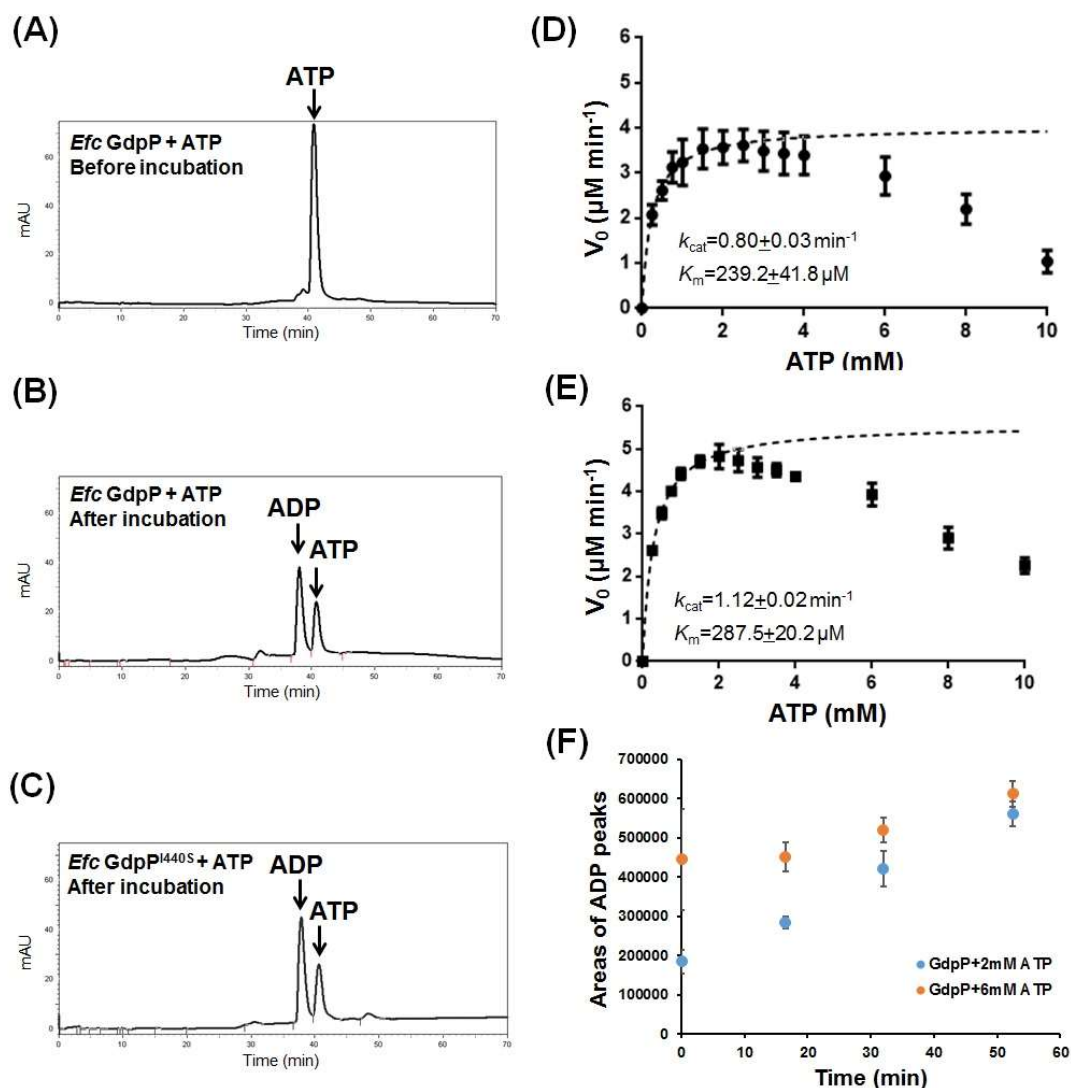
Figure 3.11 . *Efc* **GdpP and GdpP[I440S] have comparable ATPase activity.** *(A-C): Reverse phase HPLC analysis of: (A) ATP and wild-type Efc GdpP before incubation, (B) ATP and wild-type Efc GdpP after 2 h incubation at 25°C, (C) ATP and Efc GdpP[I440S] after 2 h incubation at 2562°C. (D) ATPase activity measurement of 5 μM Efc GdpP 28°C. (E) ATPase activity measurement of 5μM Efc GdpP[I440S] 28°C. Reaction buffer contains 50mM Tris pH 7.5, and 1mM MgCl₂. (F) ATP inhibition of the Efc GdpP ATPase*

activity. Reverse phase HPLC results of 10μM Efc GdpP incubated with 2 mM and 6 mM ATP at 28℃. The area of the peaks corresponding to ADP are plotted. The reaction buffer contained 40 mM Tris pH7.5 and 10 mM MgCl₂.

3.4.2. *Efc* GdpP ATPase kinetics curve shows substrate inhibition.

To quantitate *Efc* GdpP ATPase kinetics, I used the EnzChek® Phosphate Assay Kit (Life Technologies). *Efc* GdpP can hydrolyze ATP to generate inorganic phosphate (Pi), which can interact with 2-amino-6-mercapto-7-methylpurine ribonucleoside (MESG, Abs_{max}=340nm) to produce 2-amino-6-mercapto-7-methylpurine (Abs_{max}=360nm) (Upson et al., 1996). Thus, the ATPase reaction kinetics can be readily quantified. (Please see Chapter 2 for details.)

ATPase activity of *Efc* GdpP had a k_{cat} of 0.80 ± 0.03 min^{-1} and K_m of 239.2 ± 41.8 μM (Figure 3.11D), while the *B. subtilis* GdpP homolog had similar values of k$_{cat}$ but a markedly lower K_m (k_{cat}= 0.59 ± 0.03 min^{-1}, K_m= 0.90 ± 0.12 mM) (Rao et al., 2010).

To assess whether the mutation of Ile-440 to Ser in the DHH domain could affect ATPase activity in the GGDEF domain, I measured the ATPase activity of *Efc* GdpP^{I440S}. ATPase activity for *Efc* GdpP^{I440S} was comparable to wild type GdpP (Fig. 6C) with a k_{cat} of 1.12 ± 0.02 min^{-1} and K_m of 287.5 ± 20.2 μM (Figure 3.11E). Thus, it appears that the mutation I440S in the DHH domain does not affect the GGDEF domain ATPase activity (p=0.880).

The weak ATPase activity of GdpP required me to use up to 2 mM ATP to provide sufficient data for the analysis. When performing the ATPase studies, I observed unexpected substrate inhibition on the ATPase activity (Figure 3.11 D and E). Interestingly, inhibition starts at about 2.5 mM ATP which is in the range of its intracellular concentration (about 1-10 mM) (Yaginuma et al., 2014). To confirm that the inhibition was not caused by the reagents used in the colorimetric ATPase assay, I incubated 10 μM *Efc* GdpP with 2 mM and 6 mM ATP at 28°C respectively, and analyzed the products directly by reverse phase HPLC (Figure 3.11F). This data suggested that *in vitro* substrate inhibition could be biologically relevant and led me to suspect that the local cellular ATP concentration around the cell membrane could alter *Efc* GdpP ATPase activity.

3.4.3. *Efc* GdpP does not show diadenylate cyclase activity *in vitro*.

A study of *S. aureus* GdpP showed that two mutations in its GGDEF domain could increase antibiotic resistance against vancomycin and oxacillin, and that complementation with an *S. aureus* GdpP N-terminal truncation with an inactive DHH domain could restore antibiotic susceptibility (Griffiths and O'Neill, 2012). Together these observations suggest that the *Efc* GdpP GGDEF domain has additional activities *in vivo* beyond weak ATP hydrolysis. It seems likely that ATP is hydrolyzed as part of another activity of the domain and thus I sought to identify alternate activities or conditions that might stimulate any potential GdpP cyclase activity.

Recently, the GGDEF domains from deltaproteobacteria were reported to have a hybrid dinucleotide cyclase activity, and can synthesize c-di-AMP, c-di-GMP, and cyclic AMP-GMP (3',3'-cGAMP), which suggests the GGDEF domains have similar dinucleotide cyclase (Hallberg et al., 2016).

To identify whether *Efc* GdpP GGDEF has di-nucleotide cyclase activity, *Efc* GdpP purified from *E. coli* was incubated with 0.1mM, 2mM, and 6mM ATP or GTP. Potential cofactors, such as heme and NADH, and reducing agents were tested. After optimizing reaction conditions, incubation of *Efc* GdpP with ATP or GTP did not produce either c-di-AMP or c-di-GMP (data not shown). One potential reason was that c-di-GMP in *E. coli* binds to the I-site of GGDEF domain, inhibiting the dinucleotide cyclase activity. The other possibility is that the protein was expressed in *E. coli*, lacking the cofactor in enterococci for dinucleotide cyclase activity.

Efc GdpP residue tyrosine 212 was in the putative GGDEF domain I-site. To preventing the potential binding of di-nucleotides to I-site, I generated the I-site mutant *Efc* GdpP^{Y212A}. To avoid degrading of di-nucleotide by the N-terminal DHH/DHHA1 domain, I also tested *Efc* GdpP$^{D419A/D499A}$ and *Efc* GdpP$^{Y212A/D419A/D499A}$.

To allow wild-type *Efc* GdpP and its three variants to bind the potential co-factors in enterococci, proteins were incubated with *Efc* S613 cell extracts, and purified by Ni-NTA affinity chromatography. Proteins were then incubated with 1mM – 16mM ATP. The generation of c-di-AMP was tested by c-di-AMP competitive ELISA, which is an accurate method to detect low-concertation (≥2nM) c-di-AMP

(Underwood et al., 2014). However, after optimizing reaction conditions, no c-di-AMP was observed. It appears that the GGDEF domain is not a c-di-AMP or c-di-GMP synthase *in vitro* or that I was unable to identify appropriate conditions to stimulate cyclase activity.

3.5. The PAS domain in *E. faecalis* GdpP does not appear to bind heme *in vitro*.

Small Per-ARNT-Sim (PAS) domains usually function as input domains in proteins to respond to a variety of stimuli, including light and small ligands *via* different co-factors associated with the PAS fold (Taylor and Zhulin, 1999). Previously, it had been reported that PAS domains of *Efc* GdpP homologs in *B. subtilis* and *G. thermodenitrificans* are capable of binding heme, as a co-factor resulting in suppressing the phosphodiesterase activity *in vitro* (Rao et al., 2011).

In this study, heme reconstitution assays were performed to determine whether the PAS domain in *Efc* GdpP can function as sensor domain for recognizing an environmental signal through a heme cofactor. 1mM heme (in 10mM NaOH) was titrated into His-tagged or GST-tagged *Efc* GdpP solutions at 37°C to a final 1:1 molar ratio. Their UV absorbance was scanned every 1min.

As shown in Figure 3.12A, upon addition of heme, the UV spectrum of His-*Efc* GdpP showed decreases in the absorbance maxima corresponding to free heme (373nm, 630nm), whereas the absorbance maxima of hexacoordinate heme

(415nm, 542nm, 575nm) increased. My data suggests that heme binds to His-*Efc* GdpP but I was concerned that the His-tag may provide good ligands for heme in a non-physiological context (Owens et al., 2012). Although there was a TEV protease cleavage site, unfortunately, the His-tag could not be removed by TEV protease. I replaced the His-Tag with a GST-tag to test the heme-binding ability of a *Efc* GST-GdpP to rule out the potential interference of His-tag. I incubated GST-*Efc* GdpP with heme for 6 h at 37°C, there was no spectroscopic signal for a hexacoordinated heme (Figure 3.12B), suggesting GST-*Efc* GdpP could not bind heme. My data suggests that the His-tag was indeed responsible for my earlier finding and that *Efc* GdpP did not bind heme under these conditions. I have not identified a cofactor for the PAS domain in *Efc* GdpP however this remains under investigation.
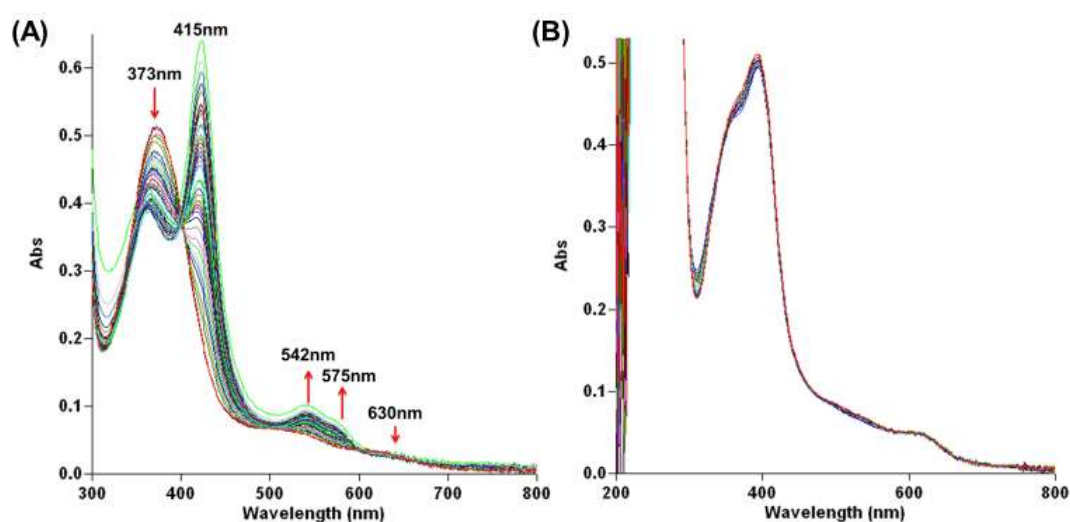
Figure 3.12 Heme reconstitution assays show *Efc* GdpP doesn't bind heme *in vitro*. *(A) UV absorbance of Efc His-GdpP with heme titration at 37°C. The reaction*

condition contains 25mM CHES pH8.6, 200mM NaCl. (B) UV absorbance of Efc GST-GdpP with heme titration at 37℃. The reaction contained 50mM Tris pH8.0, 200mM NaCl.

3.6. Discussion

Cyclic dinucleotide signaling in bacteria is widespread and is linked to a variety of regulatory responses including DNA integrity reporting (Oppenheimer-Shaanan et al., 2011a), cell wall biosynthesis (Corrigan et al., 2011), potassium homeostasis (Corrigan et al., 2013) and biofilm formation (Corrigan et al., 2011). Experimental evolution of a polymorphic population of *Efc* S613 to daptomycin resistance using a continuous evolution bioreactor identified a point mutation (*yybT*[I440S]) in a gene of unknown function initially named *yybT* (Miller et al., 2013). Based on primary sequence identity, I postulated that YybT might in fact be a cyclic dinucleotide phosphodiesterase, and based on my studies I have established phosphodiesterase activity consistent with classification as a member of the GdpP family. Therefore, I have changed the name to GdpP. As c-di-AMP signaling in enterococci had not been established, I first tested if c-di-AMP was present at levels consistent with a role in *in vivo* signaling (from 44 pM/OD_{600} to 1133 pM/OD_{600}, Figure 3.1 and Table 3.1). Having established that c-di-AMP was present *in vivo*, I went on to confirm the role of the novel GdpP in c-di-AMP homeostasis.

As shown in Figure 1.1, GdpP is comprised of three distinct domains. I purified and characterized full-length *Efc* GdpP as well as the DHH/DHHA1 domain (*Efc* GdpP$_{309-658}$). My results showed that *Efc* GdpP is indeed a cyclic-di-AMP phosphodiesterase with a strong preference for c-di-AMP over c-di-GMP. *Efc* GdpP^{I440S} shows little phosphodiesterase activity and, as expected, strains encoding *Efc* GdpP^{I440S} have increased cyclic-di-AMP levels *in vivo*. My results showed that expression of *Efc* GdpP from an inducible vector pMSP3535 in wild-type *Efc* OG1RF decreased cellular c-di-AMP level by 27% (Figure 3.8 and Table 3.1). Although I could demonstrate weak ATPase activity for the GGDEF domain and c-di-AMP phosphodiesterase activity for the DHH/DHHA1 domain, I was unable to identify the *in vivo* function of either domain. The PAS domain could be a critical regulator of the activities of the GGDEF and DHH/DHHA1 domains *in vivo*. For example, the c-di-AMP phosphodiesterase activity for the DHH/DHHA1 domain alone (GdpP$_{309-658}$) is ~13 times higher than the full-length protein suggesting that under specific conditions or stimuli *in vivo*, the kinetic rates of the activities within the GdpP domains may be quite variable and well regulated. Undoubtedly, each of the GdpP domains has relevant activities or roles *in vivo.* A study showed *S. aureus* GdpP GGDEF mutations could increase *S. aureus* vancomycin and oxacillin resistance (Griffiths and O'Neill, 2012). Together, these observations suggest that the *Efc* GdpP GGDEF domain has additional activities *in vivo* beyond weak ATP hydrolysis. However, I couldn't detect *Efc* GdpP di-nucleotide cyclase activity *in vitro*. The

functional role of the PAS and GGDEF domains is the subject of ongoing investigation.

Based on sequence homology, *E. faecalis* has only one gene coding a potential c-di-AMP synthase (*cdaA*, also referred as *ybbP*) (Mehne et al., 2013). My finding of a robust c-di-AMP pool in *E. faecalis* suggests that *Efc* CdaA is active *in vivo*. *E faecalis* has two potential genes encoding c-di-AMP phosphodiesterases, *gdpP* and *pgpH* (Huynh et al., 2015). The *Listeria monocytogenes* PgpH is a membrane protein, and can hydrolyze c-di-AMP to 5'pApA via a His-Asp (HD) domain (Huynh et al., 2015). A study of *L. monocytogenes* c-di-AMP phosphodiesterases showed that DHH/DHHA1 family phosphodiesterases are more important than HD family phosphodiesterases for bacterial virulence and intracellular growth (Huynh et al., 2015), which may be the reason that I did not observe mutations in PgpH in the clinical or experimental evolution data for enterococci.

In summary, I show that c-di-AMP is present in enterococci, and that a novel GdpP phosphodiesterase, previously associated with daptomycin resistance, is important to modulate c-di-AMP in response to cell membrane damage caused by the antibiotic.

Chapter 4

The LiaFSR-XYZ regulon interacts with the c-di-AMP signaling network.

4.1. Introduction

During adaptation to DAP, Miller *et al.* observed that the first step towards resistance was a family of mutations that, in the LiaFSR and LiaX membrane stress response pathway (Miller et al., 2013; Tran et al., 2013). In two of the evolutionary trajectories leading to DAP resistance, an Ile to Ser substitution at position 440 was observed in GdpP (Miller et al., 2013). Interestingly, GdpP^{I440S} was always found in association with a LiaR mutant (LiaR^{D191N}), suggesting a potential epistatic link between changes in LiaFSR signaling and GdpP (Miller et al., 2013). Since LiaR is the response regulator of the LiaFSR membrane-stress response system (Wolf et al., 2010), I investigated the possibility that the LiaFSR pathway effected levels of c-di-AMP.

In this chapter, I show that mutations in the LiaFSR and LiaXYZ pathways can affect intracellular c-di-AMP levels, suggesting Lia pathways are linked to c-di-AMP regulated metabolism. I also show that intracellular c-di-AMP levels change with DAP treatment, which suggests c-di-AMP participates in the cell membrane stress response. In the course of these studies I also show a new putative phosphodiesterase XpaC that is under LiaFSR regulation.

4.2. Mutations in the LiaFSR signaling pathway can affect intracellular c-di-AMP levels.

4.2.1. LiaR deletion leads to increased c-di-AMP level.

To test whether LiaFSR leads to changes in intracellular c-di-AMP regulation, I initially used a strain in which our collaborator had generated a non-polar deletion of *liaR* in *Efc*. Cell extracts from the mutant *Efc* OG1RF_Δ*liaR* (Table 3.1) were tested for c-di-AMP levels. Of note, the *liaR* deletion removes the response regulator of the LiaFSR pathway, effectively "shutting off" the LiaFSR system. Deletion of *liaR* (*Efc* OG1RF_Δ*liaR*) upregulated the levels of c-di-AMP to 351 ± 94 pM/OD$_{600}$ (Figure 4.1A and Table 3.1), a more than 3-fold increase compared to wild type *Efc* OG1RF (p=0.030). When *liaR* expression was restored in *cis* in *Efc* OG1RF_Δ*liaR* (*Efc* OG1RF_Δ*liaR*::*liaR*, Table 3.1), cellular c-di-AMP levels returned to the levels observed for wild type *Efc* OG1RF (140 ± 29 pM/OD$_{600}$, p=0.436, Figure 4.1A and

Table 3.1). These results suggest that decreases in LiaFSR signaling leads increases in intracellular c-di-AMP levels.

To demonstrate that changes in LiaFSR signaling also lead to c-di-AMP changes in other enterococcal strains, I measured the c-di-AMP levels in non-polar deletion mutants of *liaR* in *E. faecium* strains HOU503F and R497F (*Efm* HOU503F_Δ*liaR* and *Efm* R497F_Δ*liaR*, Table 3.1) which are tolerant and resistant to DAP respectively (Panesso et al., 2015). As observed with *E. faecalis*, deletion of *liaR* in *Efm* HOU503F_Δ*liaR* and *Efm* R497F_Δ*liaR* showed modest increases in c-di-AMP levels when compared to *Efm* HOU503F and *Efm* R497F (622 ± 104 pM/OD_{600} vs. 542 ± 133 pM/OD_{600}, and 736 ± 186 pM/OD_{600} vs. 549 ± 150 pM/OD_{600}, Figure 4.1B and Table 3.1) but the increases were not statistically significant ($p = 0.250$ and 0.461). It is interesting that the inactivation of the LiaFSR pathway in *E. faecium* does not increase c-di-AMP concentrations to the same extent as observed in *E. faecalis.* The basal level of c-di-AMP in *E. faecium* HOU503F and R497F was much greater than *E. faecalis* OG1RF or S613 and thus there are substantial differences in the basal c-di-AMP pools of these related organisms. The reason for the higher baseline levels in *E. faecium* is unclear but may account for my inability to measure statistically relevant differences in c-d-AMP levels as the differences of *Efm* HOU503F and *Efm* R497F to their respective LiaR knockouts was much closer in *E. faecium* (622 ± 104 pM/OD_{600} vs. 542 ± 133 pM/OD_{600}, and 736 ± 186 pM/OD_{600} vs. 549 ± 150 pM/$OD_{600,}$ Figure 4.1B). Since very high levels of c-di-AMP have been associated with decreased fitness (Mehne et al., 2013) there may be an upper end to

c-di-AMP levels beyond which there is substantial toxicity and *E. faecium* is already near that range of c-di-AMP concentrations. *Cis*-complementation with *liaR* decreased the intracellular c-di-AMP levels to 505 ± 54 pM/OD$_{600}$ and 525 ± 134 pM/OD$_{600}$ for *Efm* HOU503F_$\Delta liaR$::*liaR* and *Efm* R497F_$\Delta liaR$::*liaR*, respectively, similar to the c-di-AMP levels in wild-type strains (Figure 4.1B and Table 3.1).
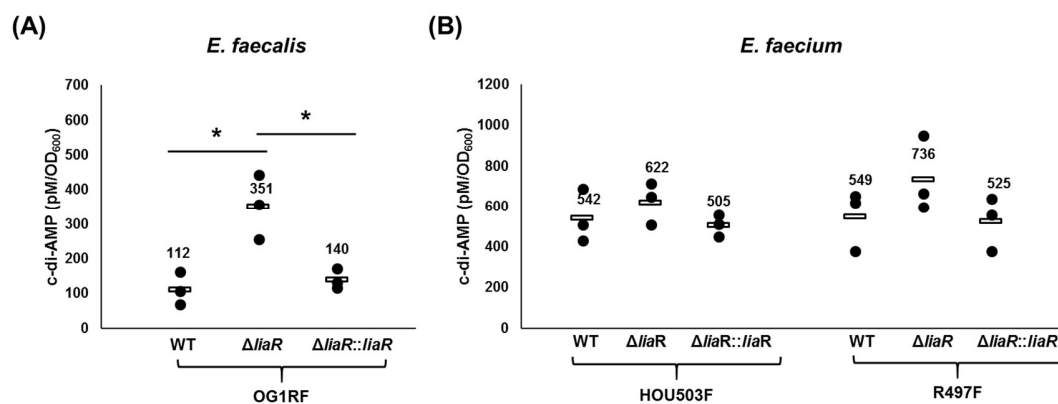
Figure 4.1 Enterococci strains with mutations in the LiaFSR signaling pathway have increased c-di-AMP levels. *Intracellular c-di-AMP concentrations were measured by an enzyme-linked immunosorbent assay (ELISA) (Underwood et al., 2014). c-di-AMP was detected in both of E. faecalis (A) and E. faecium (B). (A) E. faecalis strains: The intracellular c-di-AMP level in Efc OG1RF_ΔliaR that knocks out LiaFSR signaling increases to 351±94 pM/OD$_{600}$ (Underwood et al., 2014), complementation of liaR in cis restores c-di-AMP levels. (B) E. faecium strains: the non-polar deletion mutant of liaR causes a small but not statistically-significant increase in Efm HOU503F_ΔliaR and Efm R497F_ΔliaR. Each c-di-AMP measurement was made*

from at least three independent biological measurements. (See Table 3.1 for strain

descriptions.)

4.2.2. LiaFSR does not directly regulate the expression of c-di-AMP synthase CdaA and phosphodiesterase GdpP and PgpH.

Since deletion of LiaR in *Efc* OG1EF lead to increased c-di-AMP levels, I performed quantitative PCR (qPCR) on the putative target genes in *Efc* OG1RF and *Efc* OG1RF_ Δ*liaR* to observe whether LiaFSR directly regulates c-di-AMP signals.

As expected, deletion of *liaR* effectively turned off LiaFSR pathway, and down regulated the transcription of *liaFSR* and *liaXYZ*, which are under LiaR regulation (Figure 4.2A) (Miller et al., 2013). However, qPCR of the potential target genes *gdpP*, *pgpH*, *cdaA* and *cdaR* did not show significant changes in transcription (Figure 4.2B). CdaA is the only known c-di-AMP synthase in *Efc* OG1RF, and CdaR is the regulator of CdaA (Rismondo et al., 2016; Rosenberg et al., 2015). GdpP and PgpH are c-di-AMP phosphodiesterases (Huynh et al., 2015). My data suggests that LiaFSR pathway regulate cellular c-di-AMP levels indirectly. For example, changes in LiaFSR signaling are known to alter pools of lipids and many other aspects of cellular physiology that are likely to be integrated within other regulatory networks that may, in turn, alter c-di-AMP levels (Reyes et al., 2015).

At present the only molecule known to regulate c-di-AMP phosphodiesterase activity is the inhibitor ppGpp (Section 3.3.4). *Efc* has two putative ppGpp synthases,

RelA and RelQ (Abranches et al., 2009). If LiaFSR regulates c-di-AMP degradation through ppGpp, the expression of ppGpp synthases should decrease in *Efc* OG1RF_ Δ*liaR*. However, I did not detect significant changes of *relA* and *relQ* expression with deletion of LiaR in *Efc* OG1RF (Figure 4.2B).

All of these observations suggest there are still as yet unidentified regulatory mechanisms interacting with the LiaFSR regulon to alter c-di-AMP levels. It is certainly possible that the as yet unknown activities of the *Efc* GdpP PAS and regulation of the DHH/DHHA1 domains may be the critical 'missing piece' of the puzzle that links LiaFSR to other regulatory networks. During my studies, I discovered a novel putative c-di-AMP phosphodiesterase XpaC which is under LiaR regulation and this will be discussed further in Section 4.4.
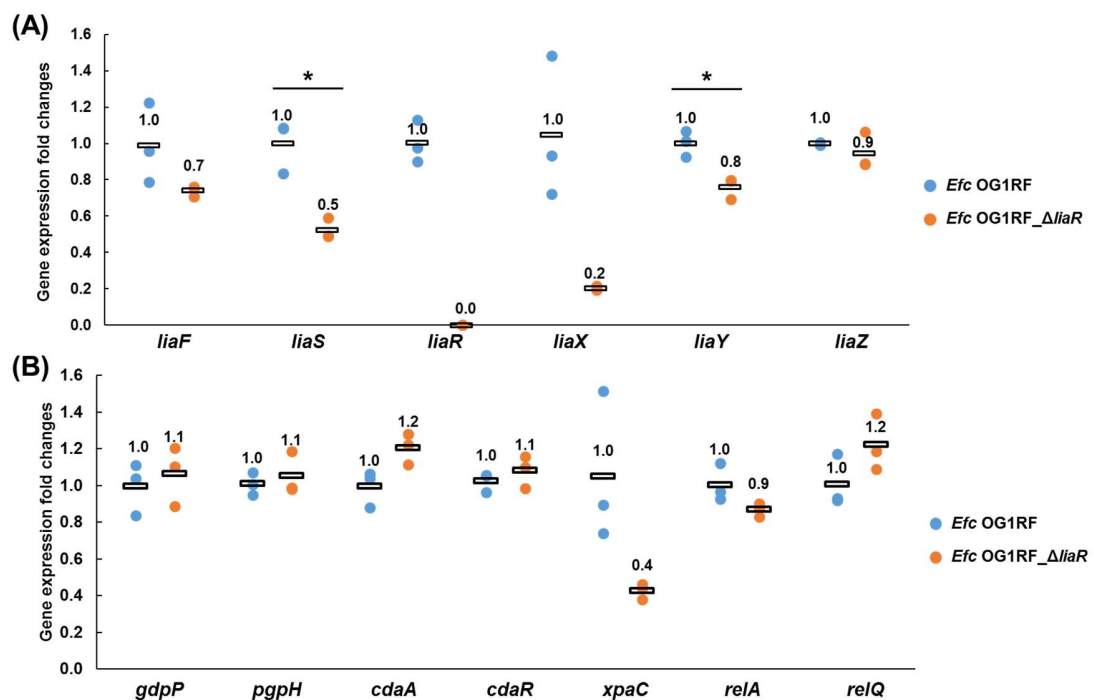
Figure 4.2 . Quantitative PCR of putative LiaFSR regulons and c-di-AMP related genes in _E. faecalis_ OG1RF_Δ_liaR_. _Transcription was analyzed in Efc OG1RF and Efc OG1RF_Δ_liaR. The non-polar deletion mutant of liaR removes the response regulator of the LiaFSR pathway, effectively "shutting off" the LiaFSR system. The transcription of liaFSR and liaXYZ operons are directly under LiaR regulation (Miller et al., 2013), and were down-regulated by deletion of liaR. Gene transcript levels of gdpP (coding c-di-AMP phosphodiesterase), pgpH (coding a putative c-di-AMP phosphodiesterase), cdaA (coding c-di-AMP synthase A, CdaA), cdaR (coding CdaR, a regulator of CdaA), relA and relQ (coding ppGpp synthase RelA and RelQ) did not change significantly with LiaR deletion (Abranches et al., 2009; Huynh et al., 2015; Rismondo et al., 2016, 2016)._

4.3. The LiaXYZ regulon interacts with the c-di-AMP network.

In addition to the adaptive mutations in LiaR and LiaF in response to DAP, a frame-shift mutation in a previously uncharacterized operon _liaXYZ_ was also identified (LiaX[V289fs]: previously referred as YvlB[V289fs]) (Miller et al., 2013). The roles LiaX, LiaY and LiaZ play in bacteria is still unclear but is under active investigation in our lab. LiaY (also referred as PspC) and LiaZ (also referred as YvlD) are membrane proteins (Davlieva et al., 2015a). LiaX (also referred as yvlB) is a potential signal sensor and interacts with LiaYZ (Davlieva et al., unpublished work). Since LiaX mutant was identified in DAP-resistant _E. faecalis_, and LiaX in under LiaR regulation, we hypothesized that LiaXYZ is embedded within the larger c-di-AMP network.

4.3.1. LiaX defects do not alter c-di-AMP signaling.

To test whether LiaX regulates cellular c-di-AMP levels, I first measured the c-di-AMP concentrations in *Efc* S613, and the experimental DAP-resistant strain *Efc* TDR7 with mutation *liaX*[V289fs] and cardiolipin synthase (*cls*[R217Q]) (Table 3.1) (Miller et al., 2013). As shown in Figure 4.3 A and B, the c-di-AMP concentration in *Efc* TDR7 was 2.4-fold higher than *Efc* S613 (268±97 pM/OD$_{600}$ versus 113±81 pM/OD$_{600}$) (Table 3.1), and did not change with DAP treatment. To rule out the possibility that *cls*[R217Q] in *Efc* TDR7 interferes c-di-AMP signaling, I tested c-di-AMP levels in wild-type *Efc* OG1RF, *Efc* OG1RF_*liaX*[1-289], and *Efc* OG1RF_Δ*liaX* (Table 3.1). Neither *liaX*[1-289] or Δ*liaX* affected intracellular c-di-AMP concentrations in *Efc* OG1RF (Figure 4.3 C and D), suggesting that LiaX defects are not enough to affect c-di-AMP signaling. On the other hand, *Efm* S447 CLS[R218Q], *cls*[R217Q] alter cardiolipin synthase activity which, in turn, alters cell membrane properties (Davlieva et al., 2013) that could certainly be linked indirectly to c-di-AMP levels. My data suggests c-di-AMP can report cell membrane changes, and participates in antibiotic-induced cell membrane stress response.
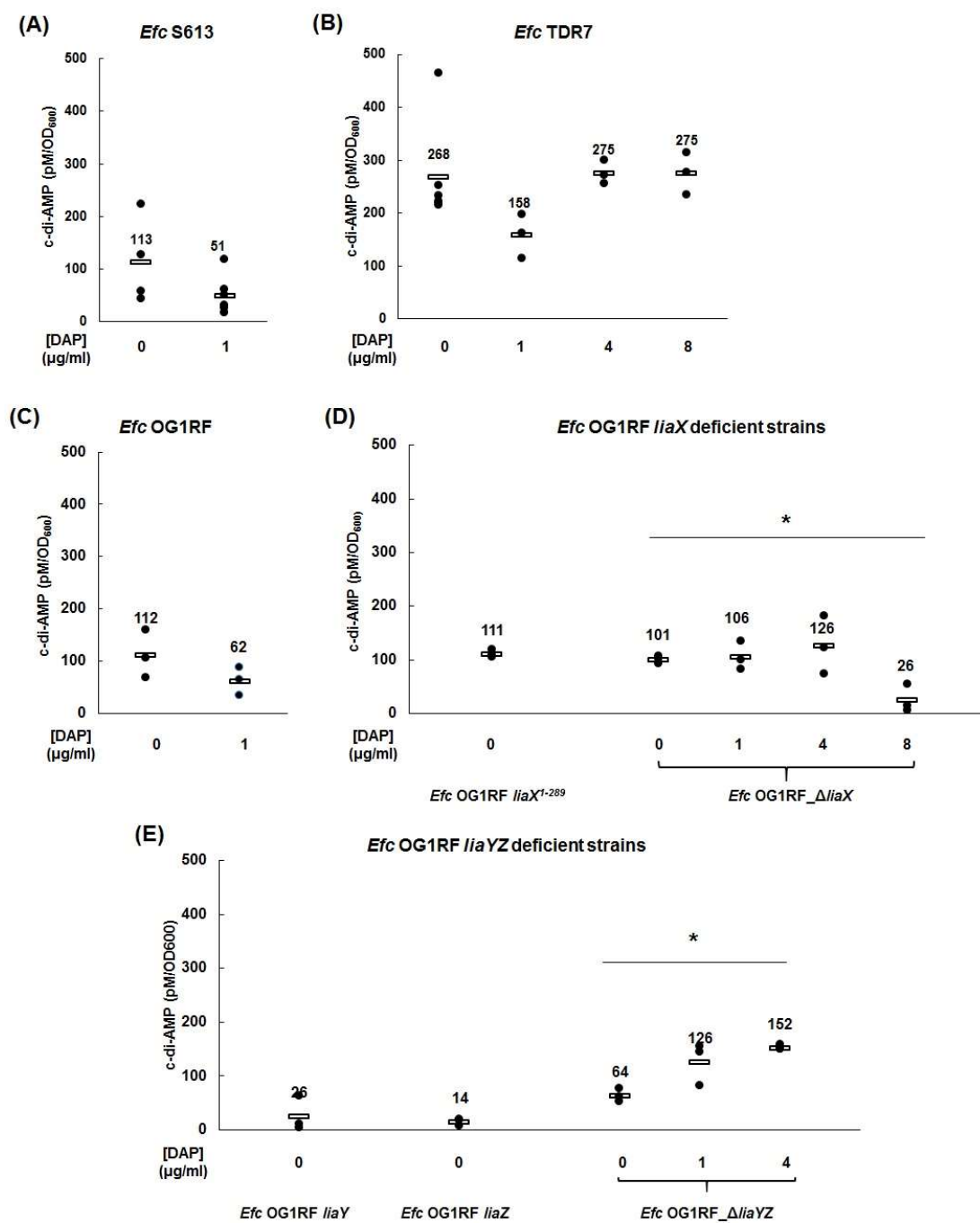
Figure 4.3 Intracellular c-di-AMP concentrations in *Efc liaXYZ* deficient strains.

Intracellular c-di-AMP concentrations were measured in Efc liaXYZ deficient strains by an enzyme-linked immunosorbent assay (ELISA) (Underwood et al., 2014)*. (A) The c-*

di-AMP levels in Efc S613 did not change with DAP treatment. (B) The c-di-AMP levels in Efc TDR7 were 2.4-fold higher than wild type, and did not change under DAP treatment. (C-D) liaX defects did not affect c-di-AMP concentration in Efc OG1RG, suggesting LiaX itself could not affect c-di-AMP signaling. (E) c-di-AMP concentrations decreased with LiaYZ defects. And c-di-AMP levels increased with higher DAP concentrations, suggesting LiaYZ was involved in c-di-AMP regulation. Each c-di-AMP measurement was made from at least three independent biological measurements. (See Table 3.1 for strain descriptions.)

4.3.2. LiaY and LiaZ are involved in c-di-AMP signaling.

As mentioned previously, LiaY and LiaZ are predicted to be membrane proteins (Davlieva et al., 2015a). The functions of LiaY and Z are still unclear, but as liaY and liaZ are in the same operon as liaX and under the regulation of LiaFSR, we reasoned that LiaYZ may be linked to the regulation of intracellular c-di-AMP levels.

To test this possibility, cell extracts from strains where *liaYZ* were knocked out (*Efc* OG1RF_Δ*liaY*, *Efc* OG1RF_Δ*liaZ*, and *Efc* OG1RF_Δ*liaYZ*) were examined (Table 3.1). In *Efc* OG1RF_Δ*liaY*, c-di-AMP levels decreased 77% to 26 ± 33 pM/OD$_{600}$ (Figure 4.3E and Table 3.1). In *Efc* OG1RF_Δ*liaZ*, c-di-AMP levels decreased 88% to 14 ± 7 pM/OD$_{600}$ (Figure 4.3E and Table 3.1). Deletion of LiaYZ also led to a 43% c-di-AMP decrease to 64 ± 12 pM/OD$_{600}$ (Figure 4.3E and Table 3.1).

liaYZ defects also made *Efc* OG1RF behave differently during DAP exposure. With 1 μg/ml DAP, the c-di-AMP levels in *Efc* OG1RF showed only a moderate decrease (Figure 4.3E). But c-di-AMP in *Efc* OG1RF_*ΔliaYZ* increased significantly with increased DAP treatment (Figure 4.3E). All of these data suggests LiaY and LiaZ are part of the larger c-di-AMP network.

4.4. XpaC is a putative c-di-AMP phosphodiesterase under LiaR regulation.

As discussed in Section 4.2, 'shutting off' the LiaFSR pathway leads to increased c-di-AMP levels in *Efc*, but the genes related to c-di-AMP synthesis and degradation (*cdaA*, *gdpP* and *pgpH*)are not under direct LiaR regulation (Figure 4.2). Taken together my data suggests that enterococci have as yet undiscovered c-di-AMP synthase/phosphodiesterases. I found one *Efc* S613 derived strain S613_D18A10 generated from the DAP adaptation assays showing up to ~14-fold higher c-di-AMP levels than wild-type *Efc* S613 (1493 ± 61 pM/OD_{600} versus 113 ± 81 pM/OD_{600}, Figure 4.4A), suggesting an important c-di-AMP regulator may have been mutated in its genome. I so analyzed the *Efc* S613 derived strains to find putative genes.
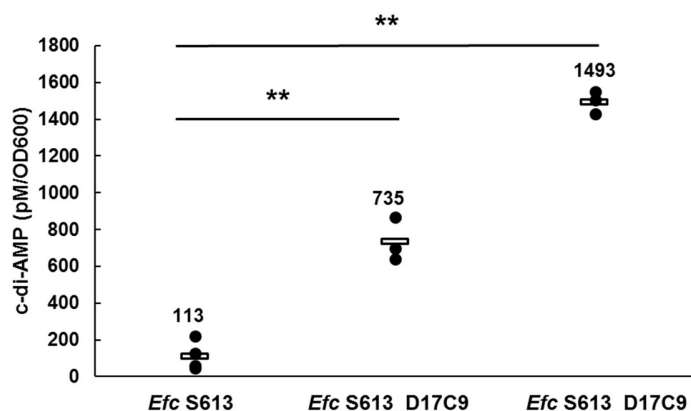
Figure 4.4 c-di-AMP levels in *Efc* S613 derived DAP-resistant strains. *c-di-AMP*

concentrations in Efc S613_D17C9 and Efc_D18A10 measured by an enzyme-linked

immunosorbent assay (ELISA) (Underwood et al., 2014)*. Each c-di-AMP measurement*

was made from at least three independent biological measurements. Please see Table

3.1 and Table 4.1 for strain descriptions.

4.4.1. Whole genome sequencing results of *E. faecalis* S613 derivative strains.
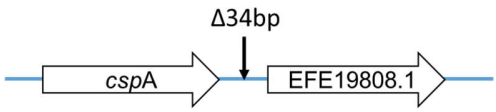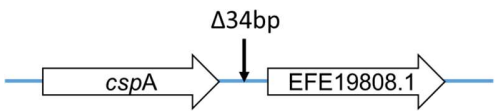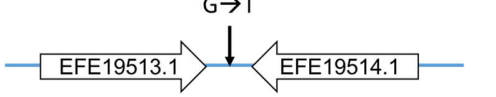
Two DAP-resistant S613 derivative strains *Efc* S613_D17C9 and *Efc*
S613_D18A10 were analyzed by whole genome sequencing (Table 4.1).

Efc S613_D17C9 has *lia*F$^{\Delta I177}$, produces a constitutively "on" state of the
LiaFSR pathway (Miller et al., 2013). Two additional mutations not observed in that
earlier study by Miller et al., (2013) were identified in this strain, including a silent
mutant *prg*U^{G105G} (with unknown function), and a 34bp intergenic deletion between
*csp*A (coding a putative cold-shock DNA-binding domain protein) and EFE19808.1

(coding a YdcF-like hypothetical cytidylyltransferase family protein). These new mutations were likely missed in our earlier studies because the reference genomes available at that time had significant gaps between contigs and thus the genomes were not closed.

Efc S613_D18A10 has $liaF^{\Delta I177}$ and 5 additional mutations (Table 4.1). Besides the same 34bp intergenic deletion ($cspA$/EFE19808.1) as in S613_D17C9, and a silent mutant $prgU^{N103N}$, Efc S613_D18A10 also has $xpaC^{K163fs}$ (coding 5-bromo-4-chloroindolyl phosphate hydrolysis protein), $dacA^{E554K}$ (coding D-alanyl-D-alanine carboxypeptidase), and an intergenic mutation G$\rightarrow$T between EFE19514.1 (coding a hypothetical protein) and EFE19513.1 (coding a putative ABC transporter or a putative permease).

Table 4.1 Genotypes of *E. faecalis* S613 derivative strains.

Strains	Genotype	Description
S613_D17C9	*liaF*$^{\Delta I177}$	LiaF$^{\Delta I177}$ is supposed to keep LiaFSR pathway in 'on' state.
	prgU^{G105G}	PrgU is an unknown functional protein.
	Δ34bp — *cspA* → EFE19808.1 →	CspA is a putative cold-shock DNA-binding domain protein. EFE19808.1 encodes a YdcF-like hypothetical cytidylyltransferase family protein.
S613_D18A10	*liaF*$^{\Delta I177}$	LiaF$^{\Delta I177}$ is supposed to keep LiaFSR pathway in 'on' state.
	xpaC^{K163fs}	XpaC is a 5-bromo-4-chloroindolyl phosphate hydrolysis protein.
	dacA^{E554K}	DacA is D-alanyl-D-alanine carboxypeptidase.
	prgU^{N103N}	PrgU is an unknown functional protein.
	Δ34bp — *cspA* → EFE19808.1 →	CspA is a putative cold-shock DNA-binding domain protein. EFE19808.1 encodes a hypothetical cytidylyltransferase family protein.
	G→T — EFE19513.1 → ← EFE19514.1	EFE19513.1 encodes a putative a putative ABC transporter or a putative permease. EFE19514.1 encodes a hypothetical protein.

Efc S613_D18A10 has a very high intracellular c-di-AMP level (1493±61 pM/OD$_{600}$), which is 2-fold higher than S613_D17C9 (735±118 pM/OD$_{600}$, p=0.002) (Figure 4.4A, Table 3.1). By comparing their genotypes, it is likely that *xpa*C, encoding a 5-bromo-4-chloroindolyl phosphate hydrolysis protein, may be the main reason. XpaC is annotated as having activity against 5-bromo-4-chloroindolyl phosphate but the actual *in vivo* substrate remains entirely unknown. The physiological function of XpaC is also unclear. XpaC may be a c-di-AMP phosphodiesterase, so the frame shift mutant (XpaC$^{1-163fs}$) may abolish or decrease its phosphodiesterase activity, leading to the increased c-di-AMP levels observed in *Efc* S613_D18A10 compared with *Efc* S613_D17C9.

4.4.2. XpaC is under direct LiaR regulation.

As mentioned in Section 4.2.1, deletion of *liaR* results in increased c-di-AMP concentrations. If *xpaC* is a c-di-AMP phosphodiesterase under LiaR regulation, XpaC expression should be down-regulated in *liaR* deficient strains. Indeed, as Figure 4.2B shows, *xpaC* transcription is significantly decreased in *Efc* OG1RF_Δ*liaR*, which agrees with my hypothesis.

To further investigate the relationship between LiaR and XpaC, I wanted to know how activated LiaR regulates *xpaC*. As DAP-induced cell membrane stress can 'turn on' the LiaFSR pathway, I incubated *Efc* S613 with DAP, and analyzed gene expression by qPCR. As expected, the LiaFSR pathway was activated by DAP exposure, and upregulated *liaFSR* and *liaXYZ* (Figure 4.5A). However, the activated

LiaFSR regulon only upregulated *xpaC*, but not other putative c-di-AMP synthases and phosphodiesterases (Figure 4.5A). Similar trends were also observed in *Efc* OG1RF (Figure 4.5B). I also identified a putative consensus motif in the upstream region of *xpaC* for that further corroborate my observation that *xpaC* is directly regulated by LiaR (Davlieva et al., 2015a).

(A)
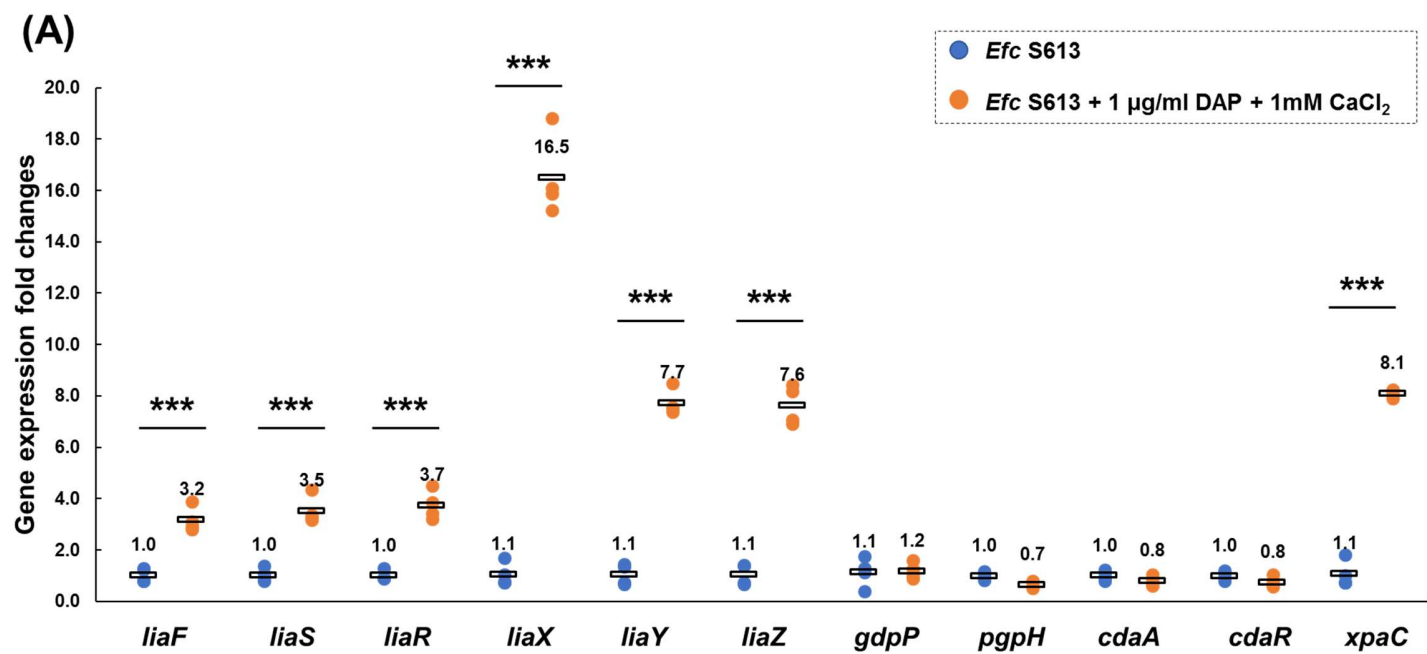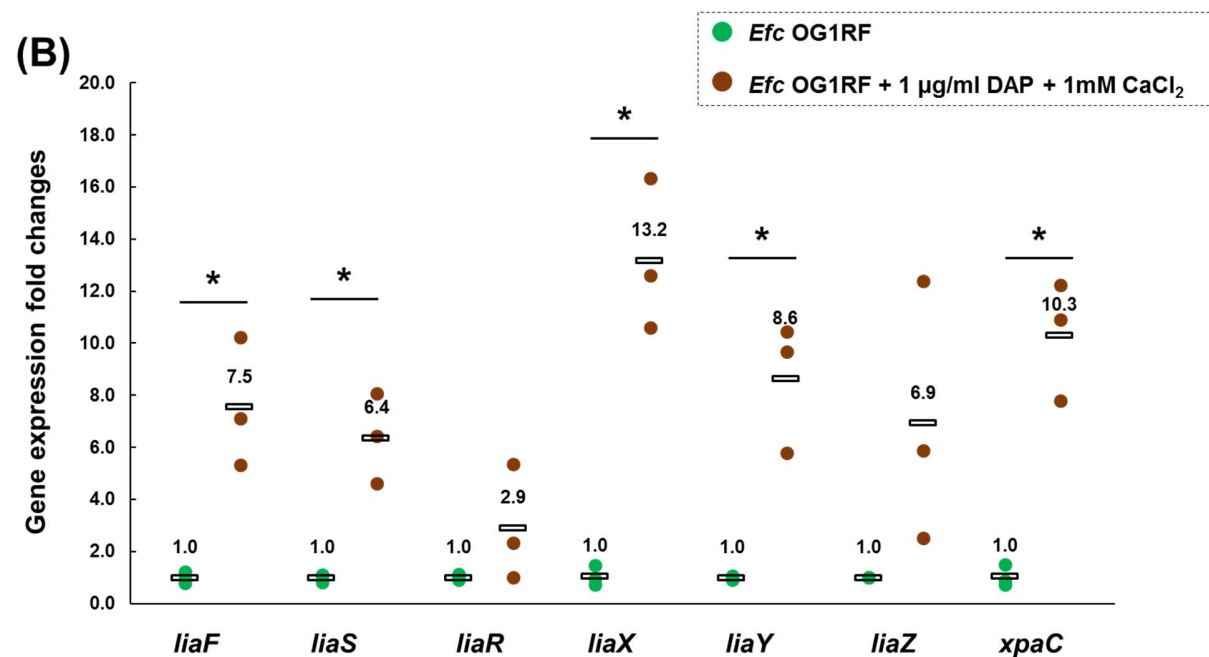
Figure 4.5 Quantitative PCR shows *xpaC* is under LiaR regulation in *E. faecalis*. *qPCR results show the gene expression in Efc S163 and Efc OG1RF during daptomycin exposure. daptomycin activates LiaFSR pathway, and upregulates LiaFSR and LiaXYZ, as well as the putative c-di-AMP phosphodiesterase XpaC. Gene transcript levels of gdpP (coding c-di-AMP phosphodiesterase), pgpH (coding a putative c-di-AMP phosphodiesterase), cdaA (coding c-di-AMP synthase A, CdaA), cdaR (coding CdaR, a regulator of CdaA) did not change significantly under daptomycin stress (Abranches et al., 2009; Huynh et al., 2015; Rismondo et al., 2016, 2016). Each measurement was made from at least three independent biological measurements.*

```
-150 TTCTTAGGAT TTCACTAAAT CATAAAATAC ATCTTCCGCT GTATGTCTTT
-100 TCTCTCACAG AGTATGCTAA AATAACTATT GTAACGAGAG CTGACTCTTT
 -50 CGAGGATTAG ATAGATAGGA GGAACTATAT AAATGAACAA ATTAAATACA
```

Figure 4.6 LiaR consensus sequence in the upstream of *xpaC*. *Putative LiaR consensus sequence (-105, -90) in the upstream of xpaC in Efc S613. The consensus sequences are highlighted in yellow. The gene start codons are highlighted in green.*

4.4.3. Current studies to elucidate Xpac structure and function.

To study the function and structure of XpaC, I attempted to clone *Efc* Xpac, the DAP adaptive mutant *Efc* XpaC[K163fs] and XpaC homologs from other Gram-positive organisms to inducible expression vectors pET-28a (for expression in *E. coli*) and pMSP3535 (for expression in *Efc* OG1RF).

In the first stage of molecular cloning, I made 30 different constructs (Table 4.2), and used *E. coli* DH5α to select ligation products. After several trials, only 4 constructs of *Efc* Xpac with N-terminal 6xHis-tag were successfully generated (Construct #1-4 in Table 4.2). Although colony PCR showed positive results for other constructs, *E. coli* lost the recombinant plasmid or the insert during overnight incubation. Expression of Constructs #1-4 could be induced in *E. coli* BL21, but the BL21 strains carrying the recombinant plasmids grew much slower than wild type BL21 even before IPTG was added to induce expression. These observations suggest even leaky expression of XpaC is very toxic for *E coli.*

Genes coding *xpaC* have only be identified in Gram-positive organisms, such as enterococci and staphylococci, suggesting Xpac is not toxic to Gram-positive bacteria. *B. subtilis* is a well-studied model organism, uses c-di-AMP as second messenger as well, and does not have *xpaC* in its genome, which makes it a potentially good host to over-express XpaC for functional studies (Oppenheimer-Shaanan et al., 2011a). My future work is to over express XpaC in *B. subtilis*. If XpaC does have c-di-AMP phosphodiesterase activity, I should be able to observe decreased c-di-AMP levels with XpaC overexpression.

Table 4.2 Summary of XpaC constructs made in this study.

#	Source Bacteria	Construct[b]	Vector	6xHis-tag	TEV cleavage site [Y/N]
1	*Efc* S613	XpaC	pET-28a	N-terminal	N
2	*Efc* S613	XpaC	pET-28a	N-terminal	Y
3	*Efc* S613	XpaC[K163fs]	pET-28a	N-terminal	N
4	*Efc* S613	XpaC[K163fs]	pET-28a	N-terminal	Y
5	*Efc* S613	XpaC	pET-28a	C-terminal	N
6	*Efc* S613	XpaC[K163fs]	pET-28a	C-terminal	N
7	*Efc* S613	XpaC	pMSP3535	No tag	N
8	*Efc* S613	XpaC	pMSP3535	N-terminal	N
9	*Efc* S613	XpaC	pMSP3535	N-terminal	Y
10	*Efc* S613	XpaC	pMSP3535	C-terminal	N
11	*Efc* S613	XpaC	pMSP3535	C-terminal	Y
12	*Efc* S613	XpaC[1-163]	pMSP3535	No tag	N
13	*Efc* S613	XpaC[1-163]	pMSP3535	N-terminal	N
14	*Efc* S613	XpaC[1-163]	pMSP3535	N-terminal	Y
15	*Efc* S613	XpaC[1-163]	pMSP3535	C-terminal	N

16	*Efc* S613	XpaC$^{1-163}$	pMSP3535	C-terminal	Y
17	*Efc* S613	XpaC^{E163fs}	pMSP3535	No tag	N
18	*Efc* S613	XpaC^{K163fs}	pMSP3535	N-terminal	N
19	*Efc* S613	XpaC^{K163fs}	pMSP3535	N-terminal	Y
20	*Efc* TX1467	XpaC	pET-28a	N-terminal	Y
21	*Efc* TX1467	XpaC	pET-28a	N-terminal	N
22	*Efc* TX1467	XpaC	pET-28a	C-terminal	N
23	*Efc* TX1467	XpaC^{K163fs}	pET-28a	N-terminal	Y
24	*Efc* TX1467	XpaC^{K163fs}	pET-28a	N-terminal	N
25	*Efc* TX1467	XpaC^{K163fs}	pET-28a	C-terminal	N
26	*Efm* HOU503	XpaC	pET-28a	N-terminal	Y
27	*Efm* HOU503	XpaC	pET-28a	C-terminal	N
28	MRSA 131[a]	XpaC	pET-28a	N-terminal	Y
29	MRSA 131[a]	XpaC	pET-28a	N-terminal	N
30	MRSA 131[a]	XpaC	pET-28a	C-terminal	N

[a]MRSA 131: Methicillin-resistant Staphylococcus aureus MRSA131.

[b]XpaC constructs: the frameshift (AAAC) deletion in XpaC generates a -RMKN tail after residue lysine 163. The construct XpaC$^{1-163}$ only covers the first 163 residues. The construct XpaC^{K163fs} covers the following -RMKN tail.

4.5. Discussion.

Since GdpP^{I440S} was identified in association with changes within the LiaFSR pathway, I tested the effect of the mutations in LiaFSR pathway upon *in vivo* c-di-AMP levels. I found that the deletion of *liaR* (*Efc* OG1RF_Δ*liaR*) led to increased c-di-AMP levels (Table 3.1 and Figure 4.1) and I observed a significant decrease in c-di-AMP levels in strains with *liaYZ* deletions (Figure 4.3).

While it is tempting to link c-di-AMP levels to LiaFSR signaling, the nature of this association is unclear. My qPCR data shows that the transcription of potential target genes *cdaA*, *gdpP* and *pgpH* were not altered in LiaR deletion strains (Figure 4.2), suggesting that the effects of mutations in LiaFSR signaling on cellular c-di-AMP levels are indirect. It is possible that cellular c-di-AMP pools will also respond dynamically through several stress regulons including LiaFSR. In addition, an unknown cofactor or stress may switch the function of GdpP from c-di-AMP phosphodiesterase (DHH/DHHA1 domain activity) to c-di-AMP synthase (putative GGDEF activity) (Hallberg et al., 2016). While I was unable to demonstrate that the *Efc* GdpP GGDEF domain had c-di-AMP synthase activity *in vitro*, GGDEF domains of other proteins do have demonstrated synthase activity (Hallberg et al., 2016). How the PAS domain of GdpP might regulate the known DHH/DHHA1 domain phosphodiesterase activity as well as the potential cryptic activities of the GGDEF domain also remains unknown. Additionally, other as yet unidentified regulatory mechanisms may also be involved in the system. For example, *xpaC* is under LiaR regulation (Figure 4.5), and the mutant *xpaC*^{K163fs} was identified in *Efc* S613_D18A10

with greatly increased intracellular c-di-AMP levels (Figure 4.4 and Table 3.1), suggesting that XpaC is a *bone fide* c-di-AMP phosphodiesterase and is involved in LiaR-mediated cell wall stress response. Although the complete signaling mechanism by which LiaFSR regulates c-di-AMP level remains to be fully elucidated, it is evident that membrane damage is faithfully transduced and converted into altered levels of c-di-AMP.

In summary, I have shown that c-di-AMP is an important second messenger in enterococci. Moreover, LiaFSR and LiaXYZ regulate c-di-AMP pools *in vivo* at physiologically relevant levels and that there is a clear, but indirect, role for the LiaFSR regulon. Further, my data shows that although there is no direct linear correlation between DAP resistance and c-di-AMP my findings suggest that c-di-AMP signaling constitutes a key aspect of the membrane damage response with important consequences for our understanding of how enterococci respond to DAP and other cationic antimicrobial peptides.

Chapter 5

Structural studies of GdpP

5.1. Structural studies of full-length wild-type *Efc* GdpP

Efc GdpP has five domains: two transmembrane motifs on its N-terminus, one PAS domain, one GGDEF domain with weak ATPase activity, and one DHH/DHHA1 domain with c-di-AMP specific phosphodiesterase activity (Figure 1.1). To date, there are no structures for any full-length proteins in this family. A high-resolution structure of GdpP would be very informative as it would reveal the overall domain structure as well as a detailed view of the actives sites responsible for its biological activities. Also, any structures solved from crystals grown with/without potential cofactors/substrates/products would potentially reveal how the activities are regulated, and the molecular mechanism for how GdpP responds and controls cyclic dinucleotide signaling.

5.1.1. Crystallization of full-length *Efc* GdpP.

    Efc GdpP with an N-terminal His-tag was over-expressed in *E. coli* BL21, purified by Ni-NTA and gel filtration chromatography (Figure 5.1) (please see Section 2.4 for details). The final yield of *Efc* GdpP was 0.1 mg/L to 0.2 mg/L, which was very low. Since Rao's group reported that *B. subtilis* GdpP had a heme-binding PAS domain, and the binding of heme helped make this protein more stable, I investigated whether the addition of heme might increase protein yield (Rao et al., 2011). The expression conditions for GdpP were optimized by adding $10\mu M$ heme with 0.5mM IPTG during induction. The yield of protein was improved by at least two times, and 0.4 mg/L to 0.5mg/L protein could be obtained after purification.
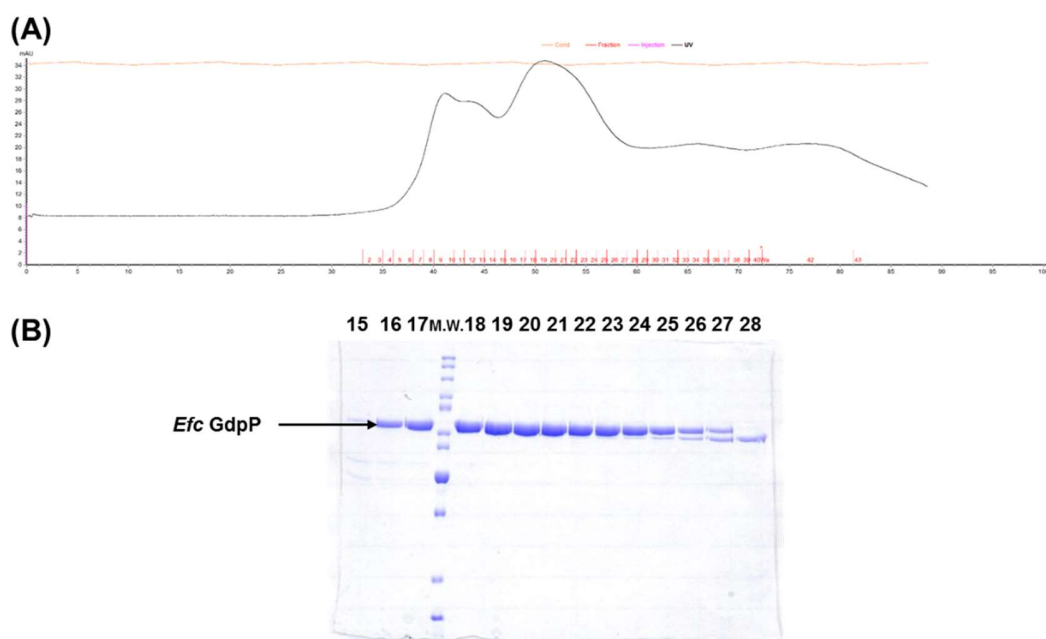
Figure 5.1 Purification of *Efc* GdpP. *Protein was purified on a Superdex-200 size exclusive column (A) and analyzed by SDS-PAGE (B). The numbers correspond to elution fractions. M.W.: protein molecular weight ladder.*

Efc GdpP was concentrated to $A_{280}=10$ (11.18 mg/ml) to set up sparse matrix screening for crystals. The crystallization conditions for primary screens are summarized in Table 5.1. Some small and micro crystals were obtained from primary screens. Small crystals could grow in five conditions and were further optimized (Table 5.2).

These five crystallization conditions were manually optimized by varying protein concentration, buffer pH, precipitant concentration, drop size, temperature, ratio between protein and mother liquor, and vapor diffusion method. Only some

small crystals were obtained during the optimization of Condition A (Figure 5.2A). And several big crystals were obtained from the optimization of Condition B (Figure 5.2B), C (Figure 5.2C) and D (Figure 5.2D). Unfortunately, all of them diffracted to 7.9Å to 12Å.

Table 5.1 Summary crystallization conditions for primary screens.

Catalog No.	Crystal Screen Kit	Temperature
Hampton HR2-130	Crystal Screen HT	
Hampton HR2-134	Index HT	
Hampton HR2-136	SaltRx HT	
QIAGEN 130901	Classics Suits	
QIAGEN 130904	PEGs Suits	
QIAGEN 130905	AmSO$_4$ Suits	
QIAGEN 130906	MPD Suite	
QIAGEN 130907	Anion Suits	4°C, 10°C, 20°C
QIAGEN 130909	pHClear Suite	
QIAGEN 130910	pHClear II Suite	
QIAGEN 130911	MbClass Suite	
QIAGEN 130912	MbClass II Suite	
QIAGEN 130916	PEGs II Suite	
QIAGEN 130920	JCSG+ Suits	
QIAGEN 130923	Classics II Suite	

Table 5.2 *Efc* GdpP crystallization conditions for optimization.

#	Crystallization Condition	Temperature
A	3.5M Sodium formate pH7.0.	10°C
B	1.0M Succinic acid pH 7.0, 0.1M HEPES pH 7.0, 1% w/v PEG 2000	10°C
C	35% v/v Tacsimate pH7.0	10°C
D	0.2M Magnesium Chloride, 0.1M HEPES Sodium Salt pH7.5, 30% (v/v) PEG 400	10°C
E	0.2M Magnesium acetate, 0.1M Sodium cacodylate pH6.5, 20% (w/v) PEG 8000.	10°C
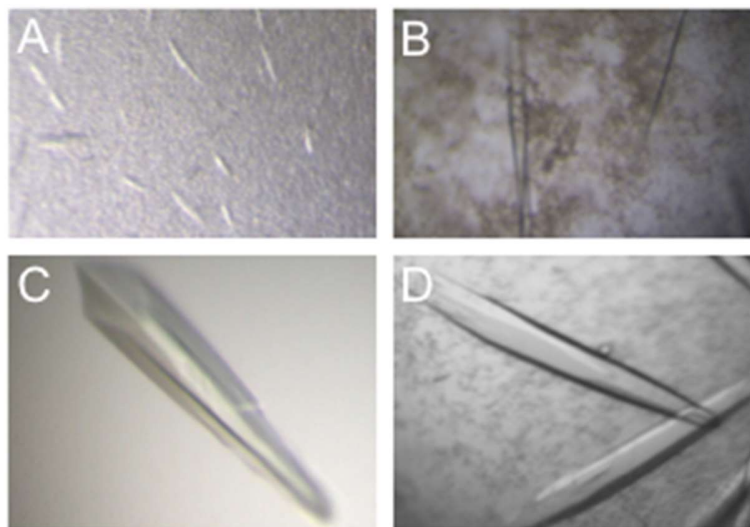
Figure 5.2 Crystals of full-length wild-type *Efc* GdpP grew in optimized conditions. *(A) Crystals grew in: 3.5M sodium formate pH7.0; (B) 1.15M succinic acid pH6.5, 0.1M HEPES pH6.5, 1% (w/v) PEG 2000 at 10°C; (C) 32% (v/v) tacsimate pH7.0 at 10°C; (D) and 0.1M magnesium chloride, 0.1M HEPES sodium salt pH7.0, 20% (v/v) PEG 400 at 10°C.*

The two crystals grown in Condition E (Table 5.2) in primary screens diffracted to 3.5 Å and 5Å (Figure 5.3A). But in the following optimizations, crystals would not grow spontaneously and so trays were set up by micro seeding using a seed bead kit (Hampton HR2-320) to establish reproducible crystal growth. Additive Screen (Hampton HR2-428), Silver Bullets Bio HT (Hampton HR2-088), and Detergent Screen HT (Hampton HR2-406) were also screened to optimize crystallization. Since *Efc* GdpP has ATPase and c-di-AMP specific phosphodiesterase

activities, its substrates (ATP and c-di-AMP), products (ADP and 5'pApA), inhibitors (AMPPNP and ppGpp), and other adenosine derivatives (such as AMP and cAMP) were also tried as additives to optimize this condition. The putative PAS domain cofactors, such as heme, bilirubin and biliverdin, were also screened. Several big crystals were obtained with ADP as an additive (Figure 5.3B).

Crystals were mounted and frozen with in cryo buffer optimized using Hampton Research Crystal Screen Cryo (HR2-122). The optimal cryo buffer contains 70% mother liquor (v/v) and 30% glycerol (v/v). Crystals were sent to Advanced Photon Source Synchrotron, and data were collected with beamline 21-TD-D. The best crystal diffracted to 3.3Å (Figure 5.3C and Table 5.3). Data was collected with 250mm distance, 1 degree oscillation angle and 1s exposure time.
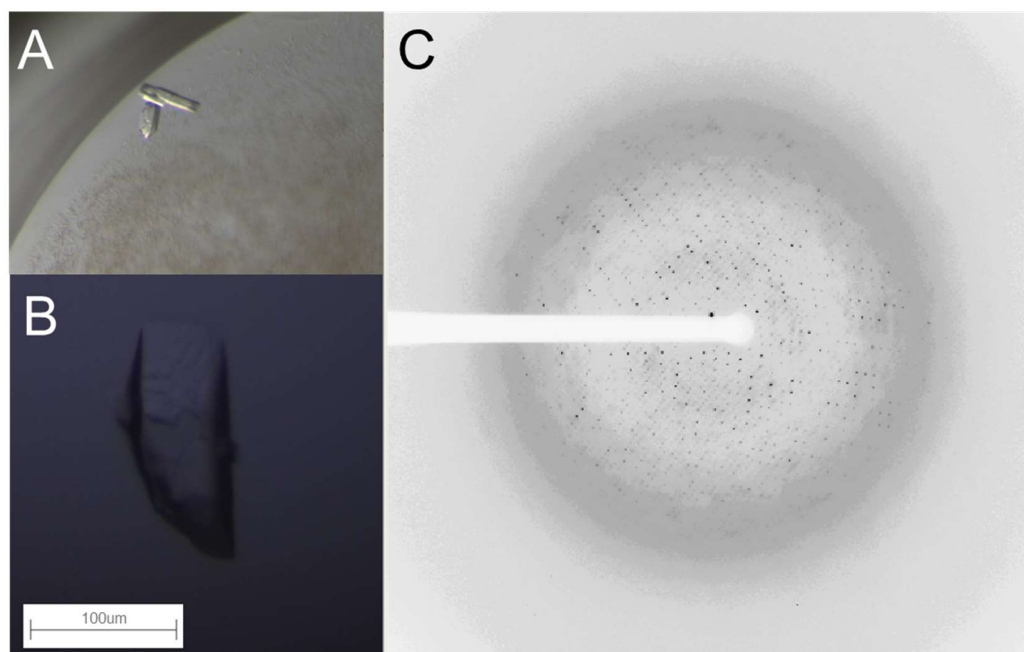
Figure 5.3 Crystals of *Efc* GdpP. *(A) Before optimization: crystals grown in 0.2M magnesium acetate, 0.1M sodium cacodylate pH6.5, and 20% (w/v) PEG 8000 at 10°C. (B) After optimization: Crystal grown in 0.2M magnesium acetate, 0.1M sodium cacodylate pH 6.5, 5% PEG8000, and 675µM ADP at 10°C. (C) Figure shows the diffraction of Efc GdpP crystal.*

Table 5.3 Data collection statistics of wild type full-length *Efc* GdpP.

Parameter	
Space group	P1
Unit cell parameters	
a, b, c (Å)	114.03, 147.33, 164.83
α, ß, γ (°)	86.58, 79.95, 89.01
Resolution limits (Å)	40.0-3.30 (3.36-3.30)
Total number of observations	608,957
Number of unique reflections	155,170
I/ σI	7.4 (2.77)
Completeness (%)	98.9 (98.3)
R_{merge} (%)	9.6 (85.2)

HKL2000 was used to index the data set. The crystal had low symmetry, and can only be indexed under P1 space group (Table 5.3). The average R_{merge} was 9.6%. The R_{merge} for the highest resolution shell 3.36Å-3.30Å is 0.852 (Table 5.4). The completeness is higher than 98% (Table 5.5). The redundancies are higher than 3.8 (Table 5.6).

Table 5.4 Summary of reflections intensities and R-factors by shells.

Shell Lower	Upper	Average	Average		Norm.	Linear	Square
limit	Angstrom	I	error	stat.	Chi**2	R-fac	R-fac
40.00	8.93	466.1	8.8	4.6	2.616	0.037	0.040
8.93	7.10	196.7	4.4	2.9	2.173	0.045	0.043
7.10	6.20	89.0	2.8	2.2	1.800	0.060	0.053
6.20	5.64	66.1	2.6	2.2	1.519	0.068	0.057
5.64	5.24	70.4	2.9	2.5	1.432	0.070	0.057
5.24	4.93	76.2	3.3	2.9	1.379	0.071	0.057
4.93	4.68	78.9	3.6	3.2	1.359	0.074	0.058
4.68	4.48	69.5	3.7	3.4	1.303	0.085	0.065
4.48	4.31	62.5	3.9	3.6	1.230	0.097	0.074
4.31	4.16	51.9	3.9	3.7	1.173	0.116	0.084
4.16	4.03	42.7	4.1	3.9	1.102	0.141	0.099
4.03	3.91	36.7	4.2	4.1	1.031	0.167	0.117
3.91	3.81	31.9	4.4	4.3	0.995	0.196	0.135
3.81	3.72	23.7	4.6	4.5	0.979	0.272	0.192
3.72	3.63	20.8	4.8	4.7	0.966	0.320	0.230
3.63	3.55	17.4	5.0	4.9	0.973	0.401	0.280
3.55	3.48	14.5	5.1	5.1	0.951	0.485	0.345
3.48	3.42	12.3	5.2	5.2	0.933	0.583	0.402
3.42	3.36	9.8	5.3	5.3	0.924	0.738	0.503
3.36	3.30	8.7	5.4	5.4	0.915	0.852	0.585
All reflections		72.2	4.4	3.9	1.285	0.096	0.052

Table 5.5 Summary of the completeness by shells.

Shell		I/Sigma in resolution shells:								
Lower	Upper	% of of reflections with I / Sigma less than								
limit	limit	0	1	2	3	5	10	20	>20	total
40.00	8.93	1.3	2.7	4.4	6.2	9.6	17.9	32.9	65.2	98.1
8.93	7.10	1.7	4.4	7.7	10.8	16.5	28.1	45.9	53.3	99.2
7.10	6.20	2.6	7.4	13.0	18.2	27.0	41.5	57.3	42.1	99.5
6.20	5.64	3.5	9.5	16.4	22.9	32.7	47.8	63.0	36.4	99.5
5.64	5.24	4.1	10.7	17.3	23.5	33.8	49.0	64.5	34.8	99.4
5.24	4.93	3.9	10.0	17.1	24.2	34.2	49.6	65.3	34.0	99.4
4.93	4.68	4.5	11.5	18.7	25.7	35.8	50.5	67.0	32.2	99.2
4.68	4.48	5.8	13.3	21.3	28.5	39.4	54.7	70.2	29.0	99.2
4.48	4.31	6.2	13.8	23.2	30.8	42.2	58.8	75.2	24.0	99.2
4.31	4.16	7.3	17.2	27.3	35.8	47.8	62.8	79.0	20.1	99.1
4.16	4.03	9.5	21.3	33.0	42.4	53.9	68.5	83.7	15.4	99.1
4.03	3.91	10.7	24.0	36.9	46.4	58.3	72.6	86.4	12.5	98.9
3.91	3.81	11.2	26.1	40.4	50.2	62.3	76.6	89.3	9.7	99.0
3.81	3.72	13.5	31.2	47.3	57.6	68.7	82.5	92.9	5.9	98.8
3.72	3.63	14.2	32.2	49.6	60.2	71.7	85.1	94.2	4.4	98.6
3.63	3.55	16.4	37.2	54.9	65.5	76.2	88.0	95.8	2.8	98.6
3.55	3.48	18.1	40.4	58.9	68.6	79.6	90.4	96.8	1.8	98.5
3.48	3.42	20.5	44.0	62.4	72.7	82.7	92.2	97.0	1.4	98.3
3.42	3.36	22.6	48.2	67.9	77.9	86.7	94.3	97.8	0.8	98.5
3.36	3.30	22.9	50.1	69.7	79.7	88.1	95.4	98.0	0.3	98.3
All hkl		10.0	22.8	34.4	42.4	52.4	65.3	77.6	21.3	98.9

Table 5.6 Summary of redundancies by shells.

Shell		Average Redundancy Per Shell
Lower limit	Upper limit	
40.00	8.93	3.8
8.93	7.10	3.9
7.10	6.20	3.9
6.20	5.64	4.0
5.64	5.24	4.0
5.24	4.93	4.0
4.93	4.68	4.0
4.68	4.48	4.0
4.48	4.31	4.0
4.31	4.16	4.0
4.16	4.03	4.0
4.03	3.91	4.0
3.91	3.81	3.9
3.81	3.72	3.9
3.72	3.63	3.9
3.63	3.55	3.9
3.55	3.48	3.9
3.48	3.42	3.9
3.42	3.36	3.9
3.36	3.30	3.9
All hkl		3.9

5.1.2. Crystallization of selenomethionine *Efc* GdpP.

To obtain the phases for structure determination, I prepared selenomethionine (Se-Met) *Efc* GdpP by replacing the Met by Se-Met for single-wavelength anomalous dispersion (MAD). There are 20 methionines in *Efc* GdpP. To prepare Set-Met *Efc* GdpP, protein was expressed in minimal medium with Se-Met and other amino acids supplied, and purified using the same protocols as the wild type (Figure 5.4 A, B). Large scale crystal screens were set up using Se-Met containing protein. The Se-Met *Efc* GdpP crystals with best diffraction were grown in the same conditions as the wild-type *Efc* GdpP (0.2M magnesium acetate, 0.1M sodium cacodylate pH 6.5, 5% PEG8000, and 675μM ADP), and diffracted to 8Å (Figure 5.4C).
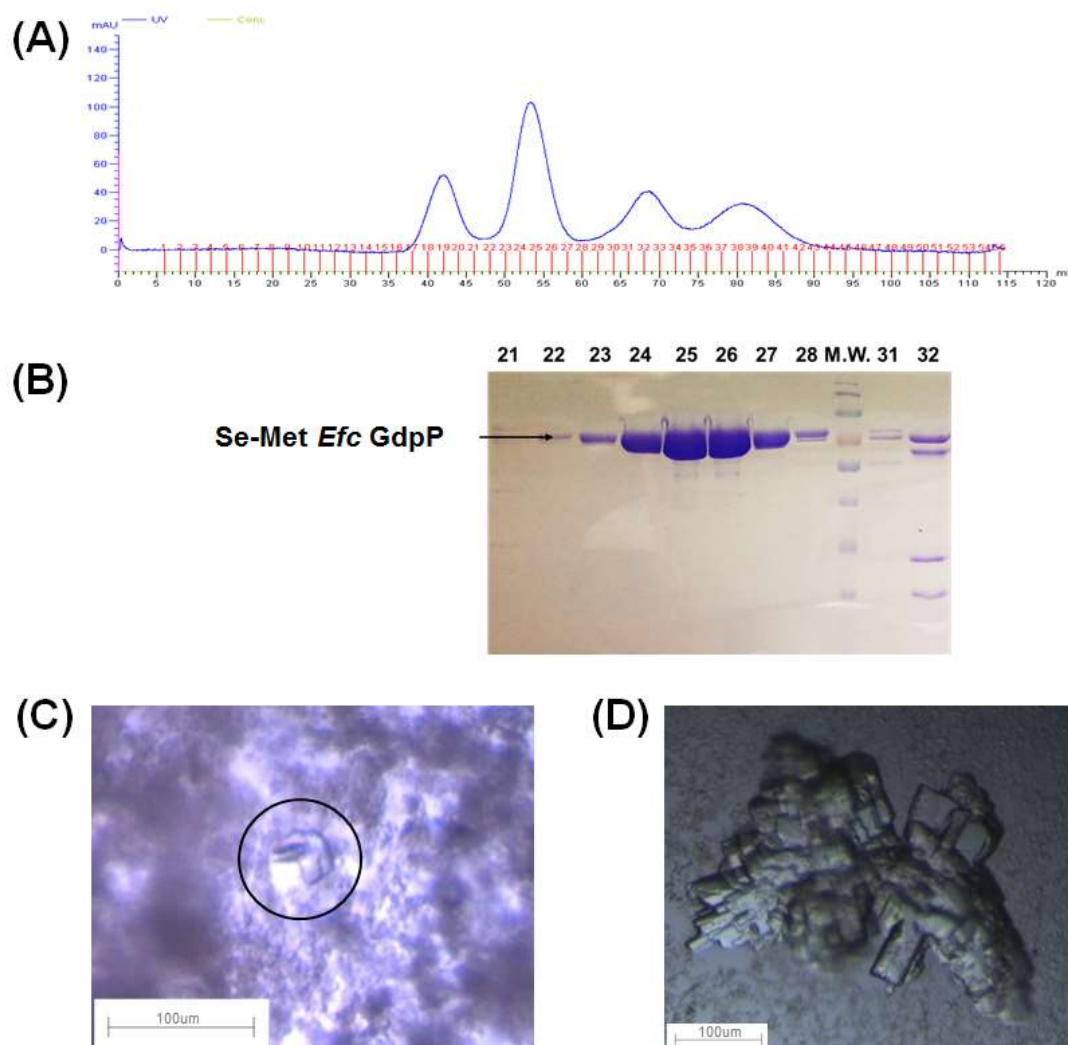
Figure 5.4 Purification and crystallization of Se-Met *Efc* GdpP. *Se-Met Efc GdpP was purified on a Superdex-200 size exclusive column (A) and analyzed by SDS-PAGE (B). The numbers correspond to elution fractions. M.W.: protein molecular weight ladder. (C) Se-Met Efc GdpP crystals grown in 0.2M magnesium acetate, 0.1M sodium cacodylate pH 6.5, 5% PEG8000, and 675µM ADP at 10°C. (D) Se-Met Efc GdpP crystals*

grown in 0.24M magnesium acetate, 0.1M sodium cacodylate pH6.5, 4% PEG8000, 6.5% pluronic F-68, and 675µM ADP at 10°C.

To further optimize Se-Met *Efc* GdpP crystals, I set up trays and varied buffer pH, protein concentration, precipitant concentration, and ratios between Se-Met *Efc* GdpP and ADP. I screened chemical reagents from Detergent Screen (Hampton HR2-408), Additive Screen HT (Hampton HR2-138), and Silver Bullet (Hampton HR2-088). I found that pluronic F-68 improved diffractions the most to 3.8Å (Figure 5.4D). However single crystals did not grow in this condition, so I broke the crystal cluster and mounted single crystals for data collection. Resolution of Se-Met *Efc* GdpP crystal was not high enough for phase determination.

To further optimize the diffraction, I prepared Se-Met *Efc* GdpP with lysine methylation as described in (Kim et al., 2008) (Figure 5.5). Reductive methylation of the solvent exposed lysine residues in protein can reduce their chains flexibilities (Kim et al., 2008). So lysine methylation may change protein properties and improve the molecular packing in crystals, which improves crystal diffractions (Kim et al., 2008). Sparse matrix screens were set up using Hampton Research kits listed in Table 5.1. Crystals were observed in 16 conditions, but none of them diffracted.
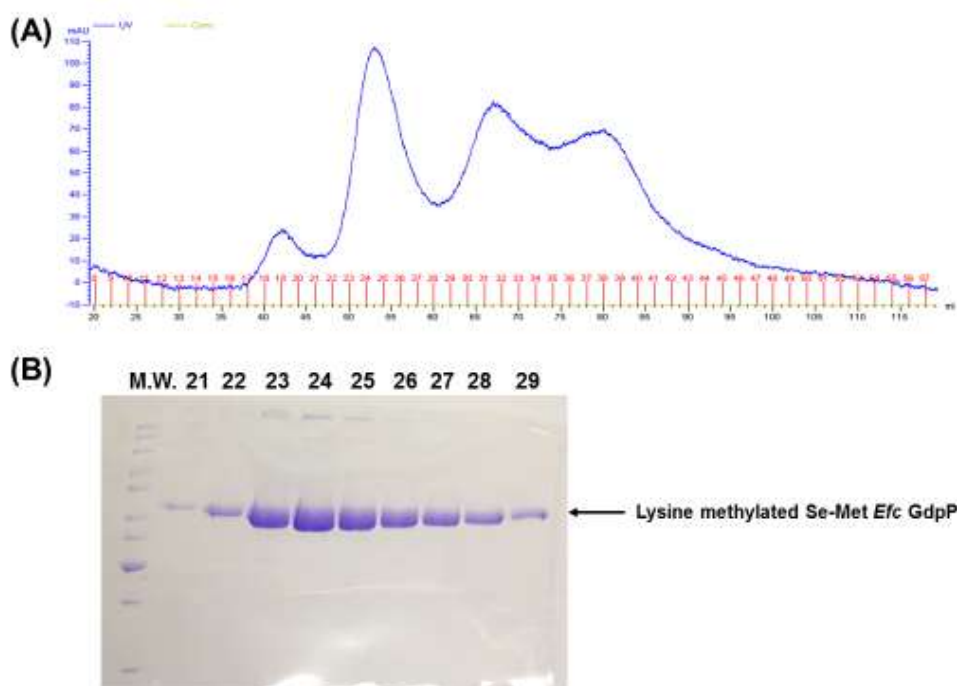
Figure 5.5 Purification of Se-Met *Efc* GdpP with lysine methylation. *Protein was purified on a Superdex-200 size exclusive column (A) and analyzed by SDS-PAGE (B). The numbers correspond to elution fractions. M.W.: protein molecular weight ladder.*

5.1.3. Heavy atom screening for multiple isomorphous replacement (MIR)

When suitable electron-dense heavy atoms bind to proteins, the scattered intensity of protein crystals will change significantly (Boggon and Shapiro, 2000). So the scattering of heavy atoms can be used to determine crystallographic phases. To find heavy atom compounds that can bind to *Efc* GdpP, I incubated the candidate compound with *Efc* GdpP, and analyzed the binding by native PAGE (Boggon and Shapiro, 2000). Protein properties such as net charge will change if heavy atoms are

bound, which usually causes a band shift in native PAGE. As shown in Figure 5.6, the native gel result suggests that $C_7H_5ClHgO_2$ bound to *Efc* GdpP, but $HoCl_3 \bullet 6H_2O$ and $NdCl_3 \bullet xH_2O$ did not. K_2HgI_4 caused extensive precipitation of *Efc* GdpP. In total, 65 heavy atom reagents from heavy atom screening kits (Hampton Research HR2-442, HR2-446, HR2-448, HR2-450) were analyzed by this method. Nine compounds gave positive results and did not cause protein precipitation (Table 5.7). These nine compounds were used to do crystal heavy atom soaking.

Efc GdpP crystals were grown in 0.2M magnesium acetate, 0.1M sodium cacodylate pH 6.5, 5% PEG8000, and 675μM ADP. Crystals were soaked in crystal mother liquor with 1mM to 10mM heavy atom compounds for 10min, 1hr, 2hr or overnight at 10°C or room temperature before being frozen. Fluorescence scans suggested that heavy atoms bound to the proteins. The *Efc* GdpP crystals usually diffracted to 3Å to 5Å, but after soaking, their diffractions dropped below 8Å. The heavy atom reagents appear to disrupt crystal order even at low concentration and with shortened soaking times.
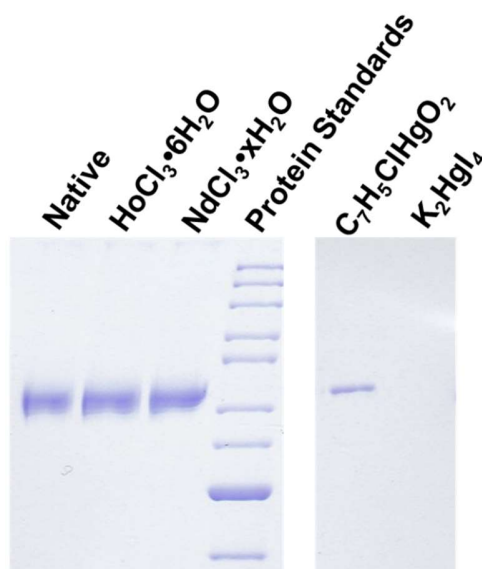
Figure 5.6 Native PAGE gel result of derivatization analysis. *2µL of 2mg/mL Efc GdpP was incubated with 2µL of 10mM heavy atom reagent solution on ice for 10min. Samples were analyzed by 10% native PAGE gel (Boggon and Shapiro, 2000). $HoCl_3 \cdot 6H_2O$: Holmium(III) chloride hexahydrate. $NdCl_3 \cdot xH_2O$: Neodymium(III) chloride hydrate. $C_7H_5ClHgO_2$: p-Chloromercuribenzoic acid. K_2HgI_4: Mercury(II) potassium iodide. All compounds are from Hampton Research.*

Table 5.7 Compounds used for heavy atom soaking.

Heavy atom compounds	Chemical formula	[1]Catalog No.
Potassium hexachloroplatinate (IV)	K_2PtCl_6	HR2-442-3
Potassium tetranitroplatinate (II)	$K_2Pt(NO_2)_4$	HR2-442-4
Phenylmercury acetate	$C_8H_8HgO_2$	HR2-446-6
p-chloromercuribenzoic acid	$C_7H_5ClHgO_2$	HR2-446-8
Lead (II) acetate trihydrate	$Pb(CH_3COO)_2 \cdot 3H_2O$	HR2-448-4
Lead (II) nitrate	$Pb(NO_3)_2$	HR2-448-5

Lead (II) chloride	$PbCl_2$	HR2-448-6
Cadmium chloride hydrate	$CdCl_2.xH_2O$	HR2-448-8
Sodium phosphotungstate	$Na_3[P(W_3O_{10})_4].aq$	HR2-450-19

[1]All compounds are from Hampton Research.

5.1.4. Post-crystallization optimization of wild-type *Efc* GdpP and Se-Met *Efc* GdpP.

5.1.4.1. Crystal dehydration

Crystal dehydration is a post-crystallization treatment to tighten the packing of protein molecules in the crystals by removing excess water and sometimes improves crystal diffraction (Heras and Martin, 2005).

Wild-type *Efc* GdpP Crystals and Se-Met *Efc* GdpP crystals were grown in three conditions including: (1) 27%~38% (v/v) tacsimate pH7.0; (2) 0.1M magnesium chloride, 0.1M HEPES sodium salt pH7.0, 15% to 26% (v/v) PEG 400; and (3) 0.2M magnesium acetate, 0.1M sodium cacodylate pH 6.5, 675μM ADP, 2% to 7% PEG8000. Crystals were soaked in the solution containing 5%-30% higher concentrations of precipitants for 30min to 1hr before being frozen (Heras and Martin, 2005). However, these dehydration-treated crystals diffracted more poorly from 8Å to 20Å.

5.1.4.2. Crystal annealing

Although cryoprotection is effective to protect protein crystals from radiation damage, uneven flash-cooling can increase crystal mosaicity and reduce

diffraction resolution (Harp et al., 1998). To avoid this problem, I performed crystal annealing by blocking the cryostream to warm the crystals to room temperature, and flash-cooling it again (Harp et al., 1998) but again crystal annealing decreased *Efc* GdpP crystal diffractions to 20Å.

5.2. Structural studies of *Efc* GdpP[I440S]

The *Efc* GdpP[I440S] was identified in several experimental DAP-resistant strains (Miller et al., 2013). The I440S mutation is located in GdpP DHH/DHHA1 domain (Figure 1.1). I have shown that I440S mutation significantly decreases GdpP phosphodiesterase activity, and can induce intracellular c-di-AMP accumulation (please see section 3.3.2 for details).

To study how the I440S mutation changes GdpP structure, *Efc* GdpP[I440S] was expressed and purified in the same way as wild-type *Efc* GdpP (Figure 5.7 A and B). Sparse matrix screens were set up using 11.18mg/ml *Efc* GdpP[I440S]. Wild-type *Efc* GdpP crystals were also broken and used as micro seeds to induce *Efc* GdpP[I440S] crystal growth.

The crystals diffracted best to 3.3Å, and were grown in 0.2M magnesium acetate, 0.1M sodium cacodylate pH 6.5, 5% PEG8000 (Figure 5.7C).
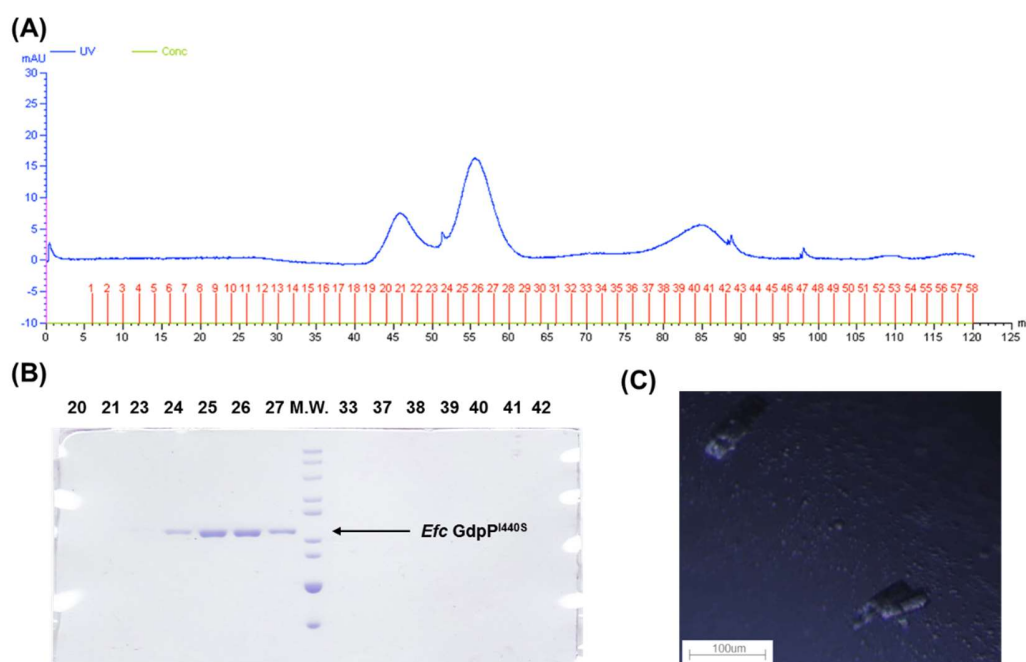
Figure 5.7 Purification and crystallization of *Efc* GdpP[I440S]. *Protein was purified on a Superdex-200 size exclusive column (A) and analyzed by SDS PAGE (B). The numbers correspond to elution fractions. M.W.: protein molecular weight ladder. (C) Crystals grew in 0.2M magnesium acetate, 0.1M sodium cacodylate pH7.0, 5% (w/v) PEG 8000 at 10°C.*

5.3. Structural studies of *Efc* GdpP[D419A] and *Efc* GdpP[D419A/D499A]

As discussed in Session 3.3.1.5, Asp[419] and Asp[499] in *Efc* GdpP DHH/DHHA1 domain are predicted to interact with divalent cations required for phosphodiesterase activity (Figure 3.7) (Corrigan et al., 2011; Rao et al., 2010). Since double mutations D429A/D499A completely abolished *Efc* GdpP phosphodiesterase activity (Figure 3.3), co-crystallization of c-di-AMP and *Efc* GdpP

mutants (*Efc* GdpP[D419A] and *Efc* GdpP[D419A/D499A]) may stabilize or reduce the conformational dynamics of the GdpP structure and improve the quality of crystals.

Efc GdpP[D419A] and *Efc* GdpP[D419A/D499A] were overexpressed in *E. coli* BL21 and purified using the same purification protocols of wild-type *Efc* GdpP (Figure 5.8 A-D). Sparse matrix screens were set up using the kits listed in Table 5.1 with or without c-di-AMP as additives. Crystals were grown in similar conditions to wild-type GdpP (Figure 5.8 E-I). After optimization, *Efc* GdpP[D419A] crystals only diffracted to 8Å ~10Å. *Efc* GdpP[D419A/D499A] crystals diffracted best to 3.3Å, and were grown in 0.2M magnesium acetate, 0.1M sodium cacodylate pH6.5, 7% PEG8000, 270µM c-di-AMP (Figure 5.8H).
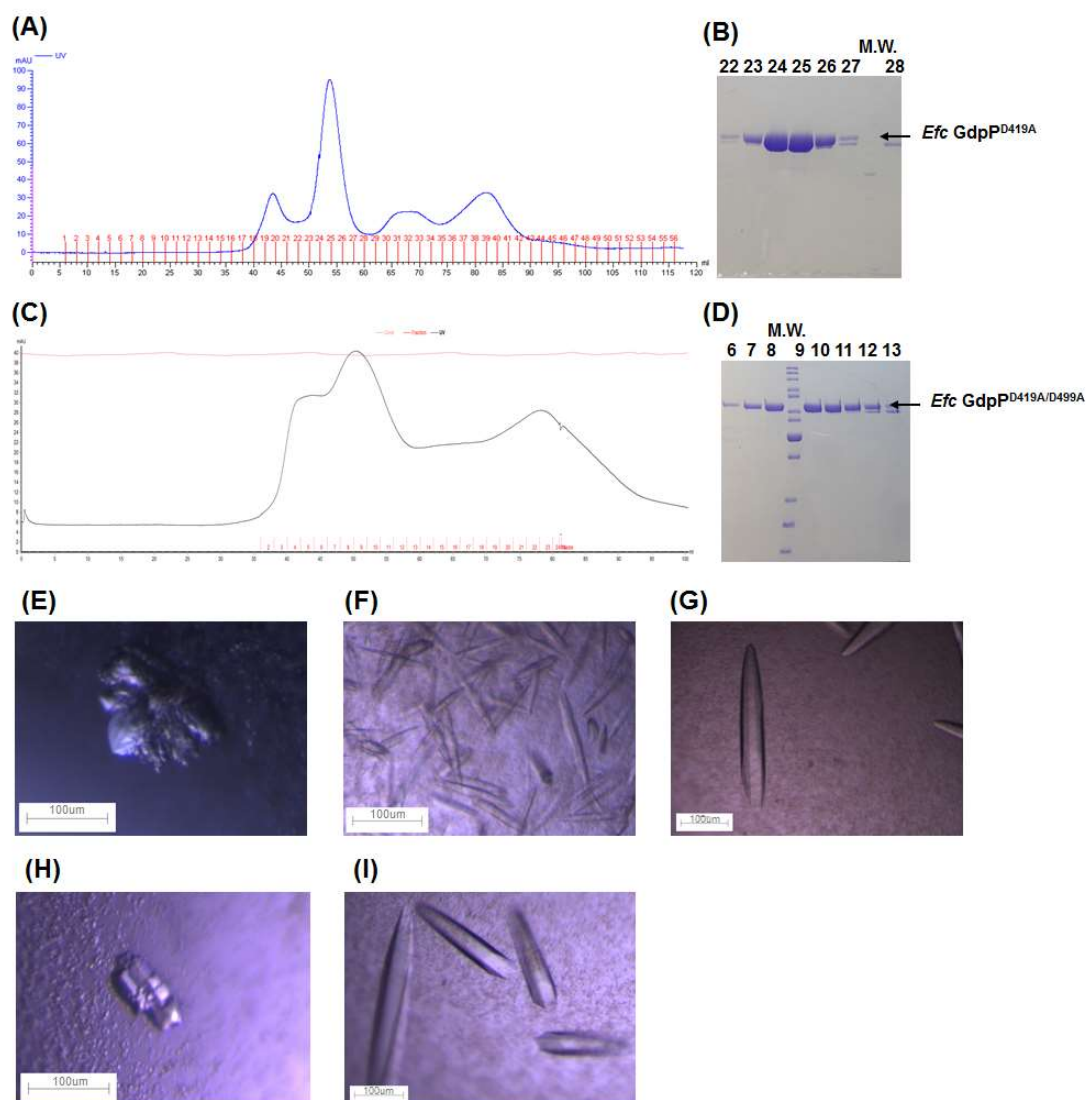
Figure 5.8 Purification and crystallization of *Efc* GdpP^{D419A} and *Efc* GdpP^{D419A/D499A}. *Efc GdpP^{D419A} was purified on a Superdex-200 size exclusive column (A) and analyzed by SDS PAGE (B). Efc GdpP^{D419A/D499A} was purified on a Superdex-200 size exclusive column (C) and analyzed by SDS PAGE (D). The numbers correspond to elution fractions. M.W.: protein molecular weight ladder. (E-G): Efc GdpP^{D419A} crystals grew in (E): 0.2M magnesium acetate, 0.1M sodium cacodylate pH6.5, 5% PEG8000,*

and 405μM c-di-AMP at 10°C; (F) 0.1M magnesium chloride, 0.1M HEPES pH7.0, 18%

PEG4000, and 270μM c-di-AMP at 10°C; (G) 30% tacsimate pH7.0, and 270μM c-di-

AMP at 10°C. (H-I): Efc GdpP^{D419A/D499A} crystals grew in (H) 0.2M magnesium acetate,

0.1M sodium cacodylate pH6.5, 7% PEG8000, 270μM c-di-AMP at 10°C; (I) 0.1M

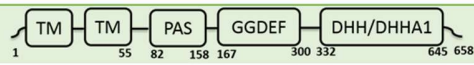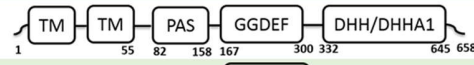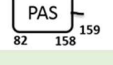*magnesium chloride, 0.1M HEPES pH7.0, 20%PEG4000, and 270μM c-di-AMP at 10°C.*
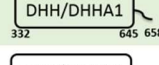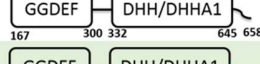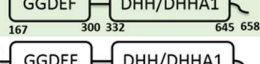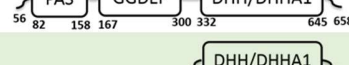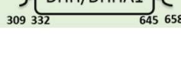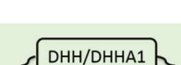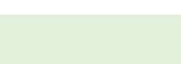
5.4. Structural studies of *Efc* GdpP truncations.

5.4.1. Construct design

Efc GdpP is a 72kDa molecule with 5 different domains. GdpP truncations with fewer domains may reduce protein flexibility and produce better crystals. To identify the flexible region in GdpP for truncation, I performed limited proteolysis by trypsin and chymotrypsin (Fontana et al., 2004). I optimized the reactions by trying different temperatures, incubation times, and ratios between protein and proteases. However, no clear limit product band could be observed by SDS-PAGE.

I analyzed *Efc* GdpP protein sequence and aligned it to other GdpP homologs that have been studied (Figure 3.2, Figure 3.10) (Cho and Kang, 2013; Corrigan et al., 2011; He et al., 2015; Rao et al., 2010; Smith et al., 2012). I also used the Phyre2 server to predict *Efc* GdpP secondary structure. Truncations were designed to avoid disrupting rigid secondary structures. Nine constructs were made for structural studies (Table 5.8).

Table 5.8 Summary of structural studies of *E. faecalis* GdpP.

Protein Construct	Expression	Solubility	Purification	Crystallization	Diffraction
Efc GdpP	✓	✓	✓	✓	3.8Å
Efc GdpP (C-His)	✓	✓	X	X	X
Efc GdpP$_{167-300}$	X	X	X	X	X
Efc GdpP$_{82-159}$	✓	X	X	X	X
Efc GdpP$_{332-658}$	✓	X	X	X	X
Efc GdpP$_{167-658}$	✓	✓	X	X	X
Efc GdpP$_{167-658}$ (C-His)	✓	✓	X	X	X
Efc GdpP$_{56-658}$	✓	✓	✓	✓	X
Efc GdpP$_{309-658}$	✓	✓	✓	✓	5Å
Efc GdpP^{I440S}	✓	✓	✓	✓	3.3Å
Efc GdpP$^{I440S}_{309-658}$					
Efc GdpP^{D419A}	✓	✓	✓	✓	X
Efc GdpP^{D419A,D499A}	✓	✓	✓	✓	3.3Å
Se-Met Efc GdpP	✓	✓	✓	✓	3.8Å
Methylated *Efc* GdpP	✓	✓	✓	✓	X

5.4.2. *Efc* GdpP with C-terminal His-tag

Full-length *Efc* GdpP with a C-terminal 6xHis-tag was constructed. Since C-His *Efc* GdpP was soluble, it was expected that the His-tag could be removed from C-terminal to make crystallization of no-tag protein possible.

C-His *Efc* GdpP was overexpressed in 10L 2xYT medium, and was first purified on a Ni-NTA column, and then on a Superdex-200 size exclusion column. The expression of C-His *Efc* GdpP was not good even after optimization. Only 2mg of protein was purified from 10 liters of cells using this modest 2-step purification. Additionally, the protein purity was lower than 30% than I had obtained from earlier purification of the full-length protein (Figure 5.9).
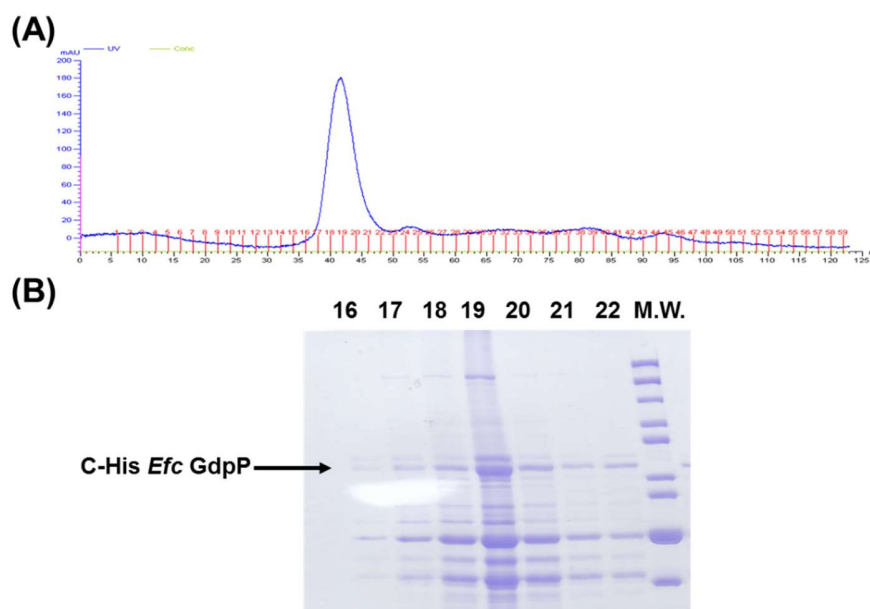
Figure 5.9 Purification of *Efc* GdpP with C-terminal His-tag. *(A) purification of C-His Efc GdpP on a Superdex-200 size exclusion column. (B) SDS-PAGE analysis of gel*

filtration purification. The numbers correspond to elution fractions. M.W.: protein molecular weight ladder.

5.4.3. GGDEF domain truncation *Efc* GdpP$_{167-300}$

Efc GdpP$_{167-300}$ includes the GdpP GGDEF domain (Table 5.8), and is predicted to be ~17kDa. *Efc* GdpP$_{167-300}$ could not be expressed despite a trying several optimization strategies such as varying temperatures (16°C, 28°C, and 37°C) and media conditions (2xYT and EnPresso™ media (BioSilta)). I was unable to obtain enough soluble protein for sparse matrix trials.

5.4.4. PAS domain truncation *Efc* GdpP$_{82-159}$ and DHH/DHHA1 domain truncation *Efc* GdpP$_{332-658}$

Efc GdpP$_{82-159}$ is the PAS domain (Table 5.8). *Efc* GdpP$_{332-658}$ is a construct that encodes the DHH/DHHA1 domain (Table 5.8). Both could be overexpressed in *E. coli* BL21, but were not soluble and thus no further crystallization studies were performed.

5.4.5. GGDEF-DHH/DHHA1 domain truncation *Efc* GdpP$_{167-658}$ with N-terminal or C-terminal His-tag

Efc GdpP$_{167-658}$ constructs could be expressed, and both were soluble. The molecular weight of *Efc* GdpP$_{167-658}$ with His-tag is 56kDa.

N-His *Efc* GdpP$_{167-658}$ was first purified on Ni-NTA column, followed with a Superdex-200 size exclusion column. After gel filtration, the purity of *Efc* GdpP$_{167-658}$ was lower than 60% with a large amount of contaminants (60kDa-75kDa, and 40kDa) co-purified (Figure 5.10A). I could not optimize sufficient yields of protein with sufficient purity for crystallization trials.

C-His *Efc* GdpP$_{167-658}$ was purified first on Ni-NTA. A large amount of lower-molecular-weight contaminants (40kDa) were co-purified (Figure 5.10B). This construct was very unstable and rapidly degraded and then precipitated after purification making it a poor candidate for crystallographic screens.

Different protein purification I tried a variety of columns and strategies were tested to remove contaminants, including Q-sepharose column (anion exchange), SP-sepharose column (cation exchange), hydrophobic interaction chromatography (HIC) column, and optimizing purification buffers. However, none of these approaches produced satisfactory results and all these aforementioned constructs proved insufficient for crystallographic trials.
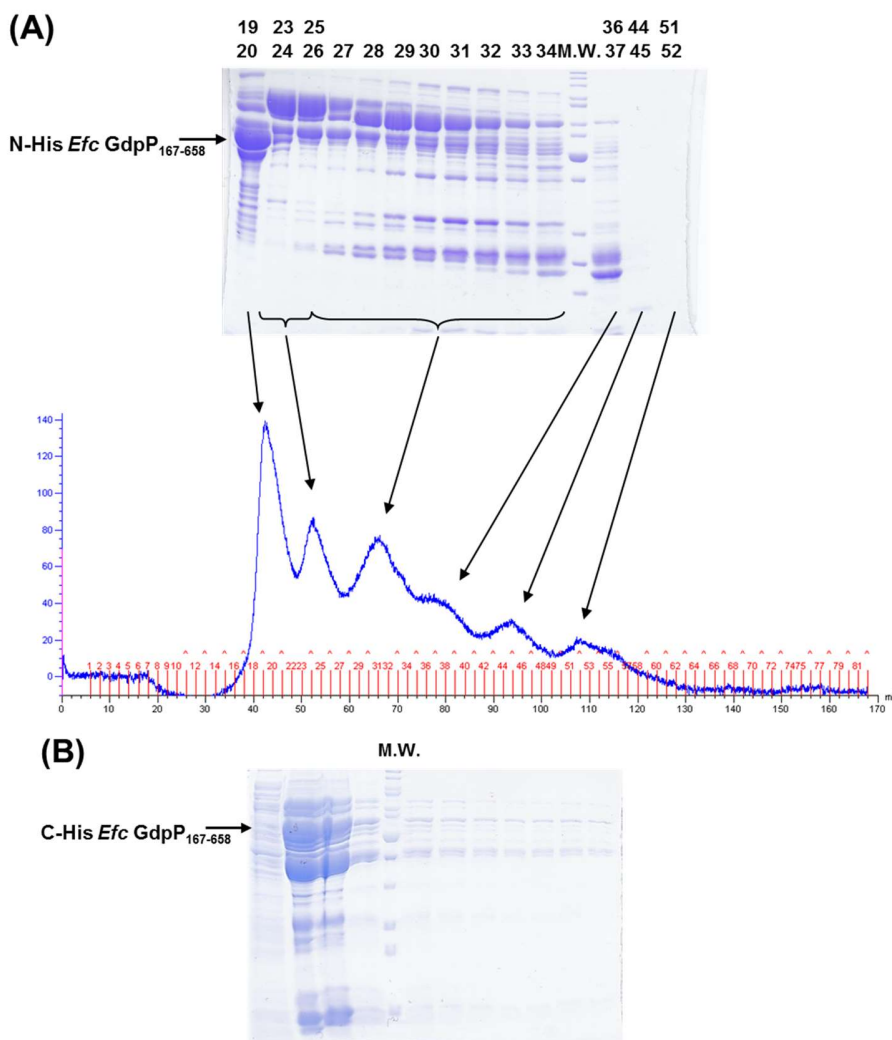
Figure 5.10 *Efc* GdpP$_{167-658}$ was co-purified with contaminants. *(A) N-His Efc GdpP$_{167-658}$ was purified on a Superdex-200 size exclusive column. The numbers correspond to elution fractions. N-His Efc GdpP$_{167-658}$ was mainly eluted in peak one (fraction #19 and #20) with contaminates. (B) C-His Efc GdpP$_{167-658}$ was purified on Ni-NTA column but had a large amount of contaminants. M.W.: protein molecular weight ladder.*

5.4.6. PAS-GGDEF-DHH/DHHA1 domain truncation *Efc* GdpP$_{56-658}$

Efc GdpP$_{56-658}$ is the truncation that includes the PAS-GGDEF-DHH/DHHA1 domains (Table 5.8). *Efc* GdpP$_{56-658}$ was purified using the same protocols as full-length *Efc* GdpP but unfortunately the yield was low. Only 0.5mg protein could be purified from 8L of cell culture (Figure 5.11 A and B). Sparse matrix screens were set up using 11.42mg/ml protein in the conditions listed in Table 5.1. Crystals only grew in one condition, and did not diffract beyond the beam stop at the synchrotron (Figure 5.11C).

Figure 5.11 Purification and crystallization of *Efc* GdpP$_{56-658}$. *(A-B) Purification of Efc GdpP$_{56-658}$ on a Superdex-200 size exclusive column. SDS-PAGE analysis shows protein purity. The numbers correspond to elution fractions. Fraction #27-#29 were*

collected for crystallization. M.W.: protein molecular weight ladder. (C) Crystals grew in 0.1M tris pH8.5, 2.0M ammonium phosphate at 10°C.

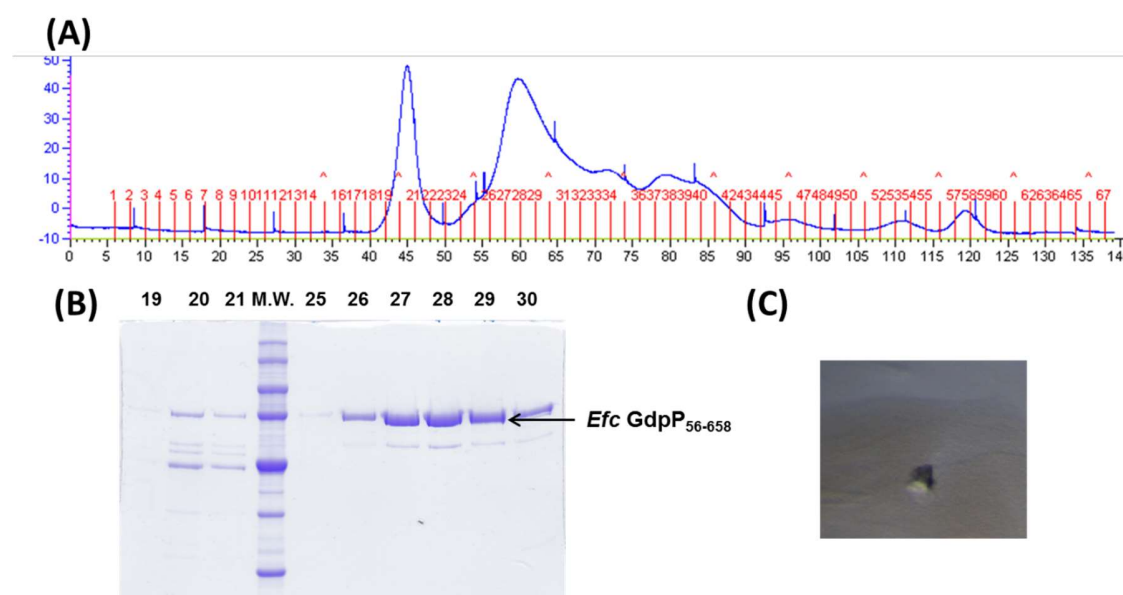## 5.4.7. DHH/DHHA1 domain truncation *Efc* GdpP$_{309\text{-}658}$ and *Efc* GdpP$_{309-658}^{\text{I440S}}$

Efc GdpP$_{309\text{-}658}$ contains the DHH/DHHA1 domain, with a longer N-terminal flexible tail than *Efc* GdpP$_{332\text{-}658}$ (Table 5.8). *Efc* GdpP$_{309-658}^{\text{I440S}}$ could not be expressed in *E. coli* BL21 despite attempts at optimization by varying temperature and media. Wild-type *Efc* GdpP$_{309\text{-}658}$ could be overexpressed in 2xYT media at 37 °C.

Efc GdpP$_{309\text{-}658}$ was purified by Ni-NTA affinity chromatography, anion exchange and gel filtration chromatography (Figure 5.12 A and B). Around 7mg protein could be purified from 5L culture. Sparse matrix crystal screening was set up using conditions listed in Table 5.1. Some small and micro crystals were obtained from primary screenings. Crystals grown in 2 conditions showed weak diffraction, and were further optimized (Figure 5.11 C and D).

In primary screening, the crystals grown in 4M sodium formate were cubic, and diffracted to 8Å (Figure 5.12C). This condition was optimized by using different concentrations of sodium formate and protein, different drop sizes, different ratios between protein and mother liquor, different temperatures, and setting up hanging drops and sitting drops. However, the cubic crystals could not be reproduced even using the earlier cubic crystals as seeds. The new crystals grown in 2.5M sodium

formate formed clusters of needles, and only diffracted to 20 Å (Figure 5.12E). I have been unable to reproduce the original crystals.

Efc GdpP$_{309-658}$ crystals grown in 0.1M MgCl$_2$, 0.05M HEPES pH7.5, 15% (w/v) PEG 2000 diffracted to 5 Å (Figure 5.12D). After optimization, bigger crystals were generated (Figure 5.12F). But none of them showed better diffraction.
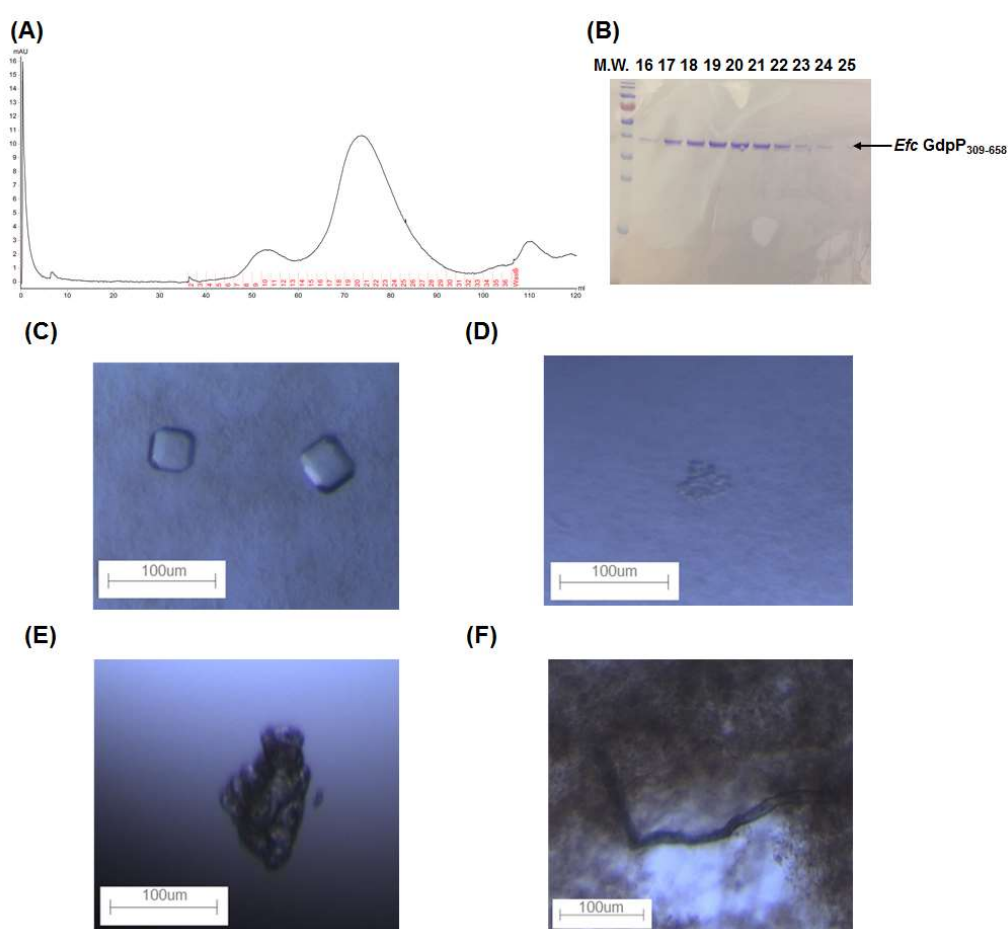
Figure 5.12 Purification and crystallization of *Efc* GdpP$_{309-658}$. *Efc* GdpP$_{309-658}$ was purified on a Superdex-200 size exclusive column (A) and analyzed by SDS-PAGE (B). *Crystals grew in (C) 4M sodium formate at 10°C; (D) 2.5M sodium formate*

at 10°C; (E) 0.1M MgCl₂, 0.05M HEPES pH7.5, 15% (w/v) PEG 2000 at 10°C; (F) 0.1M

MgCl₂, 0.1M HEPES pH7.5, 7% (w/v) PEG 2000 at 10°C.

5.5. Structural studies of *Efm* GdpP

Since *Efc* GdpP and its truncations did not behave well for crystallography,

constructs of *E. faecium* R494 GdpP (*Efm* GdpP) and its variants were also made.

Efm GdpP is a homolog of *Efs*GdpP with 58% identity at the level of amino acid

sequence. Protein blast showed there was no strong homology between *Efm* GdpP

and other PAS domains. I aligned *Efm* GdpP sequence to *B. subtilis* GdpP to predict a

putative PAS domain. However, the PAS region predicted by alignment to *Bs* GdpP

overlapped with the GGDEF domain predicted by protein blast, suggesting *Efm* GdpP

does not have a PAS domain or that it is very different than canonical PAS domains

(Figure 5.13).

Figure 5.13 Domain organization of *E. faecium* R494 GdpP. *Efm GdpP is a multi-domain protein containing two putative N-terminal transmembrane helices, a GGDEF*

domain and a DHH domain with a DHHA1 subdomain. The PAS domain predicted by alignment to B. subtilis GdP overlaps with the GGDEF domain predicted by protein blast, suggesting Efm GdpP may not have a canonical PAS domain.

Seven constructs were made with N-terminal 6xHis tag (Table 5.9), including full-length *Efm* GdpP, *Efm* GdpP$_{83-657}$, *Efm* GdpP$_{137-657}$, *Efm* GdpP$_{338-657}$, *Efm* GdpP$_{338-500}$, *Efm* GdpP$_{137-298}$, and *Efm* GdpP$_{83-167}$. The full-length *Efm* GdpP, *Efm* GdpP$_{338-657}$, and *Efm* GdpP$_{137-298}$ could be expressed, but were not soluble. *Efm* GdpP$_{83-657}$, *Efm* GdpP$_{137-657}$, *Efm* GdpP$_{338-500}$, and *Efm* GdpP$_{83-167}$ could not be expressed even after optimization.

Table 5.9 Summary of structural studies of *E. faecium* GdpP.

Protein Construct	Expression	Solubility	Purification	Crystallization	Diffraction
Efm GdpP	✓	X	X	X	X
Efm GdpP$_{338-657}$	✓	X	X	X	X
Efm GdpP$_{137-298}$	✓	X	X	X	X
Efm GdpP$_{83-657}$	X	X	X	X	X
Efm GdpP$_{137-657}$	X	X	X	X	X
Efm GdpP$_{338-500}$	X	X	X	X	X
Efm GdpP$_{83-167}$	X	X	X	X	X

5.6. Discussion and Future work

The *Efc* GdpP$_{309-658}$ crystals are under optimization. We found the detergent fluorinated octyl maltoside could dramatically increase *Efc* GdpP$_{309-658}$ phosphodiesterase activity (please see Session 3.3.1 for details). Fluorinated octyl maltoside will be used for further crystallization optimization together with additive screen kits and Silver Bullet kit.

Additionally, iodide derivatives will be tried with quick soaking to try and obtain phases for the full-length *Efc* GdpP crystals. An *Efc* GdpP structure will reveal the active site of phosphodiesterase, binding pocket of cyclic-dinucleotide and inhibitor ppGpp and is clearly a very valuable structure for understanding GdpP function. The structures solved from *Efc* GdpP and *Efc* GdpP$^{D419/D499A}$ crystals grown with/without potential cofactors/substrates/products will reveal how the activity is regulated, and the molecular mechanism of how GdpP responds and controls cyclic dinucleotide signaling.

Chapter 6

Conclusions and Future Studies

6.1. Discussion

Multidrug-resistant pathogen infections have become serious threats to public health (CDC, 2013). In the United States, 66,000 people get enterococcus infections each year, and 30% of the infections are caused by vancomycin-resistant enterococcus (VRE) (CDC, 2013). Since VRE is resistant to almost all clinically available antibiotics, daptomycin (DAP) is used as the last resort treatment against recalcitrant VRE infections (Arias and Murray, 2012). Unfortunately, DAP resistance arises during clinical application (Arias and Murray, 2008). To develop efficacious therapies for DAP-resistant VRE infections, it's important to understand the biological mechanism behind the resistance.

In this work, I show for the first time that c-di-AMP is a second messenger in enterococci. I also show that *Efc* GdpP is a c-di-AMP-specific phosphodiesterase, and

regulates the intracellular c-di-AMP concentration. The DAP adaptive mutation I440S strongly decreases *Efc* GdpP phosphodiesterase activity. Furthermore, the cell stress response module LiaFSR-LiaXYZ interacts c-di-AMP signaling. I also discover a novel putative c-di-AMP phosphodiesterase XpaC that is under direct LiaR regulation. Additionally, I show my structural studies about *Efc* GdpP and *Efm* GdpP.

6.2. Current and future works

For the structural studies of *Efc* GdpP, to solve the phase problem, I will perform quick heavy atom soaking using iodide derivatives. My previous heavy atom soaking trials show that even 10min soaking of *Efc* GdpP in heavy atom reagents could disrupt crystal diffractions (Section 5.1.3). I so will perform quick soaking of 5s to 1min.

The crystals of *Efc* GdpP$_{309-658}$ containing the DHH-DHHA1 domain diffracted to 5 Å (Section 5.4.7). Since the c-di-AMP phosphodiesterase assay results suggest the detergent fluorinated octyl maltoside can help reducing *Efc* GdpP$_{309-658}$ aggregation (Section 3.3.1.4), I will set up sparse matrix screening of *Efc* GdpP$_{309-658}$ with fluorinated octyl maltoside for crystals.

I also want to identify the putative cofactors of GdpP. As *Efc* GdpP over-expressed in *E. coli* BL21 showed weak enzyme activities, suggesting Gram-negative bacteria *E. coli* lacks the essential GdpP cofactors. I will over express *Efc* GdpP in *E. coli* BL21, and purify the protein by Ni-NTA. I will use cell extracts of *Efc* S613 for a

pull-down assay using Ni-NTA chromatography. The cofactors that can bind to GdpP will be analyzed by mass spectrometry.

On the other hand, I discover a putative phosphodiesterase XpaC under direct LiaFSR regulation (Section 4.4). Since I Couldn't over-press this protein in *E. coli* BL21, I will make recombinant plasmids to overexpress XpaC in *B. subtilis*. I will purify XpaC and use HLPC to analyze its function.

References

Abranches, J., Martinez, A.R., Kajfasz, J.K., Chávez, V., Garsin, D.A., and Lemos, J.A. (2009). The molecular alarmone (p)ppGpp mediates stress responses, vancomycin tolerance, and virulence in Enterococcus faecalis. J. Bacteriol. *191*, 2248–2256.

Arias, C.A., and Murray, B.E. (2008). Emergence and management of drug-resistant enterococcal infections. Expert Rev Anti Infect Ther *6*, 637–655.

Arias, C.A., and Murray, B.E. (2012). The rise of the Enterococcus: beyond vancomycin resistance. Nat. Rev. Microbiol. *10*, 266–278.

Arias, C.A., Panesso, D., McGrath, D.M., Qin, X., Mojica, M.F., Miller, C., Diaz, L., Tran, T.T., Rincon, S., Barbu, E.M., et al. (2011). Genetic Basis for In Vivo Daptomycin Resistance in Enterococci. New England Journal of Medicine *365*, 892–900.

Bai, Y., Yang, J., Zhou, X., Ding, X., Eisele, L.E., and Bai, G. (2012). Mycobacterium tuberculosis Rv3586 (DacA) is a diadenylate cyclase that converts ATP or ADP into c-di-AMP. PLoS ONE *7*, e35206.

Bai, Y., Yang, J., Eisele, L.E., Underwood, A.J., Koestler, B.J., Waters, C.M., Metzger, D.W., and Bai, G. (2013). Two DHH subfamily 1 proteins in Streptococcus pneumoniae possess cyclic di-AMP phosphodiesterase activity and affect bacterial growth and virulence. J. Bacteriol. *195*, 5123–5132.

Bai, Y., Yang, J., Zarrella, T.M., Zhang, Y., Metzger, D.W., and Bai, G. (2014). Cyclic di-AMP impairs potassium uptake mediated by a cyclic di-AMP binding protein in Streptococcus pneumoniae. J. Bacteriol. *196*, 614–623.

Barrick, J.E., Corbino, K.A., Winkler, W.C., Nahvi, A., Mandal, M., Collins, J., Lee, M., Roth, A., Sudarsan, N., Jona, I., et al. (2004). New RNA motifs suggest an expanded scope for riboswitches in bacterial genetic control. Proc. Natl. Acad. Sci. U.S.A. *101*, 6421–6426.

Bejerano-Sagie, M., Oppenheimer-Shaanan, Y., Berlatzky, I., Rouvinski, A., Meyerovich, M., and Ben-Yehuda, S. (2006). A Checkpoint Protein That Scans the Chromosome for Damage at the Start of Sporulation in Bacillus subtilis. Cell *125*, 679–690.

Block, K.F., Hammond, M.C., and Breaker, R.R. (2010). Evidence for widespread gene control function by the ydaO riboswitch candidate. J. Bacteriol. *192*, 3983–3989.

Boggon, T.J., and Shapiro, L. (2000). Screening for phasing atoms in protein crystallography. Structure *8*, R143-149.

Bourgogne, A., Garsin, D.A., Qin, X., Singh, K.V., Sillanpaa, J., Yerrapragada, S., Ding, Y., Dugan-Rocha, S., Buhay, C., Shen, H., et al. (2008). Large scale variation in Enterococcus faecalis illustrated by the genome analysis of strain OG1RF. Genome Biol *9*, R110.

Bryan, E.M., Bae, T., Kleerebezem, M., and Dunny, G.M. (2000). Improved Vectors for Nisin-Controlled Expression in Gram-Positive Bacteria. Plasmid *44*, 183–190.

Byappanahalli, M.N., Nevers, M.B., Korajkic, A., Staley, Z.R., and Harwood, V.J. (2012). Enterococci in the environment. Microbiol. Mol. Biol. Rev. *76*, 685–706.

CDC (2013). antibiotic resistance threats in the united states, 2013.

Cho, K.H., and Kang, S.O. (2013). Streptococcus pyogenes c-di-AMP phosphodiesterase, GdpP, influences SpeB processing and virulence. PLoS ONE *8*, e69425.

Commichau, F.M., Dickmanns, A., Gundlach, J., Ficner, R., and Stülke, J. (2015). A jack of all trades: the multiple roles of the unique essential second messenger cyclic di-AMP. Mol. Microbiol. *97*, 189–204.

Corrigan, R.M., and Gründling, A. (2013). Cyclic di-AMP: another second messenger enters the fray. Nat. Rev. Microbiol. *11*, 513–524.

Corrigan, R.M., Abbott, J.C., Burhenne, H., Kaever, V., and Gründling, A. (2011). c-di-AMP Is a New Second Messenger in Staphylococcus aureus with a Role in Controlling Cell Size and Envelope Stress. PLoS Pathog *7*.

Corrigan, R.M., Campeotto, I., Jeganathan, T., Roelofs, K.G., Lee, V.T., and Gründling, A. (2013). Systematic identification of conserved bacterial c-di-AMP receptor proteins. Proc. Natl. Acad. Sci. U.S.A. *110*, 9084–9089.

Corrigan, R.M., Bowman, L., Willis, A.R., Kaever, V., and Gründling, A. (2015). Cross-talk between Two Nucleotide-signaling Pathways in Staphylococcus aureus. J Biol Chem *290*, 5826–5839.

Davlieva, M., Zhang, W., Arias, C.A., and Shamoo, Y. (2013). Biochemical Characterization of Cardiolipin Synthase Mutations Associated with Daptomycin Resistance in Enterococci. Antimicrob Agents Chemother *57*, 289–296.

Davlieva, M., Shi, Y., Leonard, P.G., Johnson, T.A., Zianni, M.R., Arias, C.A., Ladbury, J.E., and Shamoo, Y. (2015a). A variable DNA recognition site organization establishes the LiaR-mediated cell envelope stress response of enterococci to daptomycin. Nucleic Acids Res. *43*, 4758–4773.

Davlieva, M., Shi, Y., Leonard, P.G., Johnson, T.A., Zianni, M.R., Arias, C.A., Ladbury, J.E., and Shamoo, Y. (2015b). A variable DNA recognition site organization establishes the LiaR-

mediated cell envelope stress response of enterococci to daptomycin. Nucl. Acids Res. *43*, 4758–4773.

Fontana, A., de Laureto, P.P., Spolaore, B., Frare, E., Picotti, P., and Zambonin, M. (2004). Probing protein structure by limited proteolysis. Acta Biochim. Pol. *51*, 299–321.

Griffiths, J.M., and O'Neill, A.J. (2012). Loss of Function of the GdpP Protein Leads to Joint β-Lactam/Glycopeptide Tolerance in Staphylococcus aureus. Antimicrob Agents Chemother *56*, 579–581.

Gundlach, J., Rath, H., Herzberg, C., Mäder, U., and Stülke, J. (2016). Second Messenger Signaling in Bacillus subtilis: Accumulation of Cyclic di-AMP Inhibits Biofilm Formation. Front Microbiol *7*.

Hallberg, Z.F., Wang, X.C., Wright, T.A., Nan, B., Ad, O., Yeo, J., and Hammond, M.C. (2016). Hybrid promiscuous (Hypr) GGDEF enzymes produce cyclic AMP-GMP (3′, 3′-cGAMP). PNAS *113*, 1790–1795.

Harp, J.M., Timm, D.E., and Bunick, G.J. (1998). Macromolecular crystal annealing: overcoming increased mosaicity associated with cryocrystallography. Acta Crystallogr. D Biol. Crystallogr. *54*, 622–628.

He, Q., Wang, F., Liu, S., Zhu, D., Cong, H., Gao, F., Li, B., Wang, H., Lin, Z., Liao, J., et al. (2015). Structural and Biochemical Insight into the Mechanism of Rv2837c from Mycobacterium tuberculosis as a C-di-NMP Phosphodiesterase. J. Biol. Chem. jbc.M115.699801.

Hecht, G.B., and Newton, A. (1995). Identification of a novel response regulator required for the swarmer-to-stalked-cell transition in Caulobacter crescentus. J Bacteriol *177*, 6223–6229.

Henry, J.T., and Crosson, S. (2011). Ligand-binding PAS domains in a genomic, cellular, and structural context. Annu. Rev. Microbiol. *65*, 261–286.

Heras, B., and Martin, J.L. (2005). Post-crystallization treatments for improving diffraction quality of protein crystals. Acta Crystallogr. D Biol. Crystallogr. *61*, 1173–1180.

HICPAC (1995). Recommendations for Preventing the Spread of Vancomycin Resistance Recommendations of the Hospital Infection Control Practices Advisory Committee (HICPAC).

Hodinka, R.L., Jack-Wait, K., Wannamaker, N., Walden, T.P., and Gilligan, P.H. (1987). Comparative in vitro activity of LY146032 (daptomycin), a new lipopeptide antimicrobial. Eur. J. Clin. Microbiol. *6*, 100–103.

Huynh, T.N., Luo, S., Pensinger, D., Sauer, J.-D., Tong, L., and Woodward, J.J. (2015). An HD-domain phosphodiesterase mediates cooperative hydrolysis of c-di-AMP to affect bacterial growth and virulence. Proc. Natl. Acad. Sci. U.S.A. *112*, E747-756.

Jung, D., Rozek, A., Okon, M., and Hancock, R.E.W. (2004). Structural transitions as determinants of the action of the calcium-dependent antibiotic daptomycin. Chem. Biol *11*, 949–957.

Kalia, D., Merey, G., Nakayama, S., Zheng, Y., Zhou, J., Luo, Y., Guo, M., Roembke, B.T., and Sintim, H.O. (2013). Nucleotide, c-di-GMP, c-di-AMP, cGMP, cAMP, (p)ppGpp signaling in bacteria and implications in pathogenesis. Chem Soc Rev *42*, 305–341.

Kim, H., Youn, S.-J., Kim, S.O., Ko, J., Lee, J.-O., and Choi, B.-S. (2015). Structural Studies of Potassium Transport Protein KtrA Regulator of Conductance of K+ (RCK) C Domain in Complex with Cyclic Diadenosine Monophosphate (c-di-AMP). J. Biol. Chem. *290*, 16393–16402.

Kim, Y., Quartey, P., Li, H., Volkart, L., Hatzos, C., Chang, C., Nocek, B., Cuff, M., Osipiuk, J., Tan, K., et al. (2008). Large-scale evaluation of protein reductive methylation for improving protein crystallization. Nat Methods *5*, 853–854.

Luo, Y., and Helmann, J.D. (2012). Analysis of the role of Bacillus subtilis σ(M) in β-lactam resistance reveals an essential role for c-di-AMP in peptidoglycan homeostasis. Mol. Microbiol. *83*, 623–639.

Mehne, F.M.P., Gunka, K., Eilers, H., Herzberg, C., Kaever, V., and Stülke, J. (2013). Cyclic di-AMP homeostasis in bacillus subtilis: both lack and high level accumulation of the nucleotide are detrimental for cell growth. J. Biol. Chem. *288*, 2004–2017.

Mehne, F.M.P., Schröder-Tittmann, K., Eijlander, R.T., Herzberg, C., Hewitt, L., Kaever, V., Lewis, R.J., Kuipers, O.P., Tittmann, K., and Stülke, J. (2014). Control of the diadenylate cyclase CdaS in Bacillus subtilis: an autoinhibitory domain limits cyclic di-AMP production. J. Biol. Chem. *289*, 21098–21107.

Miller, C., Kong, J., Tran, T.T., Arias, C.A., Saxer, G., and Shamoo, Y. (2013). Adaptation of Enterococcus faecalis to Daptomycin Reveals an Ordered Progression to Resistance. Antimicrob Agents Chemother *57*, 5373–5383.

Müller, A., Wenzel, M., Strahl, H., Grein, F., Saaki, T.N.V., Kohl, B., Siersma, T., Bandow, J.E., Sahl, H.-G., Schneider, T., et al. (2016). Daptomycin inhibits cell envelope synthesis by interfering with fluid membrane microdomains. PNAS *113*, E7077–E7086.

Nelson, J.W., Sudarsan, N., Furukawa, K., Weinberg, Z., Wang, J.X., and Breaker, R.R. (2013). Riboswitches in eubacteria sense the second messenger c-di-AMP. Nat. Chem. Biol. *9*, 834–839.

Oppenheimer-Shaanan, Y., Wexselblatt, E., Katzhendler, J., Yavin, E., and Ben-Yehuda, S. (2011a). c-di-AMP reports DNA integrity during sporulation in Bacillus subtilis. EMBO Rep. *12*, 594–601.

Oppenheimer-Shaanan, Y., Wexselblatt, E., Katzhendler, J., Yavin, E., and Ben-Yehuda, S. (2011b). c-di-AMP reports DNA integrity during sporulation in Bacillus subtilis. EMBO Rep. *12*, 594–601.

O'Toole, G.A. (2011). Microtiter Dish Biofilm Formation Assay. J Vis Exp.

Owens, C.P., Du, J., Dawson, J.H., and Goulding, C.W. (2012). Characterization of heme ligation properties of Rv0203, a secreted heme binding protein involved in Mycobacterium tuberculosis heme uptake. Biochemistry *51*, 1518–1531.

Palmer, K.L., Daniel, A., Hardy, C., Silverman, J., and Gilmore, M.S. (2011). Genetic Basis for Daptomycin Resistance in Enterococci. Antimicrob. Agents Chemother. *55*, 3345–3356.

Panesso, D., Reyes, J., Gaston, E.P., Deal, M., Londoño, A., Nigo, M., Munita, J.M., Miller, W.R., Shamoo, Y., Tran, T.T., et al. (2015). Deletion of liaR Reverses Daptomycin Resistance in Enterococcus faecium Independent of the Genetic Background. Antimicrob. Agents Chemother. *59*, 7327–7334.

Paul, R., Weiser, S., Amiot, N.C., Chan, C., Schirmer, T., Giese, B., and Jenal, U. (2004). Cell cycle-dependent dynamic localization of a bacterial response regulator with a novel di-guanylate cyclase output domain. Genes Dev. *18*, 715–727.

Peng, X., Zhang, Y., Bai, G., Zhou, X., and Wu, H. (2016). Cyclic di-AMP mediates biofilm formation. Molecular Microbiology *99*, 945–959.

Pogliano, J., Pogliano, N., and Silverman, J. (2012). Daptomycin mediated reorganization of membrane architecture causes mislocalization of essential cell division proteins. J. Bacteriol.

Purrello, S.M., Garau, J., Giamarellos, E., Mazzei, T., Pea, F., Soriano, A., and Stefani, S. (2016). Methicillin-resistant Staphylococcus aureus infections: A review of the currently available treatment options. J Glob Antimicrob Resist *7*, 178–186.

Rao, F., See, R.Y., Zhang, D., Toh, D.C., Ji, Q., and Liang, Z.-X. (2010). YybT is a signaling protein that contains a cyclic dinucleotide phosphodiesterase domain and a GGDEF domain with ATPase activity. J. Biol. Chem *285*, 473–482.

Rao, F., Ji, Q., Soehano, I., and Liang, Z.-X. (2011). Unusual heme-binding PAS domain from YybT family proteins. J. Bacteriol. *193*, 1543–1551.

Ren, A., and Patel, D.J. (2014). c-di-AMP binds the ydaO riboswitch in two pseudo-symmetry-related pockets. Nat Chem Biol *10*, 780–786.

Reyes, J., Panesso, D., Tran, T.T., Mishra, N.N., Cruz, M.R., Munita, J.M., Singh, K.V., Yeaman, M.R., Murray, B.E., Shamoo, Y., et al. (2015). A liaR Deletion Restores Susceptibility to Daptomycin and Antimicrobial Peptides in Multidrug-Resistant Enterococcus faecalis. J Infect Dis *211*, 1317–1325.

Rice, E.W., Messer, J.W., Johnson, C.H., and Reasoner, D.J. (1995). Occurrence of high-level aminoglycoside resistance in environmental isolates of enterococci. Appl. Environ. Microbiol. *61*, 374–376.

Rismondo, J., Gibhardt, J., Rosenberg, J., Kaever, V., Halbedel, S., and Commichau, F.M. (2016). Phenotypes Associated with the Essential Diadenylate Cyclase CdaA and Its Potential Regulator CdaR in the Human Pathogen Listeria monocytogenes. J. Bacteriol. *198*, 416–426.

Robbel, L., and Marahiel, M.A. (2010). Daptomycin, a Bacterial Lipopeptide Synthesized by a Nonribosomal Machinery. J. Biol. Chem. *285*, 27501–27508.

Römling, U. (2008). Great Times for Small Molecules: c-di-AMP, a Second Messenger Candidate in Bacteria and Archaea. Sci. Signal. *1*, pe39-pe39.

Rosenberg, J., Dickmanns, A., Neumann, P., Gunka, K., Arens, J., Kaever, V., Stülke, J., Ficner, R., and Commichau, F.M. (2015). Structural and biochemical analysis of the essential diadenylate cyclase CdaA from Listeria monocytogenes. J. Biol. Chem. *290*, 6596–6606.

Ryjenkov, D.A., Tarutina, M., Moskvin, O.V., and Gomelsky, M. (2005). Cyclic Diguanylate Is a Ubiquitous Signaling Molecule in Bacteria: Insights into Biochemistry of the GGDEF Protein Domain. J Bacteriol *187*, 1792–1798.

Schrecke, K., Jordan, S., and Mascher, T. (2013). Stoichiometry and perturbation studies of the LiaFSR system of Bacillus subtilis. Mol. Microbiol. *87*, 769–788.

Smith, W.M., Pham, T.H., Lei, L., Dou, J., Soomro, A.H., Beatson, S.A., Dykes, G.A., and Turner, M.S. (2012). Heat resistance and salt hypersensitivity in Lactococcus lactis due to spontaneous mutation of llmg_1816 (gdpP) induced by high-temperature growth. Appl. Environ. Microbiol. *78*, 7753–7759.

Taylor, B.L., and Zhulin, I.B. (1999). PAS domains: internal sensors of oxygen, redox potential, and light. Microbiol. Mol. Biol. Rev. *63*, 479–506.

Tran, T.T., Panesso, D., Mishra, N.N., Mileykovskaya, E., Guan, Z., Munita, J.M., Reyes, J., Diaz, L., Weinstock, G.M., Murray, B.E., et al. (2013). Daptomycin-Resistant Enterococcus faecalis Diverts the Antibiotic Molecule from the Division Septum and Remodels Cell Membrane Phospholipids. mBio *4*.

Underwood, A.J., Zhang, Y., Metzger, D.W., and Bai, G. (2014). Detection of cyclic di-AMP using a competitive ELISA with a unique pneumococcal cyclic di-AMP binding protein. J. Microbiol. Methods *107*, 58–62.

Upson, R.H., Haugland, R.P., Malekzadeh, M.N., and Haugland, R.P. (1996). A Spectrophotometric Method to Measure Enzymatic Activity in Reactions That Generate Inorganic Pyrophosphate. Analytical Biochemistry *243*, 41–45.

Wang, J.S., Muzevich, K., Edmond, M.B., Bearman, G., and Stevens, M.P. (2014). Central nervous system infections due to vancomycin-resistant enterococci: case series and review of the literature. Int. J. Infect. Dis. *25*, 26–31.

Witte, C.E., Whiteley, A.T., Burke, T.P., Sauer, J.-D., Portnoy, D.A., and Woodward, J.J. (2013). Cyclic di-AMP is critical for Listeria monocytogenes growth, cell wall homeostasis, and establishment of infection. MBio *4*, e00282-213.

Witte, G., Hartung, S., Büttner, K., and Hopfner, K.-P. (2008). Structural biochemistry of a bacterial checkpoint protein reveals diadenylate cyclase activity regulated by DNA recombination intermediates. Mol. Cell *30*, 167–178.

Wolf, D., Kalamorz, F., Wecke, T., Juszczak, A., Mäder, U., Homuth, G., Jordan, S., Kirstein, J., Hoppert, M., and Voigt, B. (2010). In-depth profiling of the LiaR response of Bacillus subtilis. J. Bacteriol *192*, 4680–4693.

Yaginuma, H., Kawai, S., Tabata, K.V., Tomiyama, K., Kakizuka, A., Komatsuzaki, T., Noji, H., and Imamura, H. (2014). Diversity in ATP concentrations in a single bacterial cell population revealed by quantitative single-cell imaging. Sci Rep *4*, 6522.

Zhou, J., Sayre, D.A., Zheng, Y., Szmacinski, H., and Sintim, H.O. (2014). Unexpected complex formation between coralyne and cyclic diadenosine monophosphate providing a simple fluorescent turn-on assay to detect this bacterial second messenger. Anal. Chem. *86*, 2412–2420.

Antibiotic Resistance Threats in the United States, 2013 | Antibiotic/Antimicrobial Resistance | CDC.

Appendix A

In *Efc* S613_D17C9, the 34bp *csp*A/EFE19808.1 intergenic deletion may affect intracellular c-di-AMP level.

Efc S613_D17C9 has 3 mutations, *lia*F$^{\Delta I177}$, *prg*U^{G105G} (with unknown function), and a 34bp intergenic deletion between *csp*A (coding a putative cold-shock DNA-binding domain protein) and EFE19808.1 (coding a YdcF-like hypothetical cytidylyltransferase family protein) (Please see Section 4.4.1 and Table 4.1 for details).

To study how activation of LiaFSR pathway (*lia*F$^{\Delta I177}$) affects intracellular c-di-AMP level, the strain S613_*lia*F$^{\Delta I177}$ was tested (Figure A-1). The c-di-AMP level was down-regulated in S613_*lia*F$^{\Delta I177}$ (61.5±81 pM/OD$_{600}$ versus 113±81 pM/OD$_{600}$). But the c-di-AMP level differences between S613_*lia*F$^{\Delta I177}$ and S613 are not distinctly different (p=0.329). As S613 strains are not stable, S613_*lia*F$^{\Delta I177}$ needs be sent for whole genome sequencing to confirm its genotype.

On the other hand, very high c-di-AMP levels were observed in S613_D17C9 (735±118 pM/OD$_{600}$) compared with S613 and S613_*lia*F$^{\Delta I177}$ (Table 3.1 and Figure 4.4). The 34bp intergenic deletion in S613_D17C9 deletes the entire putative terminator at the downstream of *csp*A (Figure A-2.a). To test how Δ34bp affects the gene expressions, qPCR was performed (Figure A-2.b). *perM* is the downstream gene of EFE19808.1, coding a putative permease (Figure A-2.a). EFE19808.1 and *perM* are supposed to be in the same operon (Figure A-2.a). With

Δ34bp, EFE19808.1 was upregulated by 212.3±26.6 fold (Figure A-2.b). This dramatically upregulated EFE19808.1 expression may cause the increased c-di-AMP level in S613_D17C9. EFE19808.1 encodes a hypothetical YdcF-like cytidylyltransferase family protein. How EFE19808.1 expression affects cellular c-di-AMP level is still unclear. The transcription of *cspA* was upregulated by 20.9±4.3 fold (Figure A-2). The transcription of *perM* was upregulated by 21.2±5.6 fold (Figure A-2). There is a LiaR consensus in the upstream of *cspA* (-325, -340). So the upregulation of *csp*A may be caused by the activation of LiaFSR pathway in S613_D17C9. The other possibility is that the transcription of *cspA-EFE19808.1-perM* makes a more stable RNA product than *cspA* itself, leading to the increased transcription of *cspA*.
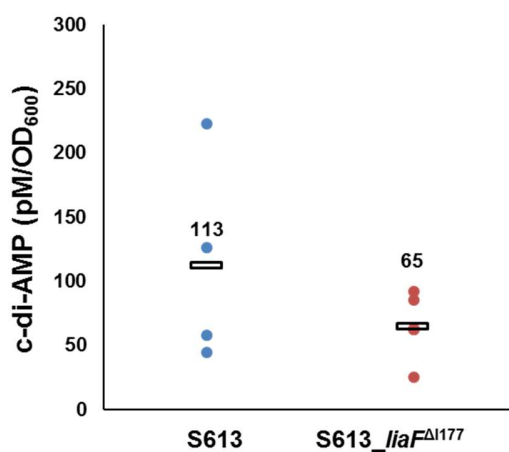

Figure A-1 Intracellular c-di-AMP levels in *Efc* S613_*lia*F^{ΔI177}. *The Intracellular c-di-AMP concentrations were measured by an enzyme-linked immunosorbent assay (ELISA) in the absence of daptomycin (Underwood et al., 2014). Mutations that are associated with activation of LiaFSR (liaF^{ΔI177}) show decreased c-di-AMP*

concentrations. There are putative additional mutations in S613_liaF$^{\Delta I177}$. Each c-di-AMP measurement was made from at least three independent biological measurements.
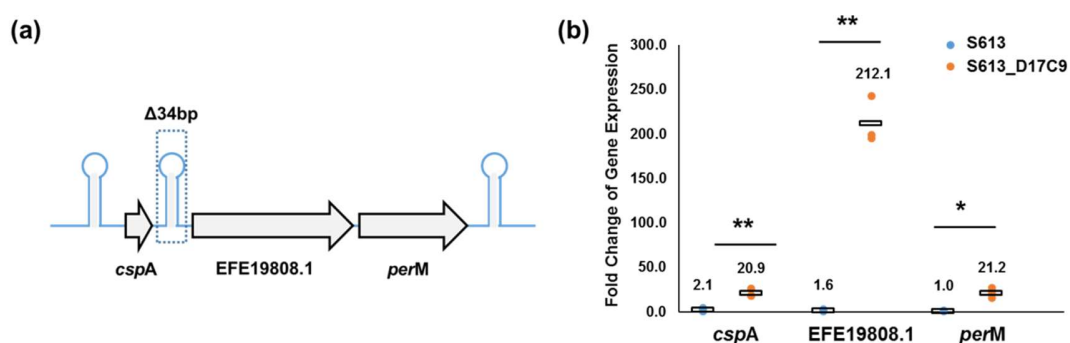

Figure A-2 Quantitative PCR results show gene expression fold change in *E. faecalis* S613_D17C9. *(a) Genetic organization in the 34bp intergenic deletion region. The predicted terminator hairpin is shown in the figure. Please see Table 4.1 for gene descriptions. (B) Quantitative PCR results of cspA, EFE19808.1, and perM in S613 and S613_D17C9. Please see Table 4.1 for gene descriptions.*

Appendix B

Growth rates of *Efc* S613 and *Efc* S613_D17C9.

      To examine the growth rates of *Efc* S613 and *Efc* S613_D17C9 (Table 3.1 and Table 4.1), the relative amount of planktonic cells within a growing culture were measured (Figure B-1). In the parental S613 strain, around 50% of cells aggregated during growth (Figure B-1.a). In *Efc* S613_D17C9, the cell line with elevated c-di-AMP levels (Table 3.1), more than 90% of the cells aggregated during growth (Figure B-1.b). S613F_D17C9 also grew more slowly than wild type S613 and reached ~73% of the total cell density measured for S613 at stationary phase. However, when biofilm formation was measured using a crystal violet staining assay (O'Toole, 2011), I did not observe a statistically significant difference between the S613 and S613_D17C9 strains (data not show).
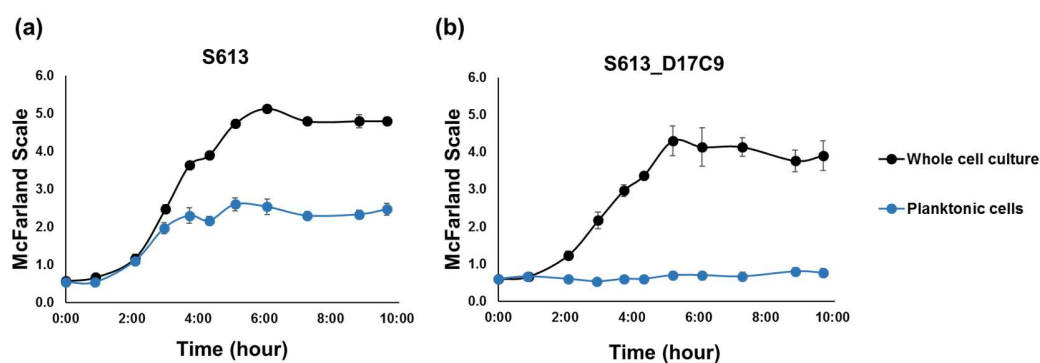

Figure B-1 Growth curves of *Efc* S613 and *Efc* S613_D17C9. *Three independent cultures were measured for whole cell culture or planktonic cells separately. Planktonic cells are defined as those in the supernatant. The growth curves show S613*

(A) and S613F_D17C9 (B) planktonic cells (blue) and whole cell cultures (black). The difference between the blue (planktonic) and black (total) illustrates the propensity of cells to aggregate. S613F_D17C9 grew slower and more cells aggregated compared with S613. Error bars correspond to standard deviations among three biological independent measurements. Please see Table 3.1 and Table 4.1 for strain details.